J.A.M. Spaninks

Department of Food Science, Agricultural University, Wageningen

Design procedures for solid-liquid extractors and the effect of hydrodynamic instabilities on extractor performance

Centre for Agricultural Publishing and Documentation

Wageningen – 1979

ISBN 90 220 0693 x

The author graduated on 6 June 1979 as Doctor in de Landbouwwetenschappen at the Agricultural University, Wageningen, the Netherlands, on a thesis with the same title.

Abstract

Spaninks, J.A.M. (1979) Design procedures for solid-liquid extractors and the effect of hydrodynamic instabilities on extractor performance. Agric. Res. Rep. (Versl. landbouwk. Onderz.) 885, ISBN 90 220 0693 X, (xi + 100 p., 44 figs, 10 tables, 155 refs, 8 app., Eng. and Dutch summaries.
Also: Doctoral thesis, Wageningen.

A design method is proposed for countercurrent mass transfer cascades with cross-flow stages, and unsteady operated fixed beds in a countercurrent arrangement. The separation performance of these cascades is calculated from mathematical models and compared with a purely countercurrent extractor. The models are based on simple equations describing mass transfer in a single stage fixed bed. The results are presented as concise correlations between the number of true and exterior apparent transfer units.

Asymptotic values of the mass transfer coefficient for transient diffusion processes in cocurrent and countercurrent extractors are calculated for particles with simple geometry. Comparing the extraction efficiency calculated from the exact solutions of the diffusion equations and the values obtained from the asymptotic mass transfer coefficient shows that differences are small under normal operating conditions for countercurrent extraction. The use of the asymptotic values in design calculations is discussed.

Due to the commonly observed viscosity and density gradients in the solvent phase, non-uniform flow of liquid through the layer of solids subjected to extraction can occur. Then some fraction of the solids is not efficiently contacted with the solvent. Experiments show that a concentration gradient rather than a concentration jump in the liquid flowing through an inert packing material reduces the effect of channelling. The effect of mass transfer between the packing and the surrounding liquid on flow stability is studied. The results indicate that channelling can reduce the extraction efficiency in solid-liquid extractors.

Free descriptors: leaching, extraction efficiency.

Contents

List of symbols most frequently used

1 Introduction 1
- 1.1 Solid liquid extraction in the food industry 1
- 1.2 Organization of the study 5
- 1.3 Some general remarks on the model system studied 10

2 Effect of local phase contact on extraction efficiency 12
- 2.1 Classification of solid-liquid extractors 13
- 2.2 Diffusion battery 14
- 2.2.1 Mathematical model of a single-stage fixed bed 15
- 2.2.2 Mathematical model of a diffusion battery 16
- 2.2.3 Efficiency of a diffusion battery 17
- 2.3 Belt type extractor 19
- 2.3.1 Mathematical model of a single-stage cross-flow device 19
- 2.3.2 Mathematical model of a belt type extractor without liquid recirculation 21
- 2.3.3 Efficiency of belt type extractors without liquid recirculation 23
- 2.3.4 Efficiency of belt type extractors with liquid recirculation 26

3 Estimation of mass transfer coefficients in solid-liquid extractors 31
- 3.1 Introduction 31
- 3.2 Estimating mass transfer coefficients in the continuous phase 33
- 3.3 Estimating mass transfer coefficients in the dispersed phase 37
- 3.3.1 Survey of literature data 38
- 3.3.2 $Sh_{d,a}$ values from solutions under coupled boundary conditions 39
- 3.3.3 $Sh_{d,a}$ values from solutions under general boundary conditions 49
- 3.4 Asymptotic $Sh_{d,a}$ numbers in engineering calculations 51

4 Liquid maldistribution in solid-liquid extractors: hydrodynamic instabilities 59
- 4.1 Introduction 59
- 4.1.1 Stability criteria 60
- 4.1.2 Flow behaviour in the unstable regime 64
- 4.1.3 Experimental verification from literature data 66
- 4.2 Experimental study of miscible liquid displacement from packed beds 68
- 4.2.1 Effect of a concentration gradient in the liquid phase on flow stability 69
- 4.2.2 Effect of mass transfer from the packing to the liquid on flow stability 73

5 Conclusions 79

Summary 80

Samenvatting 81

References 82

Appendices 86

Appendix A. Numerical solution of the equations describing mass transfer in a fixed bed 86
Appendix B. Criteria for the validity of the simplified model of a belt extractor 88
89
Appendix C. Approximate relations for estimating $Sh_{d,a}$ values 92
Appendix D. Mass transfer efficiency in the penetration period
Appendix E. Apparatus and experimental procedures: measurement of breakthrough curves 93
Appendix F. Determination of the moments of the measured breakthrough curves 96
Appendix G. Locating the position of the displacement front in downward miscible liquid displacement from packed beds 97
Appendix H. Determination of the model parameters D and $(k_0 a)$ 100

List of symbols most frequently used

a'	interfacial area per unit of solids	(m^2/m^3)
a	specific interfacial area per unit of packed volume	(m^2/m^3)
A	cross-sectional area of the extractor perpendicular to the liquid flow	(m^2)
A_d	particle surface area	(m^2)
B	dimension packed section of the extractor perpendicular to the solids flow direction	(m)
Bi	dimensionless Biot number = $m\,(D_p/2)\,k_c/\mathcal{D}_d$	(1)
Bo	dimensionless Bodenstein number = $<v>\,D_p/\mathcal{D}_E$	(1)
c'	dimensional continuous phase concentration	(kg/m^3)
c	dimensionless continuous phase concentration, Eqn 2.6	(1)
C	dimensionless continuous phase concentration, Eqn 3.44	(1)
D	distribution ratio, Eqn 2.9	(1)
$\mathcal{D}$	diffusion coefficient	(m^2/s)
$\mathcal{D}_E$	effective dispersion coefficient	(m^2/s)
D_p	equivalent particle diameter	(m)
E	frequency distribution of residence times	(1)
f	separation factor = η/Λ	(1)
F	cumulative distribution of residence times	(1)
Fo	dimensionless Fourier number = $\tau\,\mathcal{D}_d/R^2$	(1)
g	gravitational constant	(m/s^2)
h	liquid holdup, interstitial void fraction	(1)
h_m	height of the mixing zone	(m)
H	belt length	(m)
j_m	Colburn j-factor for mass transfer	(1)
k	mass transfer coefficient	(m/s)
L	extractor dimension in the direction of the liquid flow	(m)
m	slope of the equilibrium curve	(1)
M	viscosity ratio	(1)
M	moments of the distribution functions	
n	number of mass transfer sections in a countercurrent cascade	(1)
N	number of transfer units	(1)
p	pressure	(Pa)
Pe	dimensionless Péclet number = $<v>\,L/\mathcal{D}_E$	(1)
r	distance coordinate	(m)
R	particle radius = $D_p/2$	(m)
Re	dimensionless Reynolds number	(1)
s	Laplace transform variable	
s_0	initial saturation of interstitial pore liquid	(1)

S	cross-sectional area of the packed section in the extractor perpendicular to the solids flow	(m^2)
Sc	dimensionless Schmidt number = $\mu/\rho\, \mathit{ID}_c$	(1)
Sh	dimensionless Sherwood number = $k\, D_p/\mathit{ID}$	(1)
t	time	(s)
t_d	dimensionless time = $t\, \mathit{ID}_d/R^2$	(1)
t_f	time required to fill the interstitial voids of the packing	(s)
$<v>$	superficial velocity	(m/s)
v_b	belt velocity	(m/s)
v_c	superficial critical displacement velocity, Eqn 4.3	(m/s)
v_s	superficial stable displacement velocity, Eqn 4.6	(m/s)
V	volume	(m^3)
W	dimensionless dispersed phase concentration, Eqn 3.35	(1)
x,y,z	distance coordinates	(m)
ζ	dimensionless coordinate x/L	(1)
η	separation efficiency, Eqn 1.4	(1)
θ	dimensionless time, Eqn 2.11	(1)
Θ	dimensionless variable, Eqn 2.26	(1)
κ	permeability	(m^2)
λ_i	eigenvalue	
λ	wavelength perturbation	(m)
Λ	extraction factor	(1)
Λ_t	Λ for countercurrent extraction; $-\Lambda$ for cocurrent extraction	(1)
μ	viscosity	(kg/ms)
μ	eigenvalue	
ν	geometry factor; 1, 2 and 3 for slabs, cylinders and spheres respectively	(1)
ξ	dimensionless coordinate r/R	(1)
ξ_l	ratio of mixer volume and free volume column section = $V_{m,i}/V_{col}h$	(1)
ρ	density	(kg/m^3)
τ	residence time	(s)
ϕ	flow rate	(m^3/s)
ϕ''	flux	(m/s)
ω'	dimensional dispersed phase concentration	(kg/m^3)
ω	dimensionless dispersed phase concentration, Eqn 2.7	(1)

Subscript

a	asymptotic value
b	belt
c	continuous phase; operation cycle
col	column
d	dispersed phase
ext	exterior apparent
i	interface; sequence number
in	phase inlet

L	longitudinal, axial
m	mixer; mass
0	initial value; overall
out	phase outlet
ref	reference value
t	true; total flow system
T	transversal, radial
v	volumetric
Δ	entrained by the dispersed phase
∞	value at infinite time or position

Superscript

*	equilibrium
—	average

1 Introduction

1.1 Solid-liquid extraction in the food industry

Solid-liquid extraction is a unit operation aiming at the selective removal of soluble components from a solid matrix in a solvent phase. Many synonimus names for this process are used in the literature, such as leaching, washing and lixiviation. Sometimes these names are used in relation to the mechanism that is responsible for the solute transfer. This mechanism can be simple washing of adhering liquid from the surface of a solid matrix. This occurs for example in the first stage of the extraction of oil from flaked soybean, after the cells containing the oil have been broken in the pretreatment stage. In other mechanisms, solute diffuses through a permeable barrier. In the extraction of sugar from sugar-beet, the cell walls are deliberately kept intact to prevent the transfer of colloidal components. Some examples of solid-liquid extraction processes relevant to food industry are given in Table 1. The examples in this table show that for most of the important applications the liquid extract is the major product stream from an extraction plant. When the process is directed towards the removal of undesirable trace components, the solid phase is the important product. In some cases, both the solid and liquid stream are subjected to further processing. In the extraction of oil from soybean for example, the upgrading of the extracted solids is of paramount importance for the economy of the process.

Table 1. Some examples of solid-liquid extraction processes in the food industry.

Component to be extracted	Solid carrier	References
Sugar	Beets	Silin, 1964
	Cane	Brüniche Olsen, 1969
	Fruits	Wucherpfenning, 1976
Oils and Fats	Oil seeds (soybeans, cotton, peanuts, palm fruit, rapeseed), fish	Hutchins, 1976
Protein	Vegetable seeds, green leaves	Berg v.d., 1972
Coffee solubles	Roast and ground coffee beans	Sivetz, 1963
Tea solubles	Tea leaves	
Chichory	Chichory root	
Licorice	Licorice root	Molyneaux, 1975
Removal of trace components		
Aflatoxin	Cereals, seeds	US Patent 4055674, 1977
Caffeine	Green coffee beans	Bichsel, 1976

In this work attention will be focussed on solid-liquid extraction in the food industry, though most of the results have general applicability. The main reason is the growing interest in this unit operation. In the last decades, the extraction of vegetable oil shifted from mechanical pressing to solvent extraction. For oil seeds with a high oil content, the press cake obtained after mechanical prepressing by expellers is subjected to solvent extraction. Even direct solvent extraction has been proposed (Bernardini, 1976). Also there is a growing interest in solid-liquid extraction or diffusion for the production of sugar from cane (Rein, 1976), instead of the classical imbibition process. Sugar from beet has been produced by diffusion for several decades. Further, protein and carbohydrate extraction from vegetable food sources will become of increasing importance in the near future.

Compared with other unit operations such as liquid-liquid extraction, limited attention has been given in the literature to the design of solid-liquid extractors. Even though the leaching of metal ores is one of the oldest applications of this unit operation, solid-liquid extraction is of relatively minor importance to the chemical and petrochemical industries compared with distillation and liquid-liquid extraction, for example. On the other hand, in the food industry, where this process is of major importance, an overdesign of the extraction equipment normally has little impact on the final costs of the product as long as the overdesign does not increase the variable costs. For production of sugar and soybean oil, the capital cost involve only some percent of the total production costs. In the near future, with rising energy prices and an increasing scale of operation, it can be expected that a more accurate design of the extractors will be necessary.

The specific features of the solid-liquid extraction process can be elucidated by an inspection of the operation principle of the equipment used. Solid-liquid extractors are designed to transport a solid phase with a specified velocity through the extraction section. During the time that the solids reside in this part, an intensive contact between the particles and the solvent is assured to promote mass transfer. Finally, the apparatus must separate the phases efficiently before they are withdrawn from the extractor. In order to make efficient use of the solvent, the overall phase contact generally is in countercurrence. The mechanical problems associated with processing of large amounts of raw material under the conditions just mentioned have been solved more or less satisfactorily and have resulted in many widely differing designs.

In the literature, solid-liquid extractors are often classified as extractors of the percolation type and immersion type, operating in batch or continuous flow (Rickles, 1965; Milligan, 1976; Silin, 1964; Bernardini, 1976). Although this classification highlights only one specific feature of the appartus considered, it will be followed here for a description of solid-liquid extraction systems. However, it must be kept in mind that this differentiation does not provide any insight in the stage efficiencies that can be expected in a certain extractor. This disadvantage is overcome in an alternative classification that is proposed in Section 2.1. The extractortypes mentioned in the following paragraphs have been described in some detail by the authors just mentioned.

In immersion extractors the solids do not form a densely packed bed, but they are more or less dispersed in a pool of solvent. In this kind of equipment very finely ground solids can be processed, as well as particles that disintegrate upon extraction. This disintegration would certainly choke the bed of solid particles in a percolation type extractor. Normally these extraction systems are designed to operate in continuous countercurrent

flow. Examples are the Hildebrand extractor, that was in use for the extraction of oil from soybean in the 1950s, the Bonotto extractor and the BMA diffusor. The latter is used primarily for the extraction of sugar from beet. In some cases intermittent drainage of the solids is achieved by lifting the solids periodically out of the solvent. This principle is followed in the DDS and Niro diffusors, which are predominantly used for the extraction of sliced sugar-beet, and in the Kennedy extractor. The main advantages of the immersion type extractors are their insensitivity to the pretreatment of the solids, and the ease of operation as the extractor accomodates a wide range of solid-liquid flow ratios, i.e. extraction factors. Disadvantages are a low solids holdup in the system and a considerable entrainment of fines by the extract flow.

In a percolation extractor the solids are transported on a perforated support as a compact bed. The liquid flow is distributed over the bed, percolates downwards by the action of gravity, and leaves the bed dripping through the perforations in the structure supporting the bed of solids (e.g. a perforated belt). The relatively high solid phase holdup makes this extractor attractive for large scale extraction of for example oil from oil seeds and of sugar from cane. They are also in use for extraction of components from fishmeal, spices, and solubles from tea leaves.

The Bollman extractor is a well-known example of a percolation type extractor that was used in Europe and the US for the extraction of soybean oil. Most of them, however, have been replaced by extractors with a more modern design such as De Smet and Lurgi, where the solids are transported laterally through the extractor on a perforated belt, or similar types with perforated throughs connected to an endless chain. Also extractors with rotating cells provided with a perforated bottom such as Rotocell and Caroussel, or with spargers rotating over stationary cells, such as the French stationary basket extractor, are in use on a large scale. The operation principle of these extraction systems is elucidated in Fig. 1. The solvent is distributed over a section of the extractor by spargers. The liquid percolates through the bed of solids by gravity and after dripping through the perforated support, it is collected in reservoirs or pans. The net liquid flow from inlet to outlet can be accomplished in several ways. The extract from the collection pan in section i can be pumped to the sparger in section $i+1$, as indicated in the figure. In other cases, the extract from pan i is recirculated in section i while the net liquid flow is obtained by overflow of the collection pans. A combination of recirculation and transport to the sparger downstream is also possible (Milligan, 1976). To avoid entrainment of the liquid contained in the interstitial voids of the solids to the section upstream, the solids are often left to drain before leaving a section.

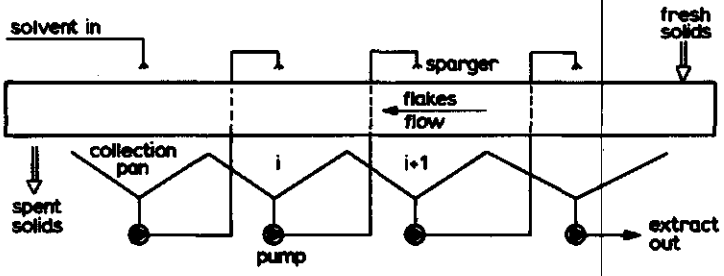

Fig. 1. Belt type percolation extractor.

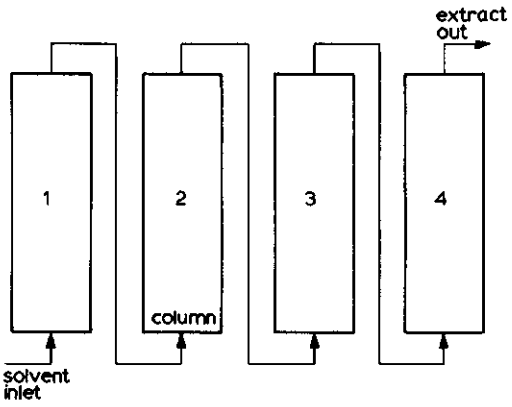

Fig. 2. Diffusion battery with 4 columns.

In a diffusion battery or Shanks extractor, the percolation velocity is controlled by pumping the solvent through the layer of solids. The extractor consists of a series of columns in which the solids are held stationary. The operation of the extractor is shown in Fig. 2. The liquid flows all the way down through the series of columns as indicated in this figure. Fig. 3 illustrates how a diffusion battery with four columns operates. After a certain 'cycle time' t_c the desired depletion of the solids in the first column is attained. The liquid inlet is then switched to the second column. The first column is then recharged with fresh solids and is put in the series of columns downstream of the last one (position IV in Fig. 3). After the extract has filled the interstitial pore volume of the freshly charged column, extract is drawn from the extractor. This cyclic operation is repeated, thus establishing an essentially countercurrent phase contacting system. This extraction system was traditionally in use for the extraction of sugar from beet but has been replaced almost entirely by continuous diffusors nowadays. The diffusion battery is still in use for the extraction of roasted and ground coffee, as the water for the extraction is

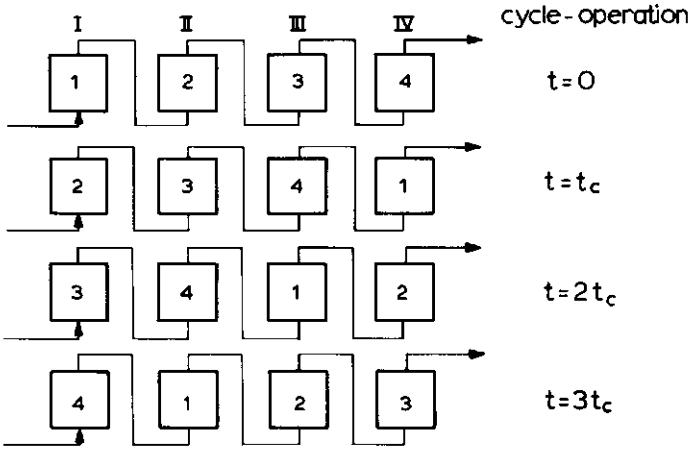

Fig. 3. Diffusion battery with 4 columns; schematic indication of operation cycles with cycle time t_c.

fed to the extractor at temperatures as high as 170 °C at a pressure of 8×10^5 Pa. Under these conditions it is difficult to feed the solids continuously to the extractor. In most cases between five and eight columns are used (Sivetz, 1963). This extractor is manufactured for small scale extraction of olive pomace (Bernardini, 1976) and consists of four columns in series.

In percolation extractors the solids are held stationary on a rigid support. This design implies that no mechanical forces act on the particles, and consequently the formation of fines is considerably reduced. Furthermore the extract is filtered while percolating through the layer of solids, so that the entrainment of fines by the liquid flow leaving the extractor is relatively small. On the other hand, a carefully designed pretreatment is required since both the particle shape and size affect the percolation velocity. As the solids subjected to the extraction are not in general repacked non-uniform liquid flow through the layer of solids may restrict the separation efficiency. In particular when particle sizes are small with consequently low permeability of the packed bed, channelling may occur. This latter phenomenon will be discussed in more detail in Section 1.2.

This description of extraction systems clearly shows that for most of the practical solutions to the mechanical problems involved in handling large amounts of particulate solids, the flow pattern of both phases through the extractor is quite complicated. Obviously, this flow pattern must be taken into account in the mathematical models underlying design procedures for solid-liquid extractors. The design methods proposed in this study incorporate these specific features of extraction into the available design procedures for other unit operations, e.g. drying and liquid-liquid extraction.

1.2 Organization of the study

The present study can be divided into two main parts: a theoretical part in which the number of transfer unit (NTU) approach for the design of solid-liquid extractors was analysed and an experimental part in which the hydrodynamic stability of the liquid flow in solid-liquid extractors was measured and analysed.

Generally the design of mass transfer processes starts from specified or assumed concentrations in inlet and outlet streams, and the flow rates of the phases. As will be shown in Chapter 3, the mass flux that occurs in solid-liquid extractors is often proportional to the overall driving force for mass transfer, i.e. the local concentration difference of the solute in both phases. In such cases, the NTU concept, in which the mass transfer resistance is lumped at the solid-liquid interface, is a convenient basis for a design procedure. An outline of the NTU approach in process design is given in Fig. 4. The separation to be attained can then be indicated by the number of exterior apparent or 'plug flow' transfer units, defined by Miyauchi & Vermeulen (1963):

$$N_{\mathrm{ext,\,c}} = \int_{c'_{\mathrm{in}}}^{c'_{\mathrm{out}}} \frac{\mathrm{d}c'}{c'^{*} - c'} \tag{1.1}$$

where c'_{in} and c'_{out} are the inlet and outlet concentrations in the continuous phase, respectively; c'^{*} is the hypothetical local concentration which would be in equilibrium with the dispersed phase if the phases were contacted in purely countercurrent plug flow.

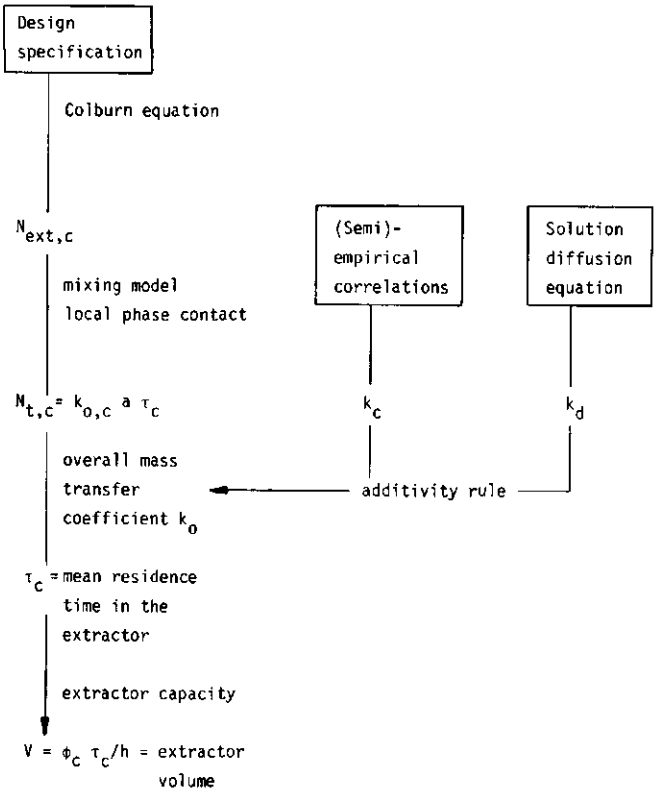

Fig. 4. Outline of the transfer unit approach to the design of solid liquid extraction equipment.

Only for purely countercurrent contact can it be shown that the number of exterior apparent transfer units is equal to the number of true transfer units (Colburn, 1939):

$$N_{\text{ext, plug flow}} = N_{t,c} = \frac{k_{oc} a V}{\phi_c} \tag{1.2}$$

where k_{oc} is the mass transfer coefficient on overall liquid phase basis and a is the effective interfacial area. Here combination of Eqn 1.1 with a mass balance yields for a linear equilibrium relation the well-known Colburn equation which is shown in Fig. 5:

$$N_{ext,c} = \frac{1}{1-\Lambda} \ln\left(\frac{1-f\Lambda}{1-f}\right) \tag{1.3}$$

The separation factor f is related to the extraction efficiency η as $f = \eta/\Lambda$ and η is defined as:

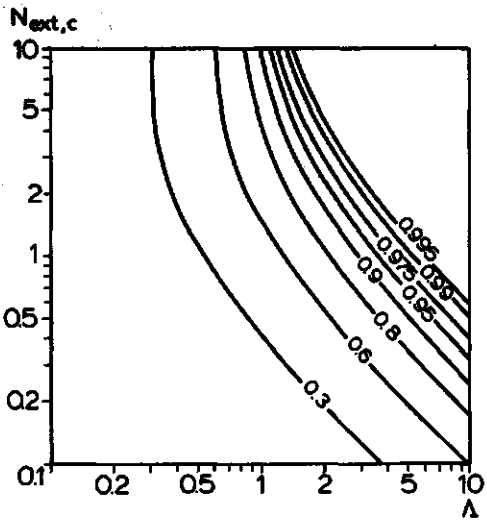

Fig. 5. Efficiency of a purely countercurrent process. Parameter: extraction efficiency η.

$$\eta = \frac{\phi_c\,(c'_{out} - c'_{in})}{\phi_d\,(\omega'_{in} - c'_{in}/m)} = \Lambda\,\frac{c'_{out} - c'_{in}}{m\omega'_{in} - c'_{in}} \tag{1.4}$$

When deviations from countercurrent plug flow occur, the number of true transfer units $N_{t,c}$ exceeds $N_{ext,c}$, the number of exterior apparent transfer units. In fact:

Table 2. Relation between the number of exterior apparent and true transfer units for some simple mass transfer stages.

Phase contact	Liquid phase	Solid phase	$\frac{c_{in}-c_{out}}{c_{in}-m\omega_{out}} =$
			$\frac{1-\exp\{(\Lambda-1)N_{ext,c}\}}{1-\Lambda}$
batch			
batch	mixed	irrelevant	$\frac{1-\exp[-N_{t,c}(1+\Lambda)]}{1+\Lambda}$
continuous flow operation			
cocurrent	unmixed	unmixed	$\frac{1-\exp[-N_{t,c}(1+\Lambda)]}{1+\Lambda}$
crosscurrent[1]	unmixed	unmixed	$\frac{1}{\Lambda}\left[\left\{\frac{1}{N_{t,c}}\int_0^{\Lambda N_{t,c}} e^{-\xi}\int_0^{N_{t,c}} e^{-\eta} I_0(2\sqrt{\xi\eta})\,d\eta\,d\xi\right\}^{-1}-1\right]^{-1}$
systematic movement of the solid phase	mixed	unmixed	$\frac{1-\exp[-N_{t,c}\Lambda]}{1-(1-\Lambda)\exp[-N_{t,c}\Lambda]}$
countercurrent	unmixed	unmixed	$\{1-\exp[-N_{t,c}(1-\Lambda)]\}/(1-\Lambda)$
continuous flow	mixed	mixed	$N_{t,c}/(1+N_{t,c})$

1. Complete mixing of both phases at the stage inlet.

$$N_{t,c} = f(N_{ext,c}, \Lambda, \text{flow situation}) \qquad (1.5)$$

The flow situation of the phases inside the apparatus is determined on a macro-scale by the local mode of phase contact, non-uniform flow of solvent through the solids etc.; and on a microscopic scale by dispersive mixing between the phases. For some simple phase contacting systems the relation between N_{ext} and N_t is given in Table 2. However, the description of extractor types in Section 1.1 has shown that the complex flow situations in practical extractors are not adequately covered by the simple examples. Deviations from these simple cases are often described by dispersive mixing or backflow models. Also these models are not likely to present a realistic picture of the flow situation in diffusion batteries and belt type extractors for example. In Chapter 2 of this work new ready-to-use correlations between N_{ext} and N_t are developed for diffusion batteries and countercurrently cascaded crossflow sections. These correlations are based on mathematical models which account for the local mode of phase contact within the apparatus.

In order to calculate the required residence time of the solids in the extractor to attain the specified separation, a sophisticated guess of the overall mass transfer coefficient k_o is inserted in the definition equation for N_t. According to the Lewis two film theory, k_o is dependent on both the mass transfer coefficient in the continuous liquid phase, k_c, and the dispersed solid phase, k_d. A constant averaged value of k_c can often be assumed throughout the extractor, as is pointed out in Section 3.1. Abundant literature data are available for estimating k_c values for widely differing process conditions and packing geometries. The dispersed phase mass transfer coefficient k_d is time dependent due to the transient nature of the diffusion process. In Section 3.1 it is shown that the Sherwood number $k_d D_p / \mathbb{D}_d$ assumes an asymptotic value for long contact times so that for a constant diffusivity $\mathbb{D}_d$ in the solid phase k_d has a constant value. These asymptotic values are calculated in Chapter 3 from the analytical solution of the diffusion equation with boundary conditions relevant to purely cocurrent and countercurrent phase contact. Using the additivity rule for mass transfer resistances, k_o can be determined from the estimated value of k_c and the asymptotic k_d value. Although this rule is exact only for a constant value of k_d and k_c, the error introduced when it is applied to transient mass transfer is small (Beek & Muttzall, 1975). The final step indicated in Fig. 4 then is the calculation of the size of the extractor from the required residence time and the specified throughput.

In both Chapters 2 and 3, concerned with the effect of local phase contact on extraction efficiency and the calculation of mass transfer coefficients, plug flow of liquid between the phases is assumed. Normally however, residence time distribution in one or both of the phases reduces the separation efficiency of the extractor. In Chapter 2, some models are discussed which can be used to account for axial dispersion in the liquid and solid phases. Another important effect that might cause residence time distribution in the liquid phase is flow maldistribution caused by a non-uniform permeability distribution in a packed bed (Stanek & Szelkeley, 1972). A well-known example of this phenomenon is the preferent flow along the wall of a column packed with particulate solids. The porosity gradient in a packed given by Pillai (1977) for example shows that the porosity near the wall exceeds the average bed porosity over the distance of about a particle diameter, see Fig. 6. The fractional wall flow resulting from this local high permeability is illustrated in Fig. 7. In general this effect can be neglected for single phase flow of a liquid with

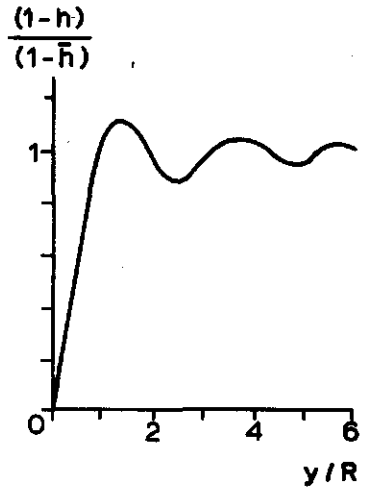

Fig. 6. Porosity gradients in packed beds, y is distance from the wall. From Pillai, 1977.

uniform physical properties when the ratio column to particle diameter is higher than 20-30. In solid-liquid extractors the physical properties of the liquid phase, i.e. density and viscosity, often increase in the direction of the liquid flow. In this case, gravity segregation can occur in upward liquid flow due to the unfavourable density gradient. In both upward and downward flow, local permeability variations can trigger the formation of channels or 'viscous fingers', through which the solvent will flow preferentially. The mechanism responsible for this phenomenon is discussed at length in Chapter 4. The existence of such stable and unstable flow regimes has been verified experimentally by many authors. Viscous fingering plays an important role in secondary recovery of oil

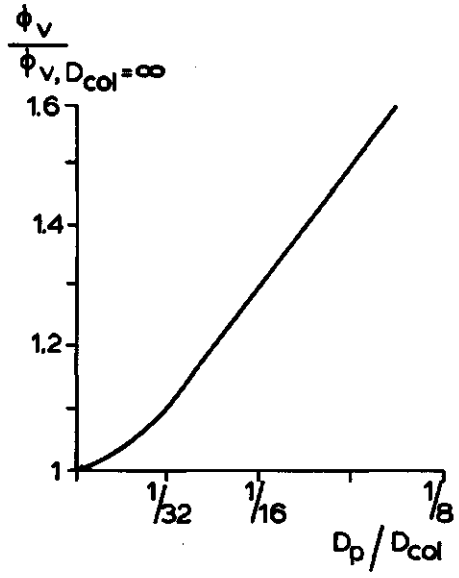

Fig. 7. Effect of particle to column diameter ratio on wall flow in packed columns. From Rietema, 1976.

from underground reservoirs, where a fluid is injected in the porous rock structure to displace residual oil (Dumoré, 1964). Examples related to the food industry are the separation of ice crystals from the mother liquor in wash columns (Vorstman & Thijssen, 1972), filter cake washing (Tondeur, 1970), sweetening on and sweetening off of char columns for decoloration of sugar solutions (Hill, 1952), and ion exclusion operations (Cooney, 1974).

Though many studies have been devoted to the onset and growth of flow instabilities during displacement of liquid from inert packed beds, little attention has been paid to systems where a concentration gradient instead of a discontinuity exists in the liquid flowing through a porous medium, as is the case in for example solid-liquid extraction. Also the effect of mass transfer between the porous packing and the liquid has not yet been studied. Chapter 4 of this work is focussed on these phenomena which can be important in solid-liquid extractors. Experiments were performed to check stability criteria which should be met in order to prevent the onset of flow instabilities in these systems.

1.3 Some general remarks on the model system studied

An effective study of the chemical engineering aspects of solid-liquid extraction is only possible when the problem is reduced to its essential elements. For this reason, if not stated otherwise, the following simplifications concerning the mass transfer process were assumed to be valid throughout this work.

– A linear equilibrium exists between the solid phase and the solvent. This assumption implies that adsorption of soluble substances on the surface of the porous matrix according to a non-linear equilibrium can be neglected. The validity of this approximation is shown experimentally by Oplatka (1954), Yang & Brier (1958) and Krasuk et al. (1967).

– The diffusivity of the extracted species is constant. The mathematics involved in solving the diffusion equation can be significantly simplified when the mass transfer rates can be described with a constant diffusion coefficient. In Table 3 some extraction processes from the food industry are given, for which the extraction rate can be described by Ficks law with a constant effective diffusion coefficient. In some cases the diffusivity is found to depend on concentration of the solute, particle size or time. Even in these cases a proper analysis of the data might sometimes reveal that the extraction can still be described by Ficks law with constant diffusion coefficient. For the extraction of flaked soybean, Bernardini (1976) found that the extraction rate is essentially constant until about 30% wt of the oil is transferred to the solvent. In a later stage of the process the mass transfer rate is governed by molecular diffusion. According to Bernardini, deviations of the initial extraction rate amount to washing off the oil adhering to the surface of the flakes. Brüniche Olsen (1962) observed that the diffusivity apparently varies with the particle size for the extraction of sugar from sliced beet. Similar effects were observed for the extraction of roast and ground coffee beans (Douwe Egberts Research, pers. commun.). This effect has been explained by a change in particle shape and fraction of disruptured cells as a result of variations in particle size.

– Constant flow rates of both phases in the extractor. When the particles can be considered as an inert solid matrix with constant internal pore volume, this approximation is valid exactly when the flow rates are expressed on a volumetric basis, e.g. m^3/s. When the

Table 3. References that report mass transfer rates that can be described with a constant diffusion coefficient.

Raw material	Extracted component	Source
Tung seed	Oil	Krasuk et al., 1975[1]
Soybean	Oil	Beek & Muttzall, 1972
Peanuts	Oil	Fan & Morris, 1948
Sugar beet	Sugar	Brüniche Olsen, 1969
Pickles	Salt	Plug et al., 1967 Bomben et al., 1974
Pickles	Sugar	Eder, 1971
Green coffee	Caffeine	Bichsel, 1976
Roast and ground coffee beans	Solubles	Douwe Egberts Research, pers. commun.
Solanum laciniatum	Solasodine	Tettamanti et al., 1975

1. At elevated temperatures only.

liquid densities are constant throughout the extractor it is also valid when the flow rates and concentrations are expressed on weigth basis. The results are not generally applicable when the particles shrink or swell considerably during extraction.

2 Effect of local phase contact on extraction efficiency

Large scale solid-liquid extractors are commonly operated in countercurrence as it is well understood that this design reduces solvent requirements. To attain pure countercurrence between solid granules or powders and a liquid phase usually involves considerable mechanical problems. For this reason one often resorts to cascading mass transfer sections in an 'overall' countercurrent fashion, while the local phase contact within a mass transfer section deviates from the overall counterflow. A classification of countercurrent separation cascades relevant to solid liquid extraction is given in Table 4. In Section 2.1. this classification is discussed in some detail and available literature dealing with the design of such mass transfer cascades is reviewed. In the subsequent sections, the efficiency of countercurrently cascaded fixed beds and cross flow sections is calculated from mathematical models. The separation efficiency of these systems is expressed as a relation between the number of exterior apparent transfer units, defined in Section 1.2, and the number of true transfer units:

$$N_{t,\,d}/\Lambda = \frac{k_{od}\ a\ V}{\phi_d}\ \frac{1}{\Lambda} \tag{2.1}$$

The results are presented in concise correlations covering the range of normal operating conditions.

Table 4. Classification of countercurrently cascaded mass transfer sections.

Local phase contact within a mass transfer stage	Examples	References covering theory on design of mass transfer cascades	
		distributed parameter model	lumped parameter model
countercurrent	U-type and J-type extractor	see Table 7	Colburn, 1939
cocurrent	Multiple batch extractors	see Table 7	
crosscurrent	Rotary and belt extractors		Thibodeaux, 1977
unsteady column	Diffusion battery	Svedberg, 1976	Chen, 1972

2.1 Classification of solid-liquid extractors

The classification of extraction systems proposed in Table 4 does not necessarilly coincide with those presented elsewhere, see Chapter 1. However, most of the percolation extractors will be found under local cross current contact, and most of the immersion extractors in the other groups. It should be kept in mind that, where as other classifications give more direct information on the raw materials that can be processed in the apparatus, this classification is related to the stage efficiencies that can be expected in the extractor.

Countercurrently cascaded mass transfer sections with local phase contact in countercurrent obviously imply a countercurrent extractor. In practice this model can be used to describe some commercial counterflow extractors approximately, such as the DDS diffusor, the NIRO and Olier extractor. Moreover purely countercurrent contact limits the separation efficiency of any extraction system. Mass transfer in countercurrent extractors is undoubtedly analysed in most detail in the literature. When plugflow of both phases occurs, the analytical solution of the distributed parameter model is given by Mikhailov (1977). Tables of analytical solutions of the diffusion equations when mass transfer rate is limited by internal diffusion have been given by Tettamanti (1975). Plachco (1970) discussed the effect of an initial concentration gradient inside a particle on the extraction efficiency for particles with slab geometry. The lumped parameter model was first solved by Colburn (1939). This latter model has been extended to deviations from pure plug flow in the phases. Exact solutions obtained by Miyauchi & Vermeulen (1963), Sleicher (1959) and Hartland & Mecklenburg (1966) using the model of plug flow with superimposed axial dispersion, and those derived by Sleicher (1960) and Mecklenburg & Hartland (1968) using the model of backmixing between complete mixed stages are not convenient for design calculations. Approximate solutions are given by Watson & Cochran (1971), Stemerding & Zuiderweg (1963), Pratt (1975), Tolic (1973) and by Pratt (1976). Kerkhof & Thijssen (1974) used a dual-cascade model, where the number of ideal mixers in both phases can be different.

Countercurrent cascades of mass transfer sections with local phase contact in cocurrence are mathematically similar to multiple batch countercurrent extractors. This extraction system is mainly used for small scale extraction of for example pharmaceutical products and spices. The operation of the extractor is described by Treyball (1968). Analytical solutions of the diffusion equation with the proper initial and boundary conditions have been numerically evaluated to obtain the efficiency of these cascades by Plachco & Lago (1972). Similar results were obtained by Schwarzberg (1977) who used a different calculation procedure. In both cases, it was assumed that geometry was spherical and that internal diffusion limits mass transfer rate. When liquid clings to the particles so that the phases are not completely separated when stage transfer occurs, the analytical solution of Plachco & Lago (1975) can be applied.

Countercurrent cascades of mass transfer sections with local phase contact in cross flow describes extraction systems that are in use for large scale extraction of oil seeds, sugarcane etc. The operating principle of this extractor is discussed in Chapter 1. In the literature little attention has been given to the mathematical modelling of these systems. For pure cross flow cascades where no entrainment of one of the phases by the other occurs, Thibodeaux (1977) recently proposed a design procedure. He assumed lumped

mass transfer resistance and complete mixing of the streams before they enter a new stage. Pure cross flow is encountered in cooling or heating of granular products (McGaw, 1976), cross-flow cooling towers (Thibodeaux, 1969) and heat exchangers (Gardner & Taborek, 1977), and is a good approximation for belt type solid-liquid extractors when the value of the distribution ratio D, defined in Eqn 2.9 is low. In his simulation model for the extraction of sugar from sugarcane, Rein (1976) accounted for entrainment of sugar juice by the moving solids. In his calculation he neglected concentration gradients over the height of the bed, perpendicular to the flow direction of the solids. No systematic analysis of the efficiency of cross-flow sections in countercurrent cascades is available in the current literature.

Countercurrent cascades of unsteady operated columns are often referred to as multiple column countercurrent extractors, diffusion batteries or Shanks extractors. Details of the operation principle of the extractor are given in Chapter 1. Multiple column countercurrent contactors are in use for ion exchange and adsorption processes. Most of the literature dealing with the design of this column arrangement is related to adsorption on active carbon from the liquid phase. The liquid residence time in a single periodically operated column was compared with a countercurrent adsorber by Neretnieks (1975). For a linear sorption isotherm, the residence time in the periodic column was at least 70% longer for the same efficiency of carbon utilization. Fornwalt & Hutchins (1966) proposed a graphical procedure to determine the number of columns in a multicolumn system. They assumed that all the columns have similarly shaped breakthrough curves, so that the apparatus is overdesigned. Chen (1972) studied adsorption from the liquid phase on activated carbon in a multiple countercurrent contactor using the model of a cascade of perfectly mixed vessels to calculate the performance of the system. An empirical relation for the equilibrium relation and the rate of mass transfer was used, so that it is difficult to generalize his results. Svedberg (1976) thoroughly studied the efficiency of multiple column adsorption from the liquid phase. Mass transfer rate was calculated from a model that takes into account film diffusion and pore diffusion with a constant diffusion coefficient. Plug flow of liquid through the column and a linear equilibrium relation were assumed. He concluded that when four or more columns are used, carbon utlization is wihin 10% of the carbon utilization in a purely countercurrent contactor, under normal operating conditions. For two columns, this figure was about 15-30% lower than in a truly countercurrent apparatus. Klaus et al. (1977) calculated carbon utilization for the adsorption of binary mixtures on active carbon. They found that the transient phase before the concentration profiles stabilize is much longer than in single component adsorption, where a periodic steady state is attained in one or two cycles.

2.2 Diffusion battery

In the following section a mathematical model of a single-stage fixed bed is derived. Subsequently it is shown how this basic model can be used as a building block in the mathematical simulation of a diffusion battery. The effect of process variables on the separation performance of the multicolumn countercurrent extractor is then calculated.

2.2.1 *Mathematical model of a single-stage fixed bed*

From Figure 8 it can be derived that mass transfer in a fixed bed can be described by Eqns 2.2 and 2.3 when a linear driving force for mass transfer is used and plug flow of liquid through the bed is assumed:

$$ALh\,\frac{\partial c'}{\partial t} = k_{oc}\,aAL\,(c'^{*} - c') - \phi_c\,\frac{\partial c'}{\partial x/L} \tag{2.2}$$

$$AL\,(1-h)\,\frac{\partial \omega'}{\partial t} = -\,k_{oc}aAL\,(c'^{*} - c') \tag{2.3}$$

with initial and boundary conditions

$$t = 0 \quad \omega' = \omega'_o\,(x) \quad c' = c'_o\,(x) \tag{2.4}$$

$$x = 0 \quad c' = c'_{in}\,(t) \tag{2.5}$$

With a linear relationship between the equilibrium concentrations in both phases, $c'^{*} = m\,\omega'$, the equations can be made dimensionless by introducing the following variables:

$$c \equiv \frac{c' - c'_o}{m\,\omega'_o - c'_o} \qquad \text{liquid phase concentration} \tag{2.6}$$

$$\omega \equiv \frac{m\,\omega' - c'_o}{m\,\omega'_o - c'_o} \qquad \text{solids phase concentration} \tag{2.7}$$

$$N_{t,c} \equiv \frac{k_{oc}\,a\,V}{\phi_c} \qquad \text{number of true transfer units on overall liquid phase basis} \tag{2.8}$$

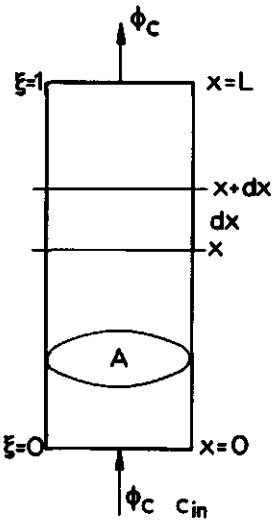

Fig. 8. Fixed bed extraction.

$$D \equiv \frac{mh}{(1-h)} \qquad \text{distribution ratio} \tag{2.9}$$

$$\zeta \equiv \frac{x}{L} \qquad \text{dimensionless distance from liquid inlet} \tag{2.10}$$

$$\theta \equiv \frac{t\phi_c}{Vh} \qquad \text{dimensionless time} \tag{2.11}$$

With these variables the differential equations with initial and boundary conditions can be written as:

$$\frac{\partial c}{\partial \theta} + \frac{\partial c}{\partial \zeta} = N_{t,c}(\omega - c) \tag{2.12}$$

$$\frac{\partial \omega}{\partial \theta} = -N_{t,c} D (\omega - c) \tag{2.13}$$

$$\theta = 0 \qquad \omega = \omega_0(\zeta) \quad c = c_0(\zeta) \tag{2.14}$$

$$\zeta = 0 \qquad c = c_{in}(\theta) \tag{2.15}$$

When at time $\theta = 0$ the concentration in the solid and the liquid phase are in equilibrium and the inlet concentration c_{in} is constant, the solution of the above equations is well known (Anzelius, 1926):

$$c = e^{-\theta_M} \int_0^{N_{t,c}} e^{-s} J_0(2i\sqrt{s\theta_M})\, ds \tag{2.16}$$

where

$$\theta_M = N_{t,c} D (\theta - 1) \tag{2.17}$$

The above relation is tabulated by Furnas (1930). Approximate solutions are given in the survey of Klinkenberg (1954) and in the paper of Roetzel & Nicole (1975). For arbitrary initial concentration profiles in both phases and time variable concentration at the liquid inlet, Klinkenberg & Harmens (1960) gave an unavoidably complicated analytical solution. As an alternative to this solution, the equations can be solved numerically. Details of the computational scheme that was used here are given in Appendix A.

2.2.2 Mathematical model of a diffusion battery

In order to simulate a diffusion battery, a number of columns can be put in series as shown in Fig. 9. Another approach that is somewhat easier to incorporate in a computer program, is to consider the diffusion battery as a single column in which the solids are transported intermittently. Since we are interested in the concentration profiles in a cyclic 'steady' state and the profiles at the beginning of a cycle are not known before-

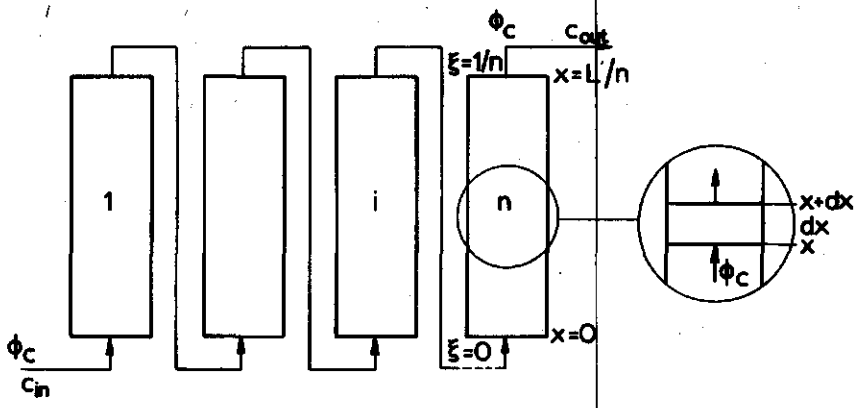

Fig. 9. Diffusion battery with n columns.

hand, the equations are solved numerically. Starting from an arbitrary initial concentration profile, the unsteady state start-up of the system of columns is simulated. At the end of every cycle the concentration profiles are shifted one column and the concentrations in both phases in the last column, i.e. where the solids are fed to the extractor, are reset according to the boundary conditions. This operation cycle is repeated until the concentration profiles in the extractor and the exit concentration of the columns averaged over one cycle time no longer change significantly. In most calculations the concentration profiles stabilized in n cycles. To allow an accurate evaluation of N_{ext}, the calculation must be continued up to a dimensionless time θ between 6 and 10. The computation is then halted and the mass balance checked, which closed within 0.5% in most cases.

In analogy to the extraction factor in continuous countercurrent processes, we defined an extraction factor or 'draw-off factor' for semi-continuous multiple column extraction as the ratio of the liquid flow drawn from the extractor to the flow of solids through the extractor, multiplied by the slope of the equilibrium curve. The flow of solids is determined by the volume of solids in one column and the cycle time t_c only. Bearing in mind that the water filling the interstitial voids in the first column is discharged with the exhausted solids, we can calculate the draw-off factor, Λ from:

$$\Lambda = m \frac{\phi_c - \frac{Vh}{n} \cdot \frac{1}{t_c}}{\frac{V(1-h)}{n} \cdot \frac{1}{t_c}} = D(n\theta_c - 1) \tag{2.18}$$

The above equation is used to determine the dimensionless cycle time θ_c required to attain a chosen draw-off factor Λ.

2.2.3 *Efficiency of a diffusion battery*

The results of the calculations are shown in Fig. 10. The plots show an almost linear relation between $N_{t,d}/\Lambda$ and N_{ext}. Increasing the number of columns results in a smaller difference between $N_{t,d}/\Lambda$ and N_{ext}, showing that the extractor approaches a truly

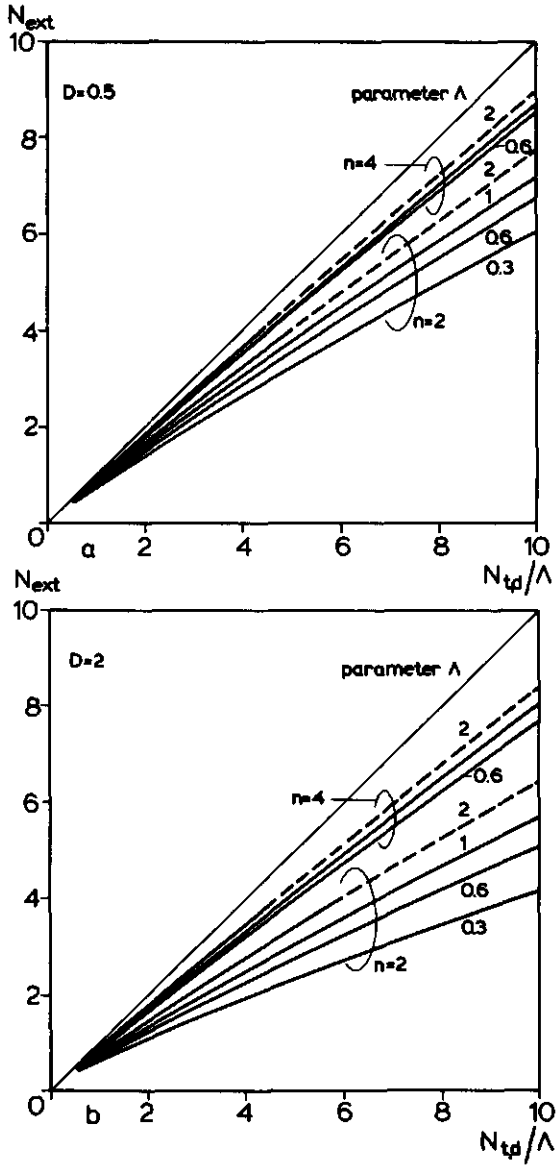

Fig. 10. Number of exterior apparent against true transfer units for a diffusion battery with n columns. D is distribution ratio; Λ is extraction factor.

countercurrent system. An increase in Λ, the draw-off factor, shows the same tendency, which is due to a more favourable ratio of draw-off and cycle time at higher values of Λ. Since the time required to fill the interstitial voids of the freshly charged column is equal to $t_f = (hV/n)/\phi_c$, one can write for this ratio with Eqns 2.9 and 2.18:

$$\frac{\theta_f}{\theta_c} = \frac{1/n}{(1 + \Lambda/D)/n} = \frac{D}{D + \Lambda} \tag{2.19}$$

The effect of D can be made clearer by writing the expression for D as follows:

$$D = \frac{mh}{1-h} = \frac{m\,\dfrac{Vh}{nt_c}}{\dfrac{V(1-h)}{nt_c}} = \frac{\phi_{c,\Delta}}{\phi_c - \phi_{c,\Delta}} \cdot \Lambda \tag{2.20}$$

D/Λ can thus be interpreted as the ratio of the liquid flow entrained by the discharged solids, $\phi_{c,\Delta}$ and the net liquid flow drawn from the extractor. Since the solubles in the liquid in the first column will be lost with the spent solids at the end of the cycle one expects a higher efficiency for a lower value of D, which is confirmed by the calculations. The results of the calculations are given in a concise form by Eqn 2.21, which covers the whole range of input parameters used in the simulation runs.

$$\frac{N_{ext}}{N_{t,d/\Lambda}} = 1 - 0.59\, n^{-1.17}\, \Lambda^{-0.3}\, N_{ext}^{0.15\Lambda/n}\, D^{0.33} \tag{2.21}$$

$2 \leq n < 6 \quad 0.25 < \Lambda < 2 \quad 0.25 < D < 4$
$0.25 < N_{ext} < 10 \quad \eta < 0.99$

Within the indicated region this correlation gives an estimated value of $(N_{t,d}/\Lambda - N_{ext})/N_{ext}$, within 5% of the numerically calculated value.

2.3 Belt type extractor

In this section a mathematical model of a single stage cross-flow device is derived. The analogy to an unsteady operated column is discussed. It is shown that the algorithm proposed in Section 2.2.1 can be used with some modifications for the mathematical simulation of a belt type extractor. For extractors without liquid recirculation, the efficiency has been obtained from numerical calculations. The efficiency of extractors with liquid recirculation is calculated from analytical solutions of approximate models.

2.3.1 Mathematical model of a single-stage cross-flow device

From Fig. 11, the following equations can be derived for cross-current extraction under steady state conditions:

$$\frac{\phi_c}{H}\frac{\partial c'}{\partial x} + \frac{v_b S h}{L}\frac{\partial c'}{\partial y} = k_{oc}\, aB\,(c^{*\prime} - c') \tag{2.22}$$

$$\frac{v_b S(1-h)}{L}\frac{\partial \omega'}{\partial y} = -\,k_{oc} aB\,(c^{*\prime} - c') \tag{2.23}$$

with boundary conditions:

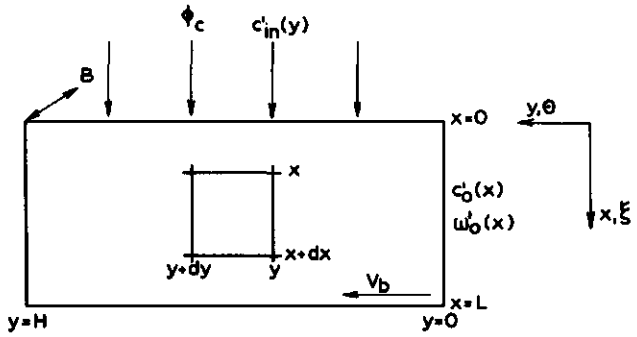

Fig. 11. Cross current phase contact.

$$y = 0 \quad \omega' = \omega'_0(x) \quad c' = c'_0(x) \tag{2.24}$$

$$x = 0 \quad c' = c'_{in}(y) \tag{2.25}$$

The equations are transformed into a dimensionless form by introducing the following variable in addition to Eqns 2.6–2.10:

$$\Theta \equiv \frac{(v/v_b)\phi_c}{Vh} \quad \text{dimensionless residence time of solids in the extractor} \tag{2.26}$$

The equations can thus be rearranged to:

$$\frac{\partial c}{\partial \Theta} + \frac{\partial c}{\partial \zeta} = N_{t,c}(\omega - c) \tag{2.27}$$

$$\frac{\partial \omega}{\partial \Theta} = -N_{t,c} D(\omega - c) \tag{2.28}$$

with boundary conditions:

$$\Theta = 0 \quad \omega = \omega_0(\zeta) \quad c = c_0(\zeta) \tag{2.29}$$

$$\zeta = 0 \quad c = c_{in}(\Theta) \tag{2.30}$$

The above equations are similar to those given in Section 2.2.1. For pure cross-current contact in single stage devices, this analogy is well understood (Nusselt, 1930). It involves that the equations describing mass transfer in unsteady operated columns can be reduced to those describing pure cross-flow contactors, by transforming the Eulerian system to Lagrangian coordinates. When liquid is displaced in the direction of the flow os solids, as in solid-liquid extraction, the analogy applies in Eulerian coordinates. This analogy will be extended here to multiple fixed beds in series in order to simulate mass transfer efficiency in a belt type extractor.

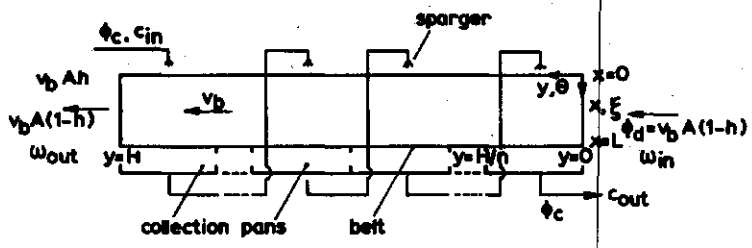

Fig. 12. Belt extractor without dripping sections.

2.3.2 Mathematical model of a belt type extractor without liquid recirculation

A sketch of the extractor considered in this section is given in Figure 12. The mean concentration of liquid leaving section i can be calculated by averaging the concentration of liquid dripping form the belt into the collection pan below, thus at $x = L$ or $\xi = 1$, from $y = 0$ to $y = H/n$, or from $\Theta = 0$ to:

$$\Theta = \Theta_c = \frac{\phi_c}{S v_b h n} \tag{2.31}$$

Θ_c, the dimensionless residence time of the solids in one section of the extractor, is related to the draw-off factor Λ, defined analogously to the extraction factor in counter-current extractors as:

$$\Lambda = m \frac{\phi_c - v_b S h}{v_b S (1-h)} \tag{2.32}$$

Combining Eqns 2.31 and 2.32 gives:

$$\Theta_c = \left(1 + \frac{\Lambda}{D}\right) / n \tag{2.33}$$

Fig. 13 gives the calculation analogue of the belt extractor from Fig. 12. The liquid leaving section i is collected in chamber A_i and mixed up. After one 'cycle time' Θ_c the liquid from A_i is transferred to B_i. The liquid entering section $(i+1)$ is withdrawn from the latter. The calculation proceeds as follows. Since the concentration profiles in steady state are unknown a priori, Eqns 2.27–2.30 are integrated starting from an arbitrary initial concentration profile in both phases. After one cycle time Θ_c, the average concentration leaving column i is determined, and the liquid concentration in B_i is set equal to this value. Concentration profiles are shifted one column. The concentration in the last column downstream is reset according to the boundary conditions. After a large number of cycles has been worked through, the average liquid concentration leaving each section reaches a constant value. The calculation is then halted and the mass balance is checked. It should be realized that this calculation method does not give any information on the unsteady operation of the extractor since we started from the steady equations 2.22 and 2.23.

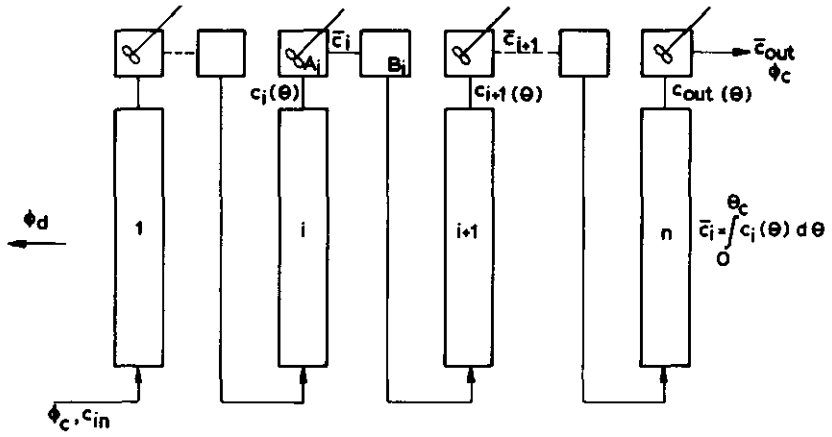

Fig. 13. Analogue of belt extractor of Fig. 12.

The mathematical simulation of a belt extractor without dripping sections has just been discussed. However, in most industrial extractors dripping sections are present. In the following the mathematical model will be extended to take these into account.

A rigorous simulation of this case is rather complicated, because both drainage rate (Beek & Muttzall, 1972) and static holdup (Dombrowski, 1954) are dependent on the physical properties of the liquid and the bed geometry. Therefore the problem is simplified considerably here by assuming a constant drainage rate, equal to the percolation rate. It is further assumed that no liquid remains in the interstitial voids of the bed after drainage. This simplified situation can be simulated by shifting the chambers collecting the percolating liquid over a distance y_f as indicated in Fig. 14. This distance is related to the time required to fill the interstitial voids in the fresh solids entering section n. In the time required for the liquid front to reach the lower end of the packing, the belt has moved over a length y_f:

$$y_f = v_b \frac{hL}{\phi_c/(BH/n)} \tag{2.34}$$

or in dimensionless form:

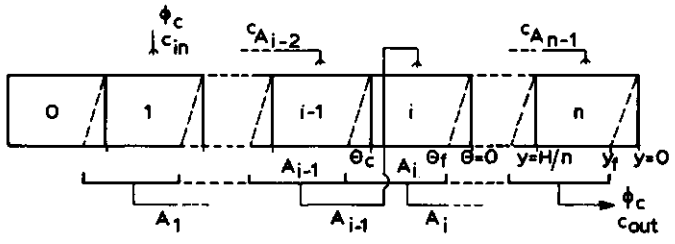

Fig. 14. Belt extractor with dripping sections.

$$\Theta_f = \frac{1}{n} \tag{2.35}$$

Since no liquid is entrained by the solids leaving the extractor, the extraction factor can now be calculated from:

$$\Lambda = m \frac{\phi_c}{v_b S(1-h)} \tag{2.36}$$

With Eqn 2.9 the dimensionless residence time of the solids in one section is obtained:

$$\Theta_c = \frac{\Lambda}{Dn} \tag{2.37}$$

The calculation proceeds as discussed in the previous section. The average concentration of liquid collected in chamber A_i is calculated from:

$$c_{A_i} = \left\{ \int_0^{\Theta_f} c_{out,\,i-1}\, d\Theta + \int_{\Theta_f}^{\Theta_c} c_{out,\,i}\, d\Theta \right\} / \Theta_c \tag{2.38}$$

Note that an extra column 0 is used in the calculation to account for mass transfer during drainage. Since only a part of this column contributes to the extractor volume, the number of true transfer units used in the simulation $N_{t,sim}$, is corrected: on inspecting Fig. 14 it is found that:

$$N_{t,c} = N_{t,sim} \cdot \frac{n\Theta_c + \Theta_f}{(n+1)\Theta_c} \tag{2.39}$$

2.3.3 Efficiency of belt type extractors without liquid recirculation

The results of the simulation of a belt extractor without recirculation of liquid and without dripping zones are presented in Fig. 15. It shows than an increase in the number of sections results in a smaller difference between N_{ext} and $N_{t,d}/\Lambda$, showing that the extractor approaches a purely countercurrent contactor. For a higher value of D, more liquid is entrained by the solids on the belt to the upstream sections. This backmixing flow $\phi_{c,\Delta}$ is related to the distribution ratio in the following way:

$$D = \frac{mhv_b S}{(1-h)v_b S} = \frac{\phi_{c,\Delta}}{\phi_c - \phi_{c,\Delta}} \Lambda \tag{2.40}$$

Solubles contained in the liquid flow $\phi_{c,\Delta}$ at the liquid feed end of the extractor will be lost with the spent solids. Compared with a diffusion battery discussed previously, the belt extractor gives a lower efficiency due to mixing of liquid in the collection pans after percolation through the bed. In Fig. 13 this mixing is illustrated in the analogue where the liquid leaving the column i (i.e. section of the belt) is mixed in the vessel A_i (i.e. the collection pan). When the extraction factor is high or the number of transfer units in each

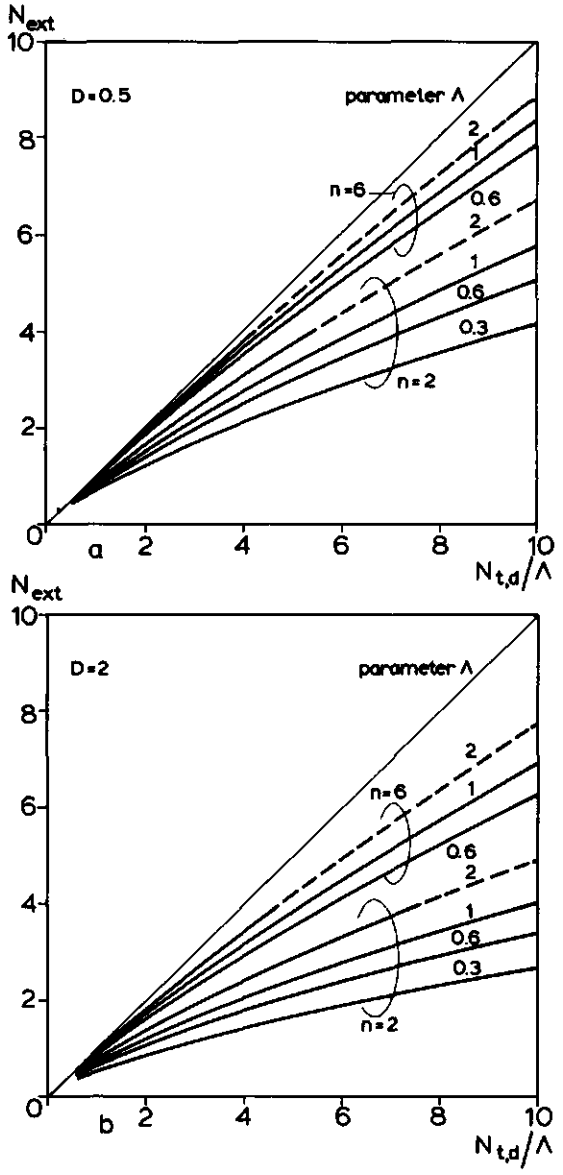

Fig. 15. Number of exterior apparent against true transfer units for a belt extractor with n sections without dripping zones. D is distribution ratio; Λ is extraction factor.

section is low, the concentration of liquid entering a collection pan does not vary significantly during a cycle. Then mixing hardly influences the extractor performance which thus approaches the performance of a diffusion battery.

For higher values of $N_{t,d}/n\Lambda$ the adverse effect of mixing becomes more important, as is clearly shown in Figs. 15 and 16. A correlation was fitted to the data so that the results can be easily applied. Within the indicated region the estimated value of $(N_{t,d} - \Lambda N_{ext})/N_{t,d}$ is within 5% of the numerically calculated value.

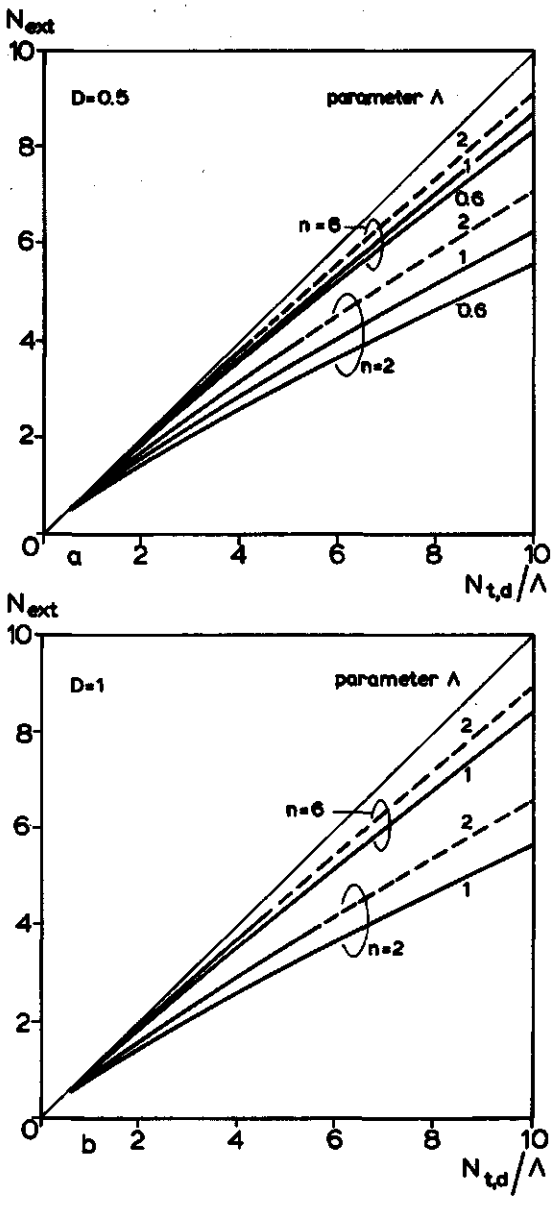

Fig. 16. Number of exterior apparent against true transfer units for a belt extractor with n sections with dripping zones. D is distribution ratio; Λ is extraction factor.

$$\frac{N_{t,d}/\Lambda}{N_{ext}} = 1 + 1.035\, n^{-1.42}\, \Lambda^{-0.71}\, D^{0.65}\, N_{ext}^{0.64} \qquad (2.41)$$

$2 \leq n \leq 7 \quad 0.3 < \Lambda < 2 \quad 0.25 < D < 2$
$0.3 < N_{ext} < 10 \quad \eta < 0.99$

If dripping zones are present, no liquid is entrained to the upstream section. The effect of the variable D/Λ is thus less pronounced than in the foregoing case. The value of $(N_{t,d}$ –

$\Lambda N_{ext})/N_{t,d}$ can be estimated with 5% accuracy from Fig. 16 or Eqn 2.42:

$$\frac{N_{t,d}/\Lambda}{N_{ext}} = 1 + 1.00\, n^{-1.44}\, \Lambda^{-0.63}\, D^{0.45}\, N_{ext}^{0.42} \tag{2.42}$$

$2 < n < 6 \quad 0.3 < \Lambda < 2 \quad 0.25 < D < 1.5$
$0.3 < N_{ext} < 10 \quad \eta < 0.99 \quad \Lambda/D > 1$

The above equation is valid only for $\Lambda/D > 1$. Since from Eqns 2.35 and 2.37:

$$\frac{\Theta_c}{\Theta_f} = \frac{\Lambda/Dn}{1/n} = \frac{\Lambda}{D} \tag{2.43}$$

the residence time in a section thus has to be longer than the time required to fill the interstitial voids of the packed section in one stage.

2.3.4 Efficiency of belt type extractors with liquid recirculation

Although the belt extractor with recirculation can be simulated analogously to the procedures we followed for the extractor without recirculation, it often suffices to apply an analytical approach for the simplified case of a completely mixed liquid phase in each section. Under what conditions this approximation is valid is discussed in Appendix B. We first note that the local mode of phase contact in each stage is immaterial because the liquid phase is completely mixed. The analytical expressions derived in this section can thus be used to estimate the efficiency of the other flow arrangements mentioned in Table 4 as well, as long as a uniform liquid phase composition in each section prevails.

Hartland & Mecklenburg (1966) derived an analytical solution for when the solids are completely separated from the interstitial liquid before they leave the extractor. In the present notation their relation reads:

$$c_i = \frac{\dfrac{h_1 - B_1^i}{(B_1 - 1)B_1^n} - \dfrac{h_2 - B_2^i}{(B_2 - 1)B_2^n}}{\dfrac{h_1(1-\Lambda B_1^n)}{(B_1 - 1)B_1^n} - \dfrac{h_2(1-\Lambda B_2^n)}{(B_2 - 1)B_2^n}} \tag{2.44}$$

where B_j is defined in Eqn 2.58 and h_j is given by:

$$h_j = 1 - \frac{D}{\Lambda}(B_j - 1) \tag{2.45}$$

In the present analysis the entrainment of liquid by the solids leaving the extractor is set equal to the interstage liquid entrainment. This assumption is believed to be physically more realistic and the results of this model can easily be compared with the correlations derived earlier. For the derivation of the equations describing the model we refer to Fig. 17.

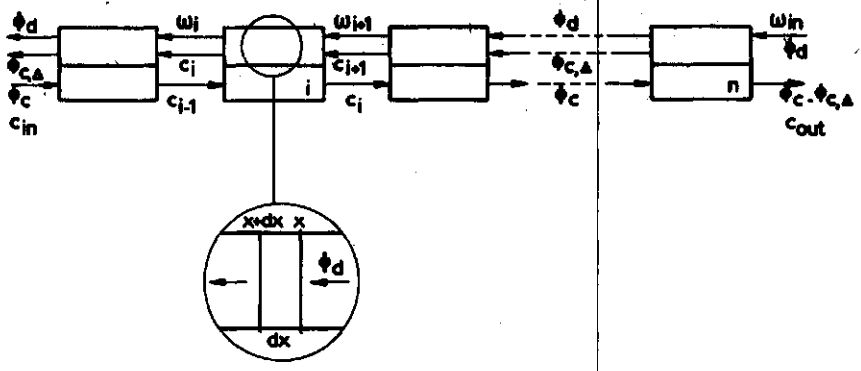

Fig. 17. Belt extractor with complete mixed liquid phase in each stage.

In this simplified model of the belt extractor, plug flow of the solids and complete mixing of the liquid within each stage is assumed. Then a mass balance on the solids in slice dx results in:

$$v_b S(1-h)\frac{d\omega_i'}{dx} = \phi_d \frac{d\omega_i'}{dx} = -k_{oc} aS(c_i'^* - c_i) \tag{2.46}$$

which can be written in a dimensionless form by introducing Eqns 2.6–2.10.

$$\frac{d\omega_i}{d\zeta} = -\frac{N_{t,d}}{n}(\omega_i - c_i) \tag{2.47}$$

The number of true transfer units on solid phase basis is defined as:

$$N_{t,d} = \frac{k_{oc} aV}{\phi_d/m} = \frac{k_{od} aV}{\phi_d} \tag{2.48}$$

Equation 2.47 can be integrated to give:

$$\frac{\omega_i - c_i}{\omega_{i+1} - c_i} = \exp(-N_{t,d}/n) \tag{2.49}$$

The mass balance on stage i, assuming complete entrainment of the interstitial liquid by the solids to the next section, gives:

$$\phi_d(\omega_{i+1}' - \omega_i') + \phi_{c,\Delta}(c_{i+1}' - c_i') + \phi_c(c_{i-1}' - c_i') = 0 \tag{2.50}$$

where the backflow $\phi_{c,\Delta}$ is defined as:

$$\phi_{c,\Delta} = v_b Sh \tag{2.51}$$

Equation 2.50 can be written in a dimensionless form using Eqn 2.9 and:

$$\Lambda = m\,(\phi_c - \phi_{c,\Delta})/\phi_d \tag{2.52}$$

Finally the following equation results:

$$(\omega_{i+1} - \omega_i) + D\,(c_{i+1} - 2c_i + c_{i-1}) + \Lambda\,(c_{i-1} - c_i) = 0 \tag{2.53}$$

For the last section the balance has to be modified since no liquid is carried by the solids entering this stage, so:

$$(\omega_{in} - \omega_n) + D\,(c_{n-1} - c_n) + \Lambda(c_{n-1} - c_n) = 0 \tag{2.54}$$

Combining Eqns 2.53 and 2.54 results in the following boundary condition at the solids inlet end of the extractor:

$$c_{n+1} = c_n \tag{2.55}$$

The solution of Eqns 2.49, 2.53 and 2.55 with the additional boundary conditions $c_{in} = 0$ and $\omega_{in} = 1$ yields:

$$c_i = \frac{(B_1^i - 1)/[B_1^n(B-1)] - (B_2^i - 1)/[B_2^n(B_2 - 1)]}{(B_1^{n+1} - g_1)/[g_1 B_1^n\,(B_1 - 1)] - (B_2^{n+1} - g_2)/[g_2 B_2^n(B_2 - 1)]} \tag{2.56}$$

where:

$$g_j = 1 - \alpha\,(B_j - 1) = 1 - (B_j - 1)/[\exp\,(N_{t,d}/n) - 1] \tag{2.57}$$

and B_j are the roots of the equation:

$$B_j^2 - \frac{1 + (\Lambda + D)\,\alpha + D(1 + \alpha)}{D\alpha}\,B_j + \frac{(1 + \alpha)\,(D + \Lambda)}{D\alpha} = 0 \tag{2.58}$$

The number of exterior apparent transfer units can be calculated from this using Eqn 1.7.

The results of the simplified model for a belt extractor with liquid recirculation in each section are shown in Fig. 18. The results are presented as graphs of $N_{ext}\Lambda/n$ plotted against $N_{t,d}/n$, the number of true transfer units in each section on overall solid phase basis in pure countercurrent flow and in the extractor under consideration, respectively. For some limiting cases of the model discussed here, a simplified solution can be given:

– No liquid entrainment to the upstream sections. Since a constant liquid concentration in each stage was assumed, the distribution ratio D will only affect liquid entrainment as shown in Eqn 2.40. This case can thus be solved by taking $D = 0$ in the foregoing equations. The resulting equation is:

$$\frac{\Lambda N_{ext}}{n} = \frac{\Lambda}{1-\Lambda}\,\ln\left[\frac{1}{\Lambda}\left\{1 - e^{-N_{t,d}/n\,(1-\Lambda)}\right\}\right] \tag{2.59}$$

This equation is shown in Fig. 18c. Equation 2.59 can also be derived from the solution

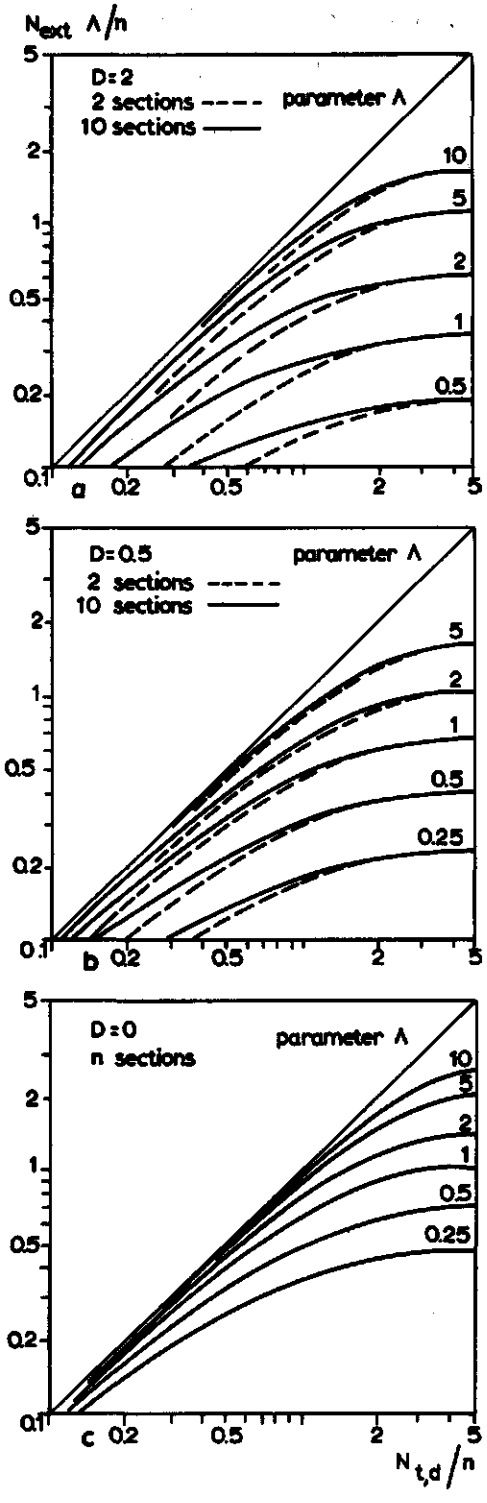

Fig. 18. Number of exterior apparent against true transfer units for a belt extractor with complete mixed liquid phase in each section. n is the number of sections; D is distribution ratio; Λ is extraction factor.

of the cascade of mixers model proposed by Kerkhof & Thijssen (1974), by taking the limit for n_y going to infinity in their equation (13a), since the solids move in plug flow.
– For a large number of true transfer units each section can be considered as an equilibrium stage. Then the resulting equation for N_{ext} is:

$$\frac{\Lambda N_{ext}}{n} = \frac{\Lambda}{1-\Lambda} \ln\left(\frac{D+1}{D+\Lambda}\right) \tag{2.60}$$

From the reasoning given above under case 1, it can be concluded that the results of this model can be used to estimate the number of true transfer units when dripping sections are present. Here the parameter D as defined in Eqn 2.9 has to be replaced by

$$D = \Lambda \frac{\nu_b S\epsilon}{\phi_c - \nu_b S\epsilon} = \frac{m\,\epsilon}{1-\epsilon} \tag{2.70}$$

where ϵ is the residual liquid hold-up after partial drainage. One should bear in mind that the extractor volume calculated from $N_{t,d}$ when dripping sections are present does not include the volume of the dripping sections itself.

3 Estimation of mass transfer coefficients in solid-liquid extractors

3.1 Introduction

In this work the NTU approach has been adopted for the design of solid liquid extractors. In the preceding chapter it has been shown how the number of true transfer units required to meet the design specifications can be determined. The present chapter deals with the estimation of mass transfer coefficients. By combining these results, the required residence time of the solids in the extractor under given process conditions can be calculated from:

$$\tau_d = V(1-h)/\phi_d = N_{t,d}/(k_{od}a') \tag{3.1}$$

where k_{od} is the mass transfer coefficient on overall dispersed phase basis. Obviously, the use of mass transfer coefficients to describe transfer rates is most convenient when k_o is independent of time, position, concentration and driving force for mass transfer. These conditions are only fulfilled approximately in solid-liquid extractors. The two film theory of Lewis states that k_o is dependent on the mass transfer coefficient in the continuous phase k_c, and in the dispersed phase k_d. This relation has been derived from the expressions for the flux through a solid-liquid interface (see Fig. 19):

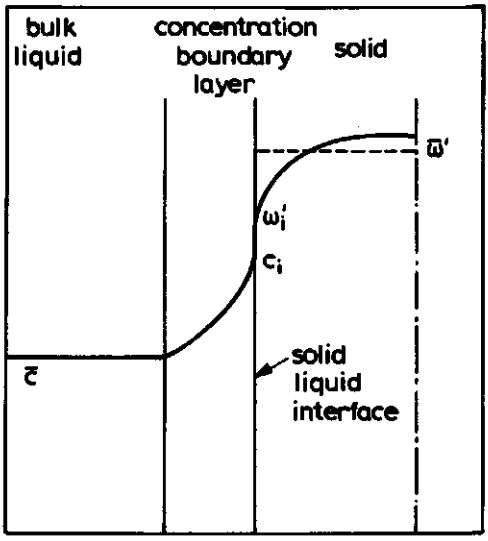

Fig. 19. Concentration profiles near a solid liquid interface.

$$\phi''_m = k_{oc}(\overline{c}'^* - \overline{c}') = k_{od}(\overline{\omega}' - \overline{\omega}'^*)$$
$$= k_c(c'_i - \overline{c}') = k_d(\overline{\omega}' - \omega'_i) \tag{3.2}$$

For a linear equilibrium relation $c'^* = m\,\omega'$, we obtain the well-known equation:

$$\frac{1}{k_{od}} = \frac{1}{mk_{oc}} = \frac{1}{k_d} + \frac{1}{mk_c} \tag{3.3}$$

which can be written in a dimensionless form as:

$$\frac{1}{Sh_{od}} = \frac{1}{Sh_d} + \frac{1}{2Bi} \tag{3.4}$$

where $Sh = k\,D_p/\mathcal{D}$, k and $\mathcal{D}$ refer to the same phase; $Bi = m(D_p/2)k_o/\mathcal{D}_d$. As will be recalled in Section 3.2, Sh_c is dependent on the physical properties and the flow velocity of the liquid surrounding the particle. Due to the mass transfer process these physical properties change with time, while in gravity percolation extractors the flow velocity might change accordingly. Moreover, even if the physical properties are uniform and the velocity is constant, k_c varies over the surface of the particle (Gillespie et al., 1968; Frössling, 1938). Fortunately, however, the Bi number which embodies the ratio of the mass transfer resistances inside and outside the particle is often rather high in solid-liquid extraction processes so that variations of k_c have a small effect on the overall mass transfer coefficient. Even for moderate Bi numbers the use of a value of k_c averaged over the particle surface and the time that the solids reside in the extractor will only slightly affect the accuracy of the design calculation. The dispersed phase Sherwood number Sh_d is time dependent due to the transient nature of the diffusion proces. The initial decrease of Sh is described by the penetration theory (Higbie, 1935). In a later stage of the extraction, the Sh_d against time curve levels off and approaches a finite asymptotic value when entering the so-called 'regular regime' (Kondratiev, 1964), Fig. 20. The value of Sh_d in this regular regime depends on the boundary conditions or concentration history at the surface of the particle, and on the geometry of the particle; but it is independent of the initial concentration distribution inside the particle. It can be expected that for high extraction efficiencies a considerable part of the process can be described with this asymptotic mass transfer coefficient.

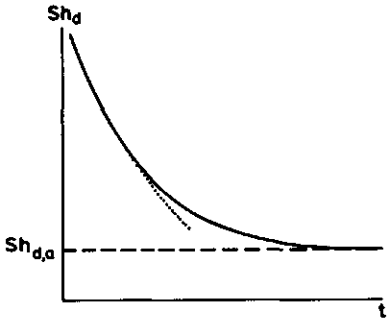

Fig. 20. Transient Sh_d numbers for unsteady diffusional mass transfer. (...) penetration period; (———) regular regime.

In Sections 3.2 and 3.3, literature data on mass transfer coefficients in continuous and dispersed phases are reviewed. This information is thereafter extended to provide a complete picture of asymptotic Sh_d values in cocurrent and countercurrent extractors for particles with simple geometry. In Section 3.3.4, the range of applicability of asymptotic Sh numbers in mass transfer calculations is discussed. Moreover it is shown in this section how one could proceed in more complicated cases that are not covered by the previous sections.

3.2 Estimating mass transfer coefficients in the continuous phase

Mass transfer coefficients in the continuous phase are commonly expressed by the dimensionless Sh_c number, defined as:

$$Sh_c = \frac{k_c D_p}{\mathcal{D}_c} \tag{3.5}$$

D_p denotes a characteristic dimension of a particle or a system that contains n particles, normally the equivalent diameter $\sqrt{A_d/n\pi}$ where A_d is the surface area of the particles. The external Sh_c number is determined by the concentration distribution in the continuous phase. The equality (Fig. 19):

$$-\mathcal{D}_c \frac{\partial c}{\partial r}\Big|_R = k_c (c_R - \bar{c}) \tag{3.6}$$

yields the following relation for Sh_c:

$$Sh_c = D_p \frac{-\partial c/\partial r|_R}{c_R - \bar{c}} \tag{3.7}$$

For a stagnant fluidum surrounding a single spherical particle the asymptotic Sh_c value is easily obtained from the solution of the diffusion equation:

$$\frac{\partial c}{\partial t} = \frac{1}{r^2}\frac{\partial}{\partial r}\left(\mathcal{D}_c r^2 \frac{\partial c}{\partial r}\right) \tag{3.8}$$

with boundary conditions:

$$r = R \qquad c = c_R \tag{3.9}$$

$$r = R_o \qquad c = c_{R_o} \tag{3.10}$$

The steady state solution for transfer from a particle submerged in a stagnant, infinitely extending fluidum is well known; when $\partial c/\partial t = 0$ and $R_o \to \infty$:

$$Sh_c = D_p \frac{-\partial c/\partial r|_R}{c_R - c_\infty} = 2 \tag{3.11}$$

Table 5. Effect of distance between two spherical particles with diameter D_p on Sh_c in an infinite stagnant medium. Data from Cornish 1965.

Distance between centers of spheres	Sh_c
D_p	1.39
$2D_p$	1.60
$50D_p$	1.98
∞	2.00

When two particles are placed in an infinite stagnant medium, the external mass transfer coefficient decreases with decreasing distance between the particles, see Table 5. For multiparticle systems in a stagnant liquid Miyauchi (1971) calculated the value of Sh_c from the concentric sphere model. In this model the particle is supposed to be surrounded by a liquid shell; the dimensions of this shell are adjusted to match the void fraction of the packing. Miyauchi assumed a concentric shell ranging from $r = R$ to $r = R_0$ around a spherical particle. When the liquid concentration at the particle surface is set equal to c_R and the concentration at the outer boundary of the liquid shell equal to c_{R_0}, the result for Sh_c in the steady state is:

$$Sh_c = D_p \frac{-\partial c/\partial r\,|_R}{c_R - c_{R_0}} = \frac{2}{1-(R/R_0)} \tag{3.12}$$

Suzuki (1975) solved Eqn 3.8 with a more realistic boundary condition at $r = R_0$:

$$r = R_0 \qquad (\partial c/\partial r) = 0 \tag{3.13}$$

thus avoiding the artificial sink term at $r = R_0$. The transient solution is used to calculate the Sh_c value, defined in Eqn 3.7, where

$$\bar{c} = 3 \int_R^{R_0} c r^2\, dr/(R_0^3 - R^3) \tag{3.14}$$

This time-dependent Sh_c number approaches an asymptotic value for long contact times t. This asymptotic solution is shown in Fig. 21, where also some measured values reported in literature are included.

For small Re-numbers, correlations for the external Sh_c number for single particles have been derived from Stokes' stream function for creeping flow around particles. For a thick concentration boundary layer or small $Re\,Sc$ numbers, the resulting equations are often presented as summation series of the form:

$$Sh_c = 2 + \tfrac{1}{2}(ReSc) + \tfrac{1}{6}(ReSc)^2 + \ldots \tag{3.15}$$

For thin boundary layers, the relation obtained after summing up the result of the above

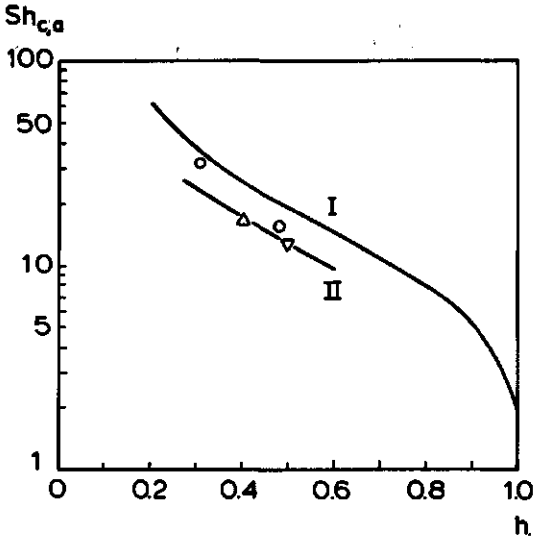

Fig. 21. Asymptotic values of Sh_c for spherical particles in a stagnant finite fluidum as a function of the void fraction h. Key: ○ Miyauchi et al., 1976b; △ Miyauchi et al., 1975; ▽ Miyauchi et al., 1976a; I Suzuki, 1975; II Miyauchi, 1971.

analysis and the limiting value 2 for a quiescent fluid reads:

$$Sh_c = 2 + b\,(ReSc)^{1/3} \tag{3.16}$$

where b ranges from 0.5 to 1 according to Sideman & Shabtai (1964). The fundamental problems associated with the interpretation of measured mass transfer rates at very low Re numbers in multiparticle systems are discussed by Gangwal (1977). This data analysis is complicated by several mechanisms that might override the effect of mass transfer rate on the measurements, e.g. dispersion effects (Wakao, 1976), channelling caused by variation in the void fraction (Martin, 1978) and free convection (Mandelbaum & Bohm, 1973). Also the often assumed symmetry of the concentration or temperature profiles inside the particles is not valid in the low Re-number regime, (Wakao, 1976). In order to provide a theoretical basis for mass transfer correlations in these systems, Pfeffer & Happel (1964) solved the spherical shell model assuming creeping flow around the particle. Their results agree reasonably well with the measured data. Nelson & Galloway (1975) combined the solution obtained by Suzuki (1975) with Danckwerts' surface renewal theory. Thus, an analytical expression was obtained for Sh_c. After scaling their solution with the Ranz Marshall correlation which applies for single spheres, they derived a correlation that has been used to predict mass transfer coefficients in the low Re-number regime. Measurements of mass transfer rates in this regime were re-evaluated by Dwivedi & Upadhyay (1977), and by Wakao & Funazkri (1978). For Re numbers below 10, the first authors proposed the following empirical correlation between the Colburn j-factor and the Reynolds number for the liquid flow, $Re = \rho \langle v \rangle D_p/\mu(1-h)$:

$$hj_m = \frac{h\,Sh_c}{Re\,(Sc)^{1/3}} = 1.1068\,Re^{-0.72} \qquad (Re > 10) \tag{3.17}$$

For higher values of Re an overwhelming amount of literature data are available. Based on Schlichtings boundary layer theory, correlations for single particles usually take the form:

$$Sh_c = 2 + b\,Re^{1/2}\,Sc^{1/3} \qquad (Re > 1) \qquad (3.18)$$

From the survey of Sideman & Shabtai (1964) it is found that the value of b is usually in the range $0.5 < b < 0.9$. Correlations for external mass transfer coefficients in multi-particle systems are reviewed (e.g. Barker (1975), Sideman (1966), Upadhyay & Tripathi (1975), Dwivedi & Upadhyay (1977) and Kumar et al. (1977)). Based on a critical examination of previous data, Dwivedi and Upadhyay proposed the following empirical correlation for higher Re numbers:

$$hj_m = 0.4548\,Re^{-0.4069} \qquad (Re > 10) \qquad (3.19)$$

These authors also suggested a generalized equation that correlates data over a wide Re number range:

$$hj_m = \frac{0.765}{Re^{0.82}} + \frac{0.365}{Re^{0.386}} \qquad (10^{-2} < Re < 15\,10^3) \qquad (3.20)$$

This relation is shown in Fig. 22 together with some literature data.

Even though no attempt has been made to be complete, the above survey clearly shows that methods for estimating the external mass transfer coefficient for widely varying conditions is extensively dealt with in literature. Moreover, as was pointed out in Section 2.1, the Biot number $Bi = m\,k_0 R/\mathcal{D}_d$ for solid-liquid extraction is often very

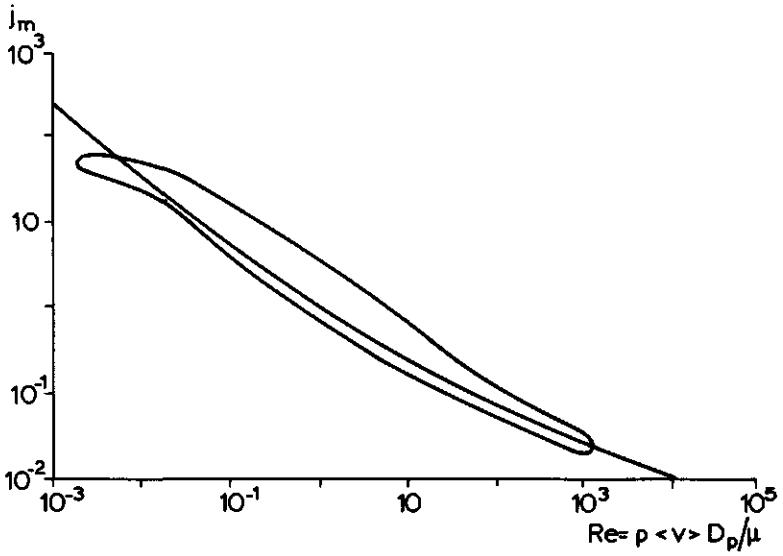

Fig. 22. Mass transfer factor in fixed beds. Solid line: Eqn 3.20; Cloud: experimental data. From Dwivedi & Upadhyay, 1977.

large. Thus a rough guess of k will prove to be sufficient in most engineering calculations. If k_c varies over the length of the extractor due to changes in viscosity or flow velocity, it is recommendable to use a constant, averaged value of k_c in the design calculation.

3.3 Estimating mass transfer coefficients in the dispersed phase

Mass transfer inside rigid particles is generally described by Ficks second law:

$$\frac{\partial \omega}{\partial t} = \frac{1}{r^{\nu-1}} \frac{\partial}{\partial r}\left(I\!D_d\, r^{\nu-1} \frac{\partial \omega}{\partial r}\right) \tag{3.21}$$

where ν, the geometrical shape factor, is 1,2 and 3 for a flat plate, cylinder and sphere, respectively. In analogy to the Sh_c number, the mass transfer coefficient in the dispersed, solid phase is embodied in the Sh_d number, which can be calculated from the concentration distribution inside the particles. An overall mass balance yields:

$$k_d A_d (\bar{\omega} - \omega_i) = - I\!D_d A_d \left.\frac{\partial \omega}{\partial r}\right|_R = - V_d \frac{d\bar{\omega}}{dt} \tag{3.22}$$

By substitution of $t_d = I\!D_d t/R^2$, $\xi = r/R$, and $\nu/2 = A_d/V_d$, the above relation can be rearranged to:

$$\frac{\nu}{2} Sh_d = \frac{-\left.(\partial\omega/\partial\xi)\right|_{\xi=1}}{\left.\bar{\omega} - \omega\right|_{\xi=1}} = \frac{-\left.d\bar{\omega}/dt_d\right|}{\left.\bar{\omega} - \omega\right|_{\xi=1}} \tag{3.23}$$

Since the concentration profile inside the particle, $\omega\,(\xi, t_d)$, is determined by the geometry of the particle and the boundary conditions imposed on Eqn 3.21, we expect Sh_d to be a function of the following parameters:

$$Sh_d = f\,(\nu, t_d, \text{initial and boundary conditions}) \tag{3.24}$$

For long contact times between the phases, the Sh_d number will approach an asymptotic value $Sh_{d,a}$, as pointed out in the introduction. This asymptotic value is essentially independent of the initial concentration profile, thus:

$$Sh_{d,a} = f\,(\nu, \text{boundary conditions}) \tag{3.25}$$

Mathematically this stems from the fact that the solution of the diffusion equation, which can be written as a summation of terms containing a weighting function $\exp(-\lambda_n t_d)$ multiplied by the related eigenfunction $f(\lambda_n)$, is governed by the term containing the smallest eigenvalue λ_1. The contribution of higher terms is negligible because of the nature of the weighting function for higher values of t_d. Many authors proposed this 'first-term approximation' for heat and mass transfer calculations (Pflug & Blaisdell, 1963; Brüniche Olsen, 1962; and others). It can be shown that the extraction rate in this regular regime can be described with a constant mass transfer coefficient, k_d.

3.3.1 *Survey of literature data*

For a constant surface concentration, $Sh_{d,a}$ values are given by Beek & Muttzall (1975). For a constant bulk liquid concentration with finite *Bi* values, these data are reported by Thijssen (1969). The solutions for constant surface concentration were extended to concentration-dependent diffusivities and shrinking systems by Schoeber (1976) (Fig. 23). The results of the analysis mentioned so far are summarized in Table 6. For cocurrent and countercurrent extraction of heating/cooling of spherical particles, several authors derived the asymptotic transfer coefficients when he phases are contacted in pure plug flow. Assuming a geometrical similar profile in the regular regime:

$$\frac{\omega - c}{\bar{\omega} - c} = f(\xi) \tag{3.26}$$

where $f(\xi)$ is a function of $\xi = r/R$ only, Gardner (1966) obtained analytical expressions for $Sh_{d,a}$ by substituting the regular concentration profile Eqn 3.26 in the diffusion equation 3.21 and combining the resulting relation with an overall mass balance:

$$(\omega_o - \omega) = -(c_{out} - c)\,\Lambda_t \tag{3.27}$$

where Λ_t is $+\Lambda$ and $-\Lambda$ for countercurrent and cocurrent phase contact, respectively. The same results were obtained by Wartman & Mertes (1966) from the transient solution of the diffusion equation with the appropriate boundary conditions. Vorstman & Thijssen (1971) calculated asymptotic $Sh_{d,a}$ values for countercurrent extraction of spherical particles by using a different mathematical approach. In solving the diffusion equation 3.21, the following general boundary condition was applied at $r = R$:

$$\frac{\partial \omega}{\partial \xi} = Bi\,\{\omega - \omega^*(t_d)\} \qquad \xi = 1 \tag{3.28}$$

The bulk liquid concentration, $m\,\omega^*(t_d)$, was then obtained from the solution of the

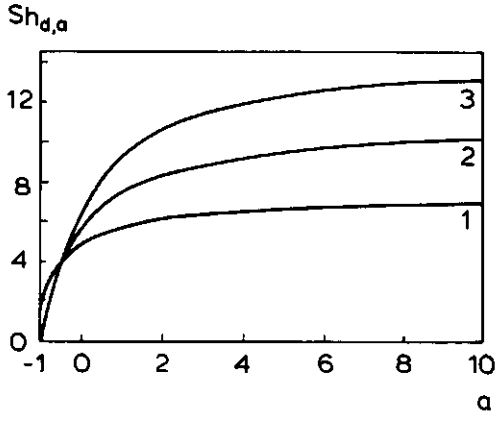

Fig. 23. Asymptotic $Sh_{d,a}$ values for concentration dependent diffusivity $\mathcal{D}_d = \omega^a$ and constant surface concentration ($Bi, \Lambda \to \infty$). Parameter is geometrical shape factor ν. From Schoeber, 1976.

Table 6. Review of Sh_{od} values for constant bulk concentration of the liquid phase in the regular regime.

Diffusion coefficient	Boundary condition	Geometry			Source
		Sphere	Cylinder	Slab	
constant	constant surface conc., $Bi = \infty$	$\frac{2\pi^2}{3}$	5.96	$\pi^2/2$	e.g. Beek & Muttzall, 1975
	finite Bi	$2\lambda_1^2/3$ $\lambda_1 =$ $(1 - Bi) \tan \lambda_1$	λ_1^2 $\lambda_1 J_1(\lambda_1) =$ $Bi\, J_0(\lambda_1)$	$2\lambda_1^2$ $\lambda_1 = Bi/\tan \lambda_1$	Thijssen, 1969
concentration dependent, $\mathcal{D} = \omega^a$	$Bi = \infty$	Fig. 23	Fig. 23	Fig. 23	Schoeber, 1976
$\mathcal{D} = \omega^a$, $a \to \infty$	$Bi = \infty$	exp(8/3)	4e	exp(2)	Schoeber, 1976

lumped parameter model, i.e. the Colburn equation. Their results coincide with those obtained by the methods discussed earlier.

In the subsequent sections $Sh_{d,a}$ values are calculated for both cocurrent and countercurrent extraction of particles which can be approximated by slabs, cylinders or spheres. Some general procedures for generating these asymptotic mass transfer coefficients are discussed.

3.3.2 *$Sh_{d,a}$ values from solutions under coupled boundary conditions*

During the extraction of rigid particles, the transient concentration distribution can be obtained from the solution of the diffusion equation, which can be written in a dimensionless form as:

$$\frac{\partial \omega}{\partial t_d} = \frac{1}{\xi^{\nu-1}} \left\{ \frac{\partial}{\partial \xi} \; \xi^{\nu-1} \; \frac{\partial \omega}{\partial \xi} \right\} \tag{3.29}$$

In general, the following initial and boundary conditions apply:

$$t_d = 0 \qquad \omega(\xi, 0) = f(\xi) \qquad 0 < \xi < 1 \tag{3.30}$$

$$\xi = 0 \qquad \partial\omega/\partial\xi = 0 \qquad t_d > 0 \tag{3.31}$$

$$\xi = 1 \qquad \partial\omega/\partial\xi = -Bi\,\{\omega - c(t_d)/m\} \qquad t_d > 0 \tag{3.32}$$

The concentration in the continuous phase, $c(t_d)$, can be calculated from a mass balance. For cocurrent and countercurrent extraction this results in the following relations:

$$\left.\begin{aligned} \frac{dc}{dt_d} &= -\frac{1}{\Lambda}\frac{d\bar{\omega}}{dt_d} \\ t_d = 0 \quad c &= c_{in} \end{aligned}\right\} \text{ cocurrent or batch} \tag{3.33}$$

$$\left.\begin{aligned} \frac{dc}{dt_d} &= +\frac{1}{\Lambda}\frac{d\bar{\omega}}{dt_d} \\ t_d = 0 \quad c &= c_{out} \end{aligned}\right\} \text{ countercurrent} \tag{3.34}$$

We will indicate this system of equations by the term 'coupled boundary conditions', i.e. coupling of $c(t_d)$ from the boundary condition Eqn 3.32 with a mass balance relation 3.33 or 3.34. Analytical solutions of the above equations are summarized in Table 7, with special reference to cocurrent and countercurrent phase contact. Only those solutions not dealt with extensively in the handbooks (Luikov, 1968; Crank, 1956; Carslaw & Jaeger, 1959) are included in the table. From these solutions the $Sh_{d,a}$ values can be derived

Tabel 7. Analytical solutions of the diffusion equation with coupled and general boundary conditions.

Geometry factor	*Bi*	f(ξ)	Remarks	Source
cocurrent				
1, 2, 3	∞	ω_0	tables, graphs	Tettamanti et al., 1975
1	∞	f(ξ)		Plachco & Krasuk, 1972
3	∞	f(ξ)		Plachco & Lago, 1972
1, 2, 3	finite	ω_0	tables, graphs	Mikhailov, 1966
2	finite	ω_0		Edeskuty & Amundson, 1952
3	finite	ω_0		Farritor & Tao, 1972
all	finite	f(ξ)	arbitrary geometry	Mikhailov, 1977
countercurrent				
1, 2, 3	∞	ω_0	tables, graphs	Tettamanti et al., 1975
1	∞	f(ξ)	graphs	Plachco & Krasuk, 1970
1	finite	ω_0		Jeschar, 1966
3	finite	ω_0	mass generation included	Munro & Amundson, 1950
			sorption included	Kasten & Amundson, 1952 Barbouteau, 1956 Wartman & Mertes, 1966
			axial dispersion included	Neretnieks, 1974
general				
3	finite	ω_0	$c = c(t)$	Vorstman & Thijssen, 1971
all	finite	f(ξ)	$c = c(t)$	Olçer, 1964
1, 2, 3	finite	f(ξ)	$c = c(t)$	Mikhailov, 1973

from Eqn 3.23.

The solution of the transient diffusion equation can be written in a generalized form:

$$W(t_d) = \frac{\omega' - \omega'(t_d=0)}{(c'/m - \omega')_{t_d=0}} = A_0 + g(\mu)e^{\mu^2 t_d} + \sum_{j=1}^{\infty} f(\lambda_j)e^{-\lambda_j^2 t_d} \tag{3.35}$$

where $f(\lambda_j)$, j=0, ∞ and $g(\mu)$ are functions that depend on the boundary and initial conditions and λ_j and μ are the nonzero roots of the characteristic equation, if those roots exist. $W(t_d)$ is defined in Table 8 for cocurrent and countercurrent flow. The value of A_0 is also given, which can be verified easily for cocurrent extraction, and for countercurrent extraction with an extraction factor $\Lambda > 1$ by taking the limit for $t_d \to \infty$ in Eqn 3.35 since no root μ exists in these cases. Combining Eqn 3.35 with the mass balance on both phases, the value of $C(t_d)$ defined in Table 8 is obtained. The definition of the *Sh* number given in Eqn 3.23 can now be written as:

$$Sh_{od}(t_d) = \frac{\mu^2 g(\mu)e^{\mu^2 t_d} - \sum_{j=1}^{\infty} \lambda_j^2 f(\lambda_j)e^{-\lambda_j^2 t_d}}{(1-\Lambda_t^{-1})\{g(\mu)e^{\mu^2 t_d} + \sum_{j=1}^{\infty} f(\lambda_j)e^{-\lambda_j^2 t_d}\}} \tag{3.36}$$

where $\Lambda_t = \Lambda$ or $-\Lambda$ for countercurrent and cocurrent phase contact respectively. For longer contact times between the phases, the solution will be determined by the smallest

Table 8. Asymptotic *Sh*-numbers and some related properties of the differential equations involved. $\gamma = \Lambda_t/\nu$; J_k is the Bessel function of the first kind and k-th order; I_k is the modified Bessel function of the first kind and k-th order; λ is the first non-zero root of the related trancedental equation.

phase contact	W	C	A_0	$Sh_{od,a}$	ν	λ or μ
cocurrent	$\frac{\omega-\omega_0}{c_0-\omega_0}$	$\frac{c-\omega_0}{c_0-\omega_0}$	$\frac{\Lambda}{\Lambda+1}$	$\frac{2A_0}{\nu}\lambda^2$	1	$\tan\lambda = \frac{\gamma Bi\,\lambda}{Bi+\gamma\lambda^2}$
countercurrent $\Lambda > 1$	$\frac{\omega-\omega_0}{c_{out}-\omega_0}$	$\frac{c-\omega_0}{c_{out}-\omega_0}$	$\frac{\Lambda}{\Lambda-1}$	$\frac{2A_0}{\nu}\lambda^2$	2	$\frac{J_1(\lambda)}{J_0(\lambda)} = \frac{\gamma Bi\lambda}{Bi+\gamma\lambda^2}$
					3	$\tan\lambda = \frac{\lambda(Bi+\gamma\lambda^2)}{Bi+\gamma(1-Bi)\lambda^2}$
countercurrent $\Lambda < 1$	$\frac{\omega-\omega_0}{c_{out}-\omega_0}$	$\frac{c-\omega_0}{c_{out}-\omega_0}$	$\frac{\Lambda}{1-\Lambda}$	$\frac{2A_0}{\nu}\mu^2$	1	$\tanh\mu = \frac{\gamma Bi\,\mu}{Bi+\gamma\mu^2}$
					2	$\frac{I_1(\mu)}{I_0(\mu)} = \frac{\gamma Bi\,\mu}{Bi+\gamma\mu^2}$
					3	$\tanh\mu = \frac{\mu(Bi+\gamma\mu^2)}{Bi+\gamma(1-Bi)\mu^2}$

eigenvalue λ_1, or by the eigenvalue μ if the latter exists. Thus the calculation of the asymptotic *Sh* numbers can be reduced to an analysis of these smallest eigenvalues. In the subsequent treatment, we will use Laplace transform techniques to determine the characteristic equations that generate the eigenvalues.

The solution of Eqn 3.29 with initial and boundary conditions 3.30 and 3.31 in the Laplace domain is given by:

$$\widetilde{W} = \int_0^\infty e^{-st_d} W(\xi, t_d)\, dt_d$$

$$= A_3 \sinh(\xi\sqrt{s})/\sqrt{s} \qquad \text{when } \nu = 3 \tag{3.37}$$

$$= A_2 I_o(\xi\sqrt{s}) \qquad \text{when } \nu = 2 \tag{3.38}$$

$$= A_1 \sinh(\xi\sqrt{s}) \qquad \text{when } \nu = 1$$

The value of the constant A_ν can be obtained from boundary condition 3.32 and the overall mass balance equation 3.33 or 3.34. Thus, the characteristic equation is obtained by setting the denominator of the resulting expression for $\widetilde{W}$ equal to zero and solving for *s*. These equations are given below:

$$\tanh(\sqrt{s}) = \frac{(Bi - \gamma s)\sqrt{s}}{Bi - \gamma s(1 - Bi)} \qquad \text{when } \nu = 3 \tag{3.40}$$

$$\frac{I_1(\sqrt{s})}{I_0(\sqrt{s})} \quad \frac{\gamma Bi\sqrt{s}}{Bi - \gamma s} \qquad \text{when } \nu = 2 \tag{3.41}$$

$$\tanh(\sqrt{s}) = \frac{\gamma Bi\sqrt{s}}{Bi - \gamma s} \qquad \text{when } \nu = 1 \tag{3.42}$$

where $\gamma = \Lambda_t/\nu$. It can be shown that the above equations have a non-zero real root μ only in case $\Lambda < 1$ in the countercurrent situation. This single root determines the asymptotic solution for $W(t_d)$. In other cases, an infinite number of roots is obtained by substituting $\lambda = i\sqrt{s}$. The smallest non-zero root determines the asymptotic solution in this case. The resulting characteristic equations are included in Table 8. The $Sh_{od,a}$ values obtained from the equations in this table, together with the $Sh_{d,a}$ values calculated from Eqn 3.4 are shown in Fig. 24-29. Both for cocurrent and countercurrent extraction the solution approaches the constant bulk concentration limit when the extraction factor Λ goes to infinity. These solutions were already summarized in Table 5. The asymptotic mass transfer coefficient increases from slab to cylindrical to spherical geometry of the particles subjected to extraction. In fact, this is a consequence of the definition of the *Sh* number given in Eqn 3.23. Due to the higher value of $\nu = 2\,A_d/V_d$, a certain flux $-\mathcal{D}_d(\partial\omega'/\partial r)_R$ causes a more pronounced concentration reduction in terms of average solute concentration for spherical particles. Decreasing the external mass transfer coefficient or *Bi* number shifts the $Sh_{d,a}$ value towards the value obtained for $\Lambda = 1$. For countercurrent extraction, an increase in Λ causes a reduction in the asymptotic mass

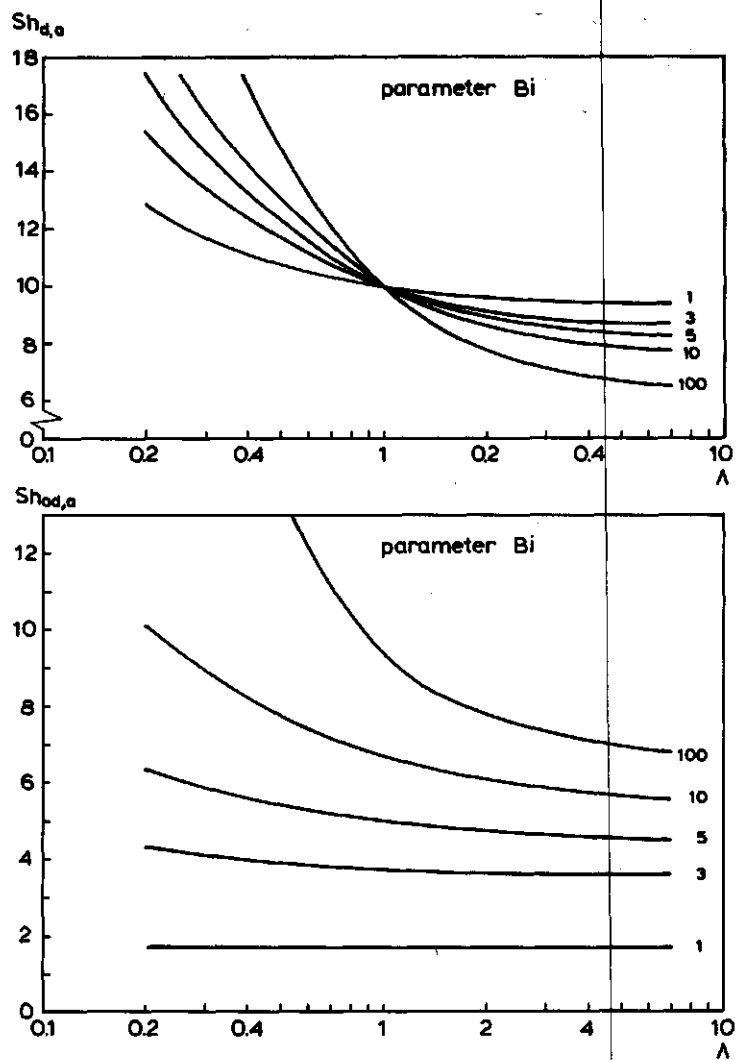

Fig. 24. Asymptotic Sh_d and Sh_{od} values for countercurrent extraction of spherical particles. $Bi = mk_cR/\mathbb{D}_d$ is the Biot number.

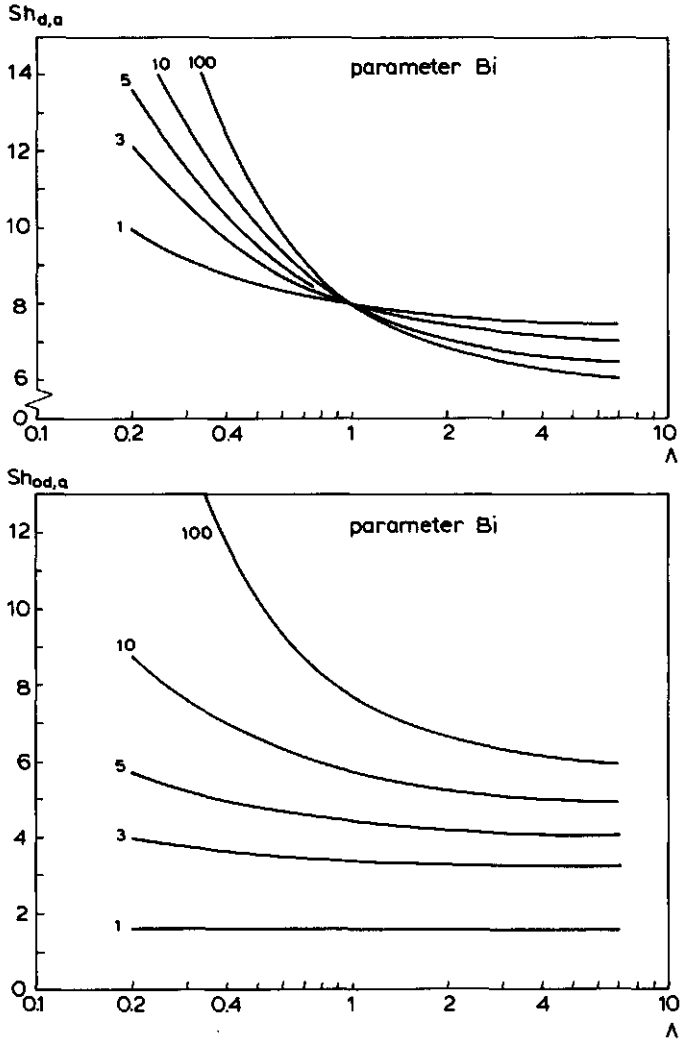

Fig. 25. Asymptotic Sh_d and Sh_{od} values for countercurrent extraction of cylindrical particles. $Bi = mk_cR/\mathbb{D}_d$ is the Biot number.

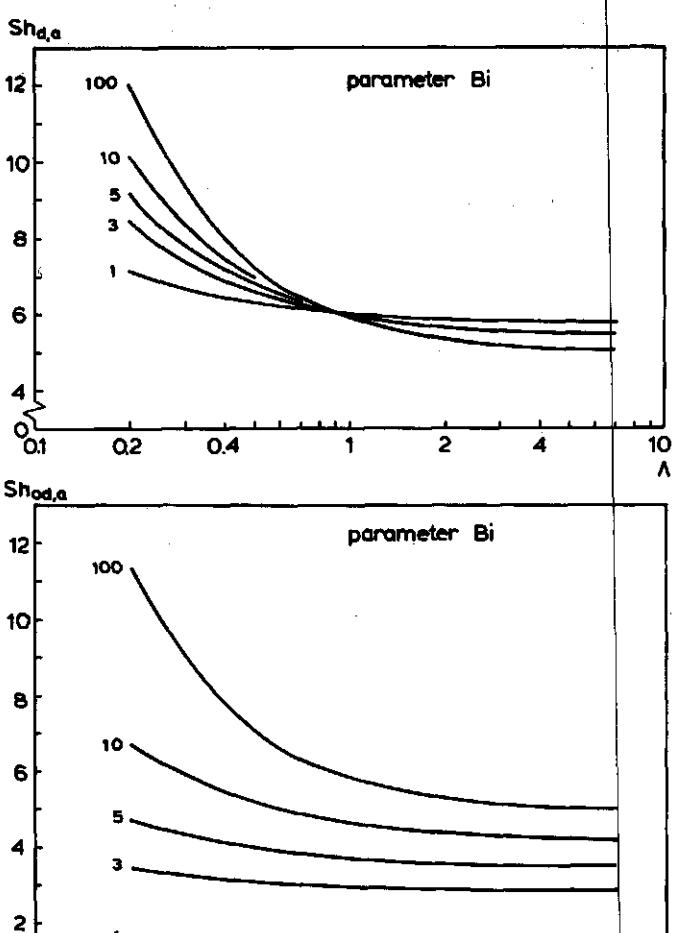

Fig. 26. Asymptotic Sh_d and Sh_{od} values for countercurrent extraction of particles with slab geometry. $Bi = mk_cR/\mathbb{D}_d$ is the Biot number.

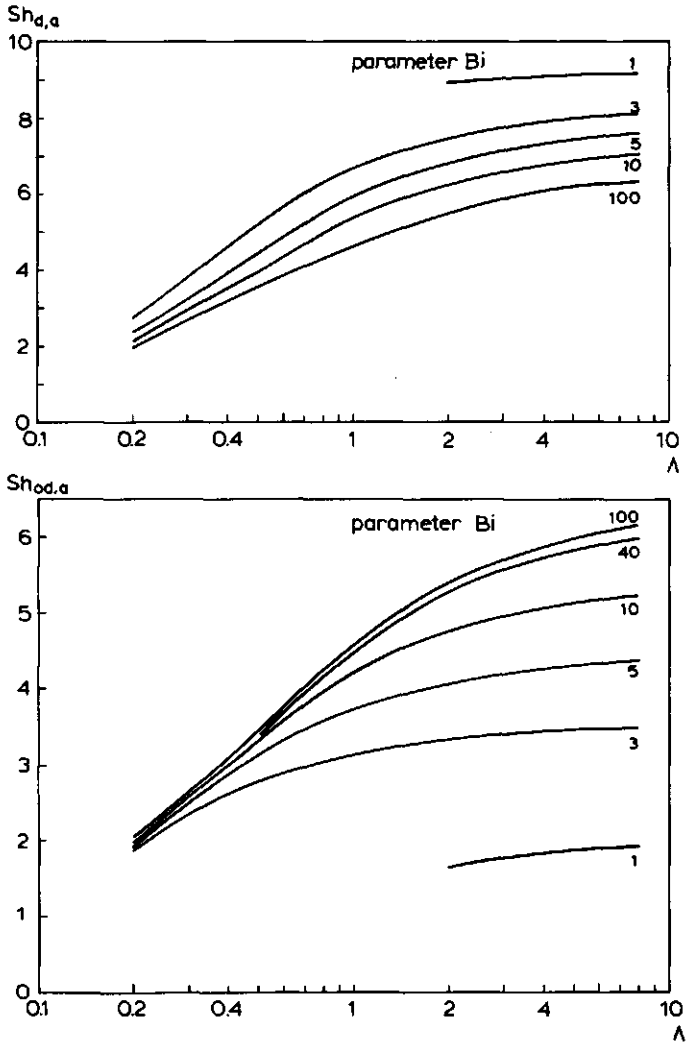

Fig. 27. Asymptotic Sh_d and Sh_{od} values for cocurrent extraction of spherical particles. $Bi = mk_cR/\mathbb{D}_d$ is the Biot number.

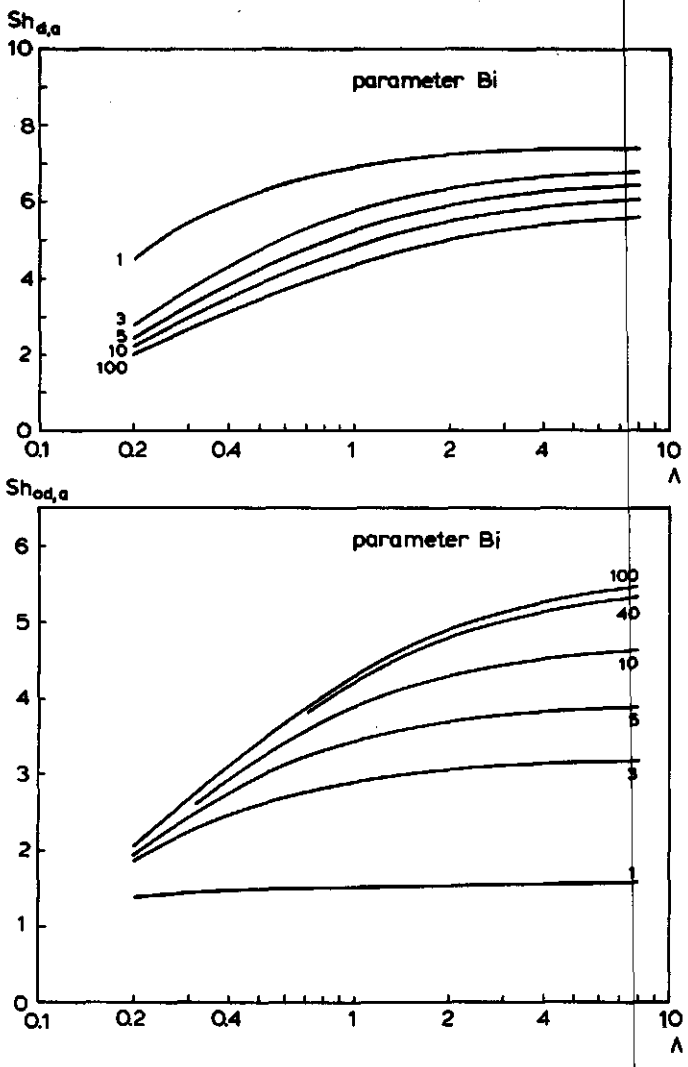

Fig. 28. Asymptotic Sh_d and Sh_{od} values for cocurrent extraction of cylindrical particles. $Bi = mk_cR/\mathbb{D}_d$ is the Biot number.

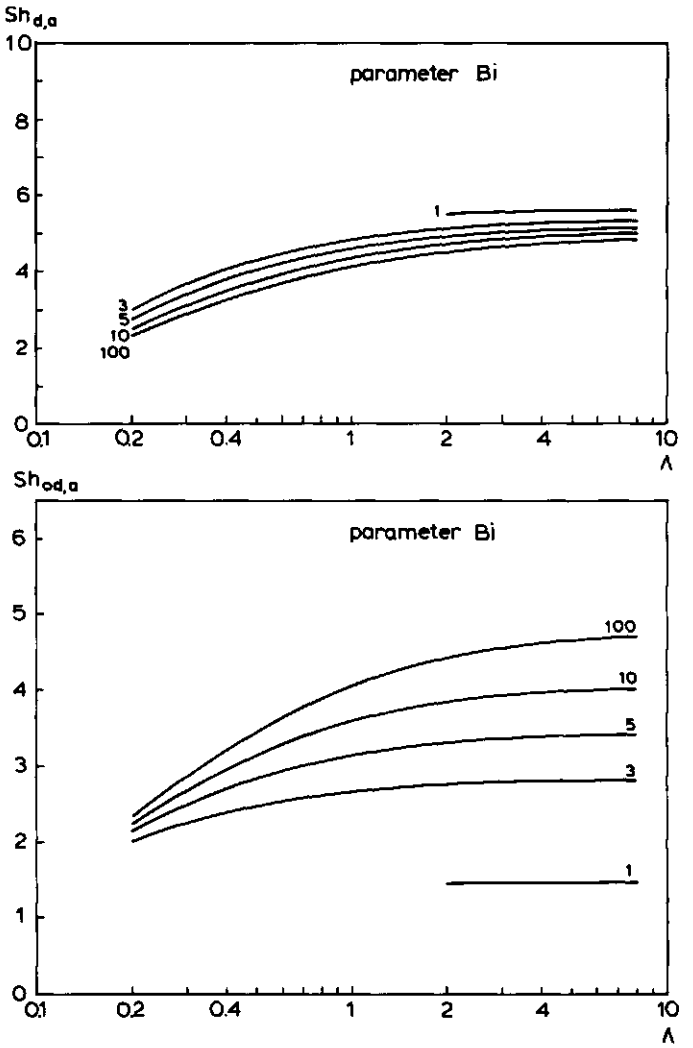

Fig. 29. Asymptotic Sh_d and Sh_{od} values for cocurrent extraction of particles with slab geometry. $Bi = mk_cR/\mathbb{D}_d$ is the Biot number.

transfer coefficient. Due to the falling concentration in the liquid surrounding the particle, the concentration gradients at the solid-liquid interface $(\partial\omega'/\partial r)_R$ are steepened with the result that was mentioned above. The reserve is true for cocurrent extraction where the liquid concentration rises during the extraction process.

3.3.3 $Sh_{d,a}$ values from solutions under general boundary conditions

The analytical solution of the diffusion equation 3.29 with boundary conditions 3.30 through 3.32 can be derived from the generalized solutions presented by e.g. Mikhailov (1973). For the basic geometries these solutions are summarized below:

$$\bar{W} = \frac{\bar{\omega}' - \omega_0'}{c'(t_d = 0)/m - \omega_0'} =$$

$$2\nu Bi^2 \sum_{n=1}^{\infty} \left[\int_0^{t_d} C(\eta)\, e^{-\lambda_n^2 (t_d - \eta)} d\eta \right] / [\lambda_n^2 + Bi(Bi + 2 - \nu)] \qquad (3.43)$$

where $C(t_d)$, the bulk liquid concentration at the dimensionless time t_d, is embodied by:

$$C(t_d) = \frac{c'(t_d)/m - \omega_0'}{c'(0)/m - \omega_0'} = \frac{1}{1 - c(t_d)} \qquad (3.44)$$

and λ_n are the positive, non-zero roots of the characteristic equations:

$$\tan \lambda_n = Bi/\lambda_n \qquad \text{when } \nu = 1 \qquad (3.45)$$

$$J_1(\lambda_n)/J_0(\lambda_n) = Bi/\lambda_n \qquad \text{when } \nu = 2 \qquad (3.46)$$

$$\tan \lambda_n = \lambda_n (1 - Bi) \qquad \text{when } \nu = 3 \qquad (3.47)$$

For longer contact times, the regular regime solutions result in a mass flux that can be described with a constant mass transfer coefficient k_{od}. For the calculation of $Sh_{od,a}$ values, we are only interested in this limiting behaviour. Therefore, the time variant bulk liquid concentration $C(t_d)$ can be calculated from the solutions of the lumped parameter model. In Section 2.1, some solutions of this model for various flow systems were given. For cocurrent and countercurrent contact in plug flow, $C(t_d)$ can be determined from Table 2 when the number of transfer units is replaced by:

$$N_{t,d} = k_{od}\, a'\, \tau_d\, (x/L) = Sh_{od}\, t_d\, \nu/2 \qquad (3.48)$$

where x is the coordinate in the liquid flow direction and $Sh_{od} = k_{od} 2R/\mathcal{D}_d$. In this way the following relation is obtained:

$$C(t_d) = \frac{\Lambda_t - \exp\left\{\frac{\nu}{2}\, t_d\, Sh_{od}\, \frac{1-\Lambda_t}{\Lambda_t}\right\}}{\Lambda_t - 1} \tag{3.49}$$

where Λ_t equals Λ for countercurrent phase contact, and $-\Lambda$ for cocurrent extraction. The extraction rate $-\,\mathrm{d}\,\bar{\omega}/\mathrm{d}\,t_d$ can be calculated by substitution of the former equation in Eqn 3.43, which yields:

$$-\frac{\mathrm{d}\bar{\omega}}{\mathrm{d}t_d} = -\frac{2\nu Bi^2}{\Lambda_t - 1} \sum_{n=1}^{\infty} \frac{[(\Lambda_t - 1)\lambda_n^2 + \Lambda_t A]\, e^{-\lambda_n^2 t_d} - A\, e^{A t_d}}{(\lambda_n^2 + A)\,[\lambda_n^2 + Bi\,(Bi + 2 - \nu)]} \tag{3.50}$$

where $A = (\nu/2)\, Sh_{od}\, (1 - \Lambda_t)/\Lambda_t$. An expression for the driving force for mass transfer is obtained from a mass balance 3.27:

$$(\bar{\omega}' - \omega_0')/\Lambda_t + (c'_{out} - c')/m = 0 \tag{3.51}$$

or in dimensionless notation:

$$\bar{\omega} - c = (\Lambda_t - 1)\, c - \Lambda_t \tag{3.52}$$

The overall driving force can now be derived from Eqns. 3.49 and 3.52:

$$\bar{\omega} - c = -\exp\left\{\frac{\nu}{2}\, Sh_{od}\, \frac{1-\Lambda_t}{\Lambda_t}\, t_d\right\} = -\exp\left(-A\, t_d\right) \tag{3.53}$$

In fact, this expression is proportional to the extraction rate calculated from the lumped parameter model. The Sh_{od} number can now be obtained easily from Eqns 3.50 and 3.53 for a contact time $t_d = Fo$:

$$\frac{\nu}{2}\, Sh_{od} = \frac{-2\nu Bi^2 \sum_{n=1}^{\infty} \dfrac{(\lambda_n^2 + \dfrac{\Lambda_t}{\Lambda_t - 1} A)\, e^{-\lambda_n^2 Fo} - A\, \dfrac{1}{\Lambda_t - 1}\, e^{A\, Fo}}{(\lambda_n^2 + A)\,[\lambda_n^2 + Bi\,(Bi + 2 - \nu)]}}{-\exp\left(A Fo\right)}$$

$$= 2\nu Bi^2 \sum_{n=1}^{\infty} \frac{(\lambda_n^2 + \dfrac{\Lambda_t}{\Lambda_t - 1} A)\, e^{-(\lambda_n^2 + A)\, Fo} - A\, \dfrac{1}{\Lambda_t - 1}}{(\lambda_n^2 + A)\,[\lambda_n^2 + Bi\,(Bi + 2 - \nu)]} \tag{3.54}$$

The asymptotic Sh_{od} number for long contact times is derived from this equation by taking the limit for $Fo \to \infty$. This raises the problem that no information is available beforehand about the value of $-(\lambda_n^2 + A)$. However, it is known that the $Sh_{od,a}$ value is the lower limiting value of the actual Sh_{od} value, and we can only accept finite mass

transfer rates. Thus $-(\lambda_n^2 + A)$ must always be less then zero. Thus the following relation is derived for $Fo \to \infty$:

$$\frac{\Lambda_t}{2\nu Bi^2} = \sum_{n=1}^{\infty} \{(\lambda_n^2 + A)[\lambda_n^2 + Bi(Bi + 2 - \nu)]\}^{-1} \tag{3.55}$$

where A is a function of the asymptotic Sh number. The iterative solution of this equation yields Sh values for arbitrary values of Bi, Λ_t and ν. The solutions are identical to those presented in the previous section.

3.4 Asymptotic $Sh_{d,a}$ numbers in engineering calculations

The practical use of the asymptotic Sh values obtained from the theory presented in the previous sections is restricted to the extraction of uniform particles with simple geometry, cocurrent or countercurrent phase contact in pure flug flow and relatively long contact times between the phases. In this section attention is paid to the applicability of the asymptotic transfer coefficients in practical design calculations, where more complicated cases are encountered. The error introduced when $Sh_{od,a}$ numbers are applied at finite Fo values is discussed. The determination of these asymptotic transfer coefficients for other boundary conditions will be outlined. Subsequently, the estimation of $Sh_{od,a}$ for irregular particles and for non-uniform particle size distributions is discussed. Finally, an approximate explicit relation is derived that predicts $Sh_{od,a}$ values in countercurrent extractors when the extraction factor is close to or larger than unity.

Range of applicability. The practical significance of asymptotic $Sh_{od,a}$ numbers can be measured by the critical Fo value, above which the time-averaged Sh differs less than a specified percentage from the asymptotic value. On this basis the range of applicability is discussed in this paragraph. The approximate Fo time required to perform a certain separation is calculated from the lumped parameter model using the asymptotic $Sh_{od,a}$ value, see Eqn 3.48. Also, the exact Fo' value is determined from the analytical solution of the diffusion equation. The relative difference between those two is then plotted against Fo'. Due to the large number of parameters involved: Bi, Λ, ν, mode of phase contact and Fo', only some sample cases are covered by the figures. Fig. 30 shows the results for cocurrent extraction of particles with slab geometry. It clearly shows the expected increasing accuracy of the method with rising Fo' value. For higher Bi numbers, the critical Fo' value increases since the overall mass transfer coefficient becomes more and more determined by the time-dependent Sh_d; the contribution of the constant valued Sh_c is gradually reduced. The effect of the extraction factor is shown in Fig. 31. This graph indicates that an increase in Λ reduces the critical Fo' value for cocurrent extraction. The reverse is true for countercurrent extraction. The latter conclusion is in agreement with the results of Vorstman & Thijssen (1971) and of Brüniche Olsen (1962). The curve for $\Lambda_t = -30$ is essentially identical to the curve obtained for a constant bulk concentration. The figure clearly shows that the critical Fo' value increases from countercurrent to cocurrent phase contact. To determine whether the critical Fo' values are met in a process, the extraction efficiency has to be calculated from the analytical solution of the diffusion equation as a function of the Fo time. The results are shown in Fig. 32,

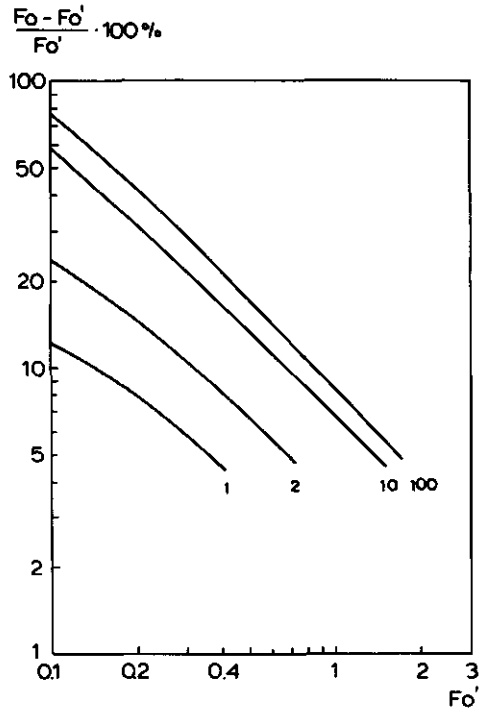

Fig. 30. Relative error in the Fourier value calculated from the $Sh_{d,a}$ value for cocurrent extraction. Slab geometry, $\nu = 1$; Extraction factor $\Lambda = 10$; Parameter *Bi*.

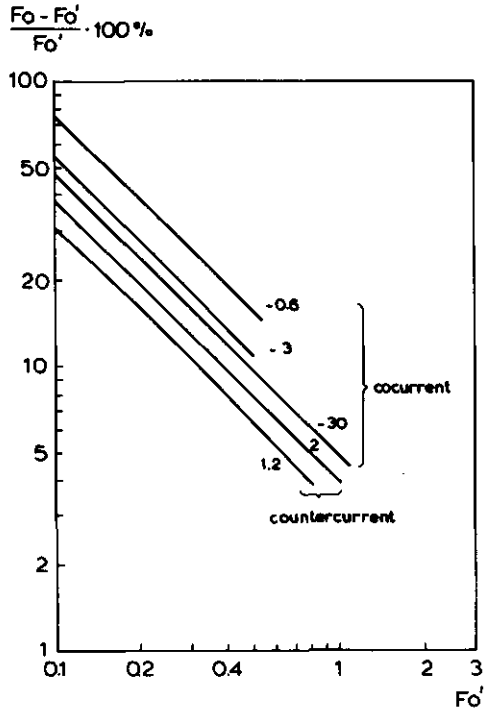

Fig. 31. Relative error in the Fourier value calculated from the $Sh_{d,a}$ value for cocurrent and countercurrent extraction. Spherical geometry, $\nu = 3$; $Bi = 100$; parameter Λ_t.

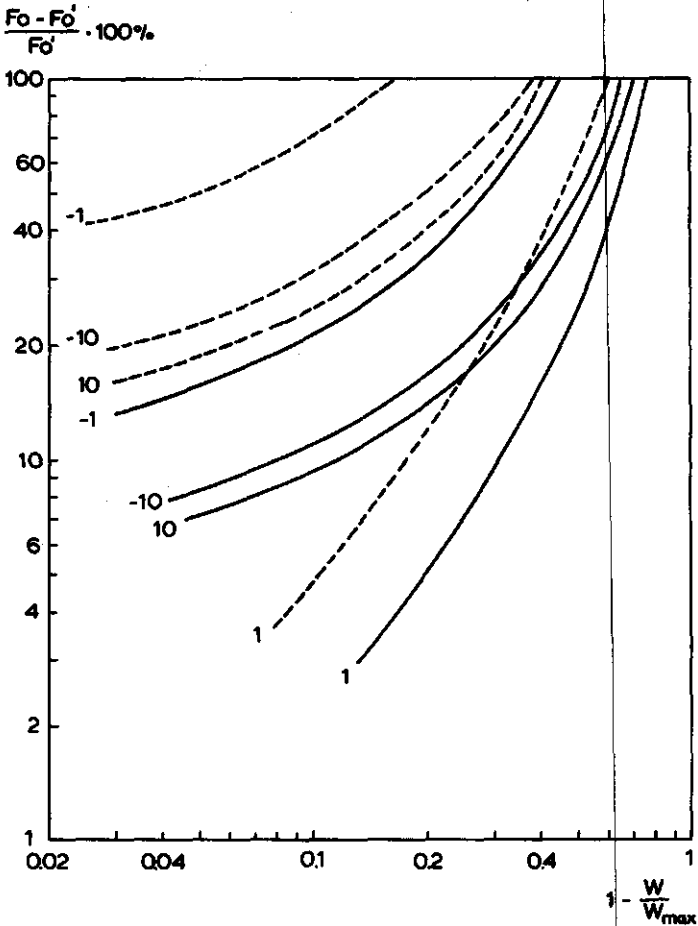

Fig. 32. Error in extraction calculations using asymptotic Sh_{od} values for cocurrent and countercurrent extractors. $Bi = \infty$; (– – –) $\nu = 3$; (——) $\nu = 1$; Parameter Λ_t.

where the relative error in the Fo value required for the separation, as calculated from the asymptotic Sh number, is plotted against the fraction of the solubles remaining in the solids, $1\text{-}W/W_{Fo\to\infty} = (\omega'_{in} - \omega'_{out})/(\omega'_{in} - \omega'_{out})_{Fo\to\infty}$. For countercurrent extraction and plane sheet geometry, the relative error is less than 10% when the extracted fraction is higher than 0.9, or $1\text{-}W/W_{max} < 0.1$. This value will often be attained in solid-liquid extraction processes in the food industry. For either cocurrent or batch extraction, Fig. 32 shows considerable discrepancy between actual and approximated Fo value; in particular for spherical particles the minimum extracted fraction will not be met in practice.

The asymptotic $Sh_{od,s}$ value only determines the extraction rate attained after long contact times between the phases, Fig. 33. The extracted fraction f can be calculated more accurately when a fictious initial condition $t_d = 0$, $f = f_0$ is incorporated in the

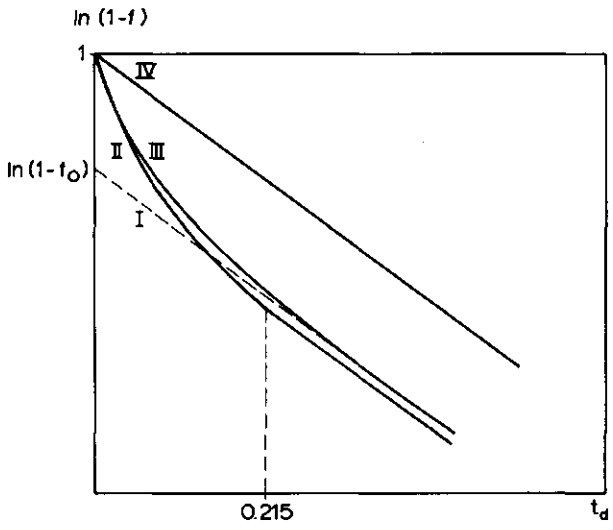

Fig. 33. Graphical representation of calculation procedures for heat and mass transfer problems. I first term approximation; II penetration/regular regime; III exact solution diffusion equation; IV asymptotic transfer coefficients.

calculation. In fact, this procedure forms the basis of the first term approximations (Pflug & Blaisdell, 1963). It has the disadvantage that the solution of the diffusion equation with proper initial and boundary conditions must be available. Here, a calculation procedure is adopted, which is similar to the one proposed for drying calculations by Schoeber (1976), that can be used to increase the accuracy of the calculation at small *Fo* values. The first part of the extraction process is calculated from the penetration theory. In a later stage the regular regime solution is applied. In Appendix D an analytical solution for short contact times is derived, for a plane sheet subjected to cocurrent or countercurrent extraction with finite mass transfer rate in the solvent phase. The time-dependent Sh_{od} numbers obtained from this solution are shown in Fig. 34. From this figure we learn, that the Sh_{od} value decreases rapidly from $Sh_{od} = Bi$ at $t_d = 0$ to some minimum value. In all cases, this minimum is located close to $\sqrt{t_d} = 0.45$ or $t_d = 0.215$, independent of *Bi*, Λ and the mode of phase contact. Furthermore, this minimum value is very close to the asymptotic Sh_{od} value. In most cases it is not more than 3% higher. The increase of the Sh_{od} number at longer times is caused by the fact that the boundary condition (D.4) for a semi-infinite slab is applied to a finite particle with finite storage capacity for the solute. This increase in the mass transfer coefficient is physically unrealistic. The above results suggest the use of the solution of the diffusion equation in the penetration period in the calculation up to $t_d = 0.215$. The subsequent part of the extractor is designed with the lumped parameter model, using the asymptotic value of Sh_{od} attained in the regular regime. The initial conditions of the solid and liquid phases in the second stage of the process are then obtained from the solution in the penetration period. The extraction efficiency:

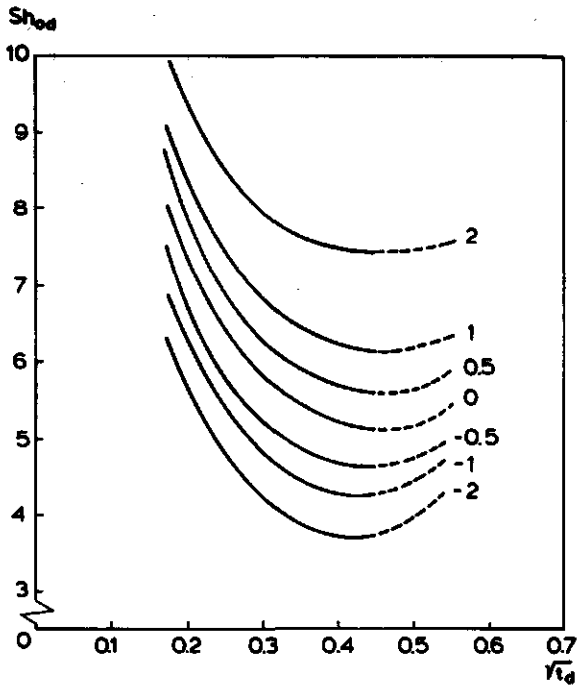

Fig. 34a. Sh_{od} values in penetration period for semi infinite slab geometry. $Bi = \infty$; Parameter $1/\Lambda_t$.

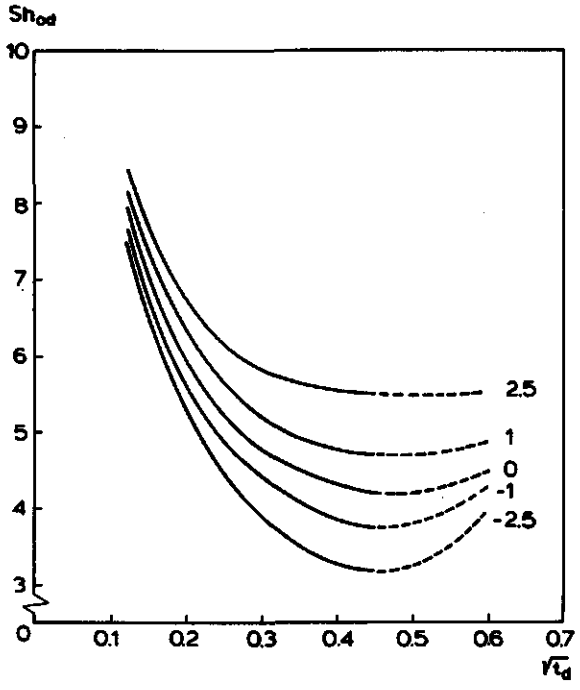

Fig. 34b. Sh_{od} values in penetration period for semi infinite slab geometry. $Bi = 10$; Parameter $1/\Lambda_t$.

$$\bar{W} = \frac{\bar{\omega}' - \omega'_o}{c'_o/m - \omega'_o} \tag{3.56}$$

at $Fo = 0.215$ is shown in Fig. 35 for both cocurrent and countercurrent extraction. The overall residence time required for the specified separation is then obtained from:

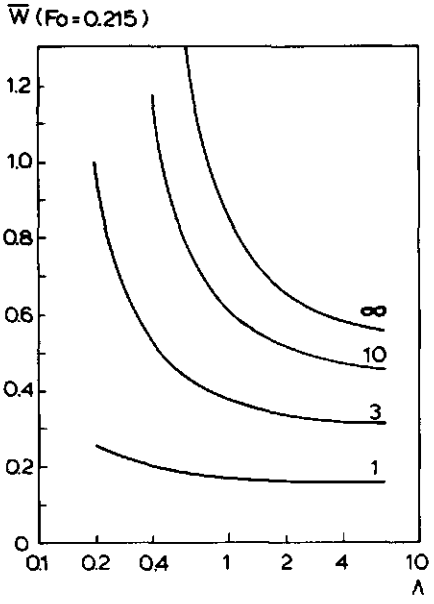

Fig. 35a. Extracted fraction in penetration period at $Fo = 0.215$ for semi infinite slab subjected to countercurrent extraction. Parameter *Bi*.

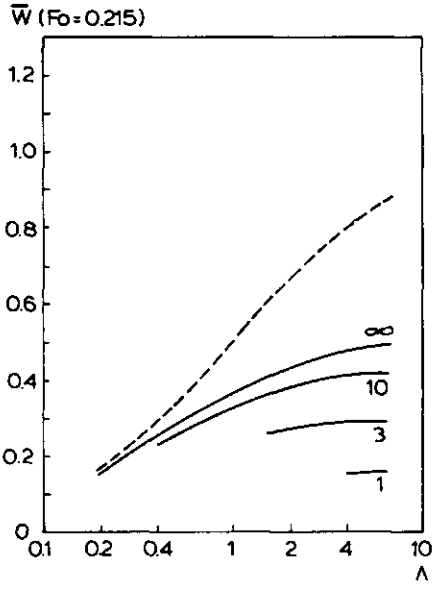

Fig. 35b. Extracted fraction in penetration period at $Fo = 0.215$ for semi infinite slab subjected to cocurrent extraction. (– – –) extracted fraction at equilibrium ($Fo \to \infty$), $\bar{W} = \Lambda/(1 + \Lambda)$; Parameter *Bi*.

$$Fo = 0.215 + \frac{2}{p}\,\frac{1}{Sh_{od,a}}\ln\frac{p\,\bar{W}(Fo=0.215)-1}{p\,\bar{W}(Fo)-1} \qquad Fo > 0.215 \tag{3.57}$$

where $p = (1-1/\Lambda_t)$. The Fo value calculated by the above procedure agrees up to a few percent with the exact solution for slabs. For Fo values smaller than 0.215 the Fo value has to be determined from the equations given in Appendix D.

Irregular shapes and particle size distributions. From the graphs presented in this chapter, the $Sh_{od,a}$ values for the extraction of particles with a simple geometry can be determined. For irregularly shaped particles, the common procedure is to approximate the particle shape by one of the basic geometries. Rutov (1958) suggested a method to improve the estimated k_d value for slightly irregular shapes. For Bi-numbers greater than 1, the diffusion coefficient has to be replaced by an effective diffusivity $\mathbb{D}'_d$:

$$\mathbb{D}'_d = \mathbb{D}_d A_d / A_{d,v} \tag{3.58}$$

where A_d is the surface area of the particle and $A_{d,v}$ is the surface area equivalent regular particle.

For non-uniformly sized particles, Gardner (1966) proposed a method to estimate an effective overall transfer coefficient when the particle size distribution is known. This procedure involves the determination of the particle size r_0^* which follows the average concentration of the particle cloud. When m is the cumulative particle size distribution function, the following relation results:

$$\int_0^1 \frac{\mathrm{d}(m)}{1+\dfrac{\Lambda_t}{1-\Lambda_t}\,\dfrac{k_{od}/r_o v}{(k_{od}/r_o v)^*}} = 1-\Lambda_t \tag{3.59}$$

where v is the particle velocity relative to the wall. r_0^* can be determined by trial and error. When $\Lambda_t = 1$, a somewhat simpler equation is obtained:

$$\int_0^1 \frac{\mathrm{d}(m)}{k_{od}/r_o v} = \frac{1}{(k_{od}/r_o v)^*} \tag{3.60}$$

Boundary conditions. When a specific flow pattern in the extractor gives rise to a boundary condition $\omega^*(t_d)$ that cannot be adequately described by one of the cases treated in this section, one of the methods discussed in Section 3.3.2 or Section 3.3.3 should be used to calculate $Sh_{od,a}$ values. The coupled boundary condition solution method as discussed in Section 3.3.2 produces relatively simple equations for $Sh_{od,a}$. However, the related characteristic equations may be rather complex, and the eigenvalues are normally not found in literature. Fortunately only one eigenvalue is required for the calculations. The general boundary condition method presented in Section 3.3.3 involves trial and error solution of an equation containing an infinite summation series to determine $Sh_{od,a}$. The advantage of this method is that for numerous cases the lumped parameter solutions are published in literature. Furthermore, the expression for $Sh_{od,a}$ is applicable

to all kinds of boundary conditions $C(t_d)$, without modification of the characteristic equations. The first 7 eigenvalues are readily obtained from the common handbooks, while additional roots are tabulated by Hayakawa (1975) for $\nu = 2$ and $\nu = 3$ and by Bakal et al. (1970) for $\nu = 1$. For these reasons the method discussed in Section 3.3.2 is only recommended for a rather simple problem. When complicated boundary conditions are involved, and consequently complex characteristic equations, the method outlined in Section 3.3.3 is more suitable.

Explicit relation for $Sh_{od,a}$. A quick estimation of $Sh_{od,a}$ values without resorting to the graphs presented in this chapter can be obtained from the approximate relation explicit in $Sh_{od,a}$. The equation is valid for countercurrent phase contact, when the extraction factor Λ is close to or greater than 1. The derivation of the equation is discussed in Appendix C. For plane sheet geometry the relation reads:

$$Sh_{d,a} = \frac{Bi\,\{6\,(Bi + 2.25) + (\Lambda - 1)\,(Bi + 3)\,\pi^2/2\}}{Bi\,\Lambda(Bi + 2.25) + (\Lambda - 1)\,\{3\,(Bi + 2.25) - (Bi + 3)\,\pi^2/4\}} \tag{3.61}$$

The solution for other geometries can be generated by the conversion rule

$$Sh_{d,a,\nu} = \nu\, Sh_{d,a,\nu=1} - 4(\nu - 1) \tag{3.62}$$

For extraction factor $\Lambda = 1$, these equations are exact.

4 Liquid maldistribution in solid-liquid extractors: hydrodynamic instabilities

4.1 Introduction

It was mentioned in Chapter 1 that viscous fingering may occur in systems where viscosity gradients exist in the liquid flowing through a densely packed bed. The mechanism that is responsible for the formation of viscous fingers can be elucidated by means of a simple model shown in Fig. 36. For the sake of simplicity, any interaction between the liquid and the packing material is not considered. The figure shows the situation where a liquid 2 is displaced downwards by a miscible liquid 1, which has the lower viscosity. Since in general density increases with viscosity, the displaced liquid is also said to be the denser one. A protrusion of the displacing liquid is supposed to be formed at the liquid-liquid interface due to, for example, a local permeability variation in the packing material. The displacing liquid will now flow preferentially through this protrusion, since the mobility of the liquid in this region is higher than that in the surrounding liquid. Hence, the disturbance tends to grow. On the other hand, especially at low displacement velocities, the favourable density difference counteracts any distortion of the displacement front. The flow can thus be stabilized by gravity segregation. The overall effect of viscous and gravity forces depends on the displacement velocity, physical properties of the liquids and properties of the packing material. Table 9 gives a schematic overview of the relative stability of several displacement conditions. In solid-liquid extractors viscosity differences may arise from concentration gradients in the solvent phase. Since both the shape of the concentration gradient and mass transfer between the solvent and the packing material affect the flow stability, the hydrodynamics of the flow in solid liquid extraction equipment present a much more complicated picture than the simple case just described. It is the aim of this section to provide information on whether viscous fingering affects extraction efficiency. In order to do so, the stabilizing effect of a concentration gradient in the liquid flowing through an inert packed bed is first examined. Subsequently, mass transfer between the packing and the solvent is taken into

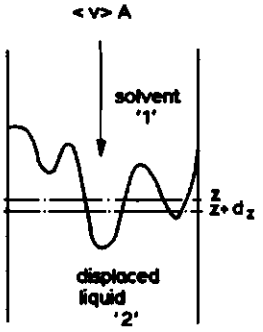

Fig. 36. Definition sketch for the phenomenological description of unstable displacement.

Table 9. Effect of flow conditions on the stability of displacement from packed beds. Index 1 refers to the upper liquid.

Flow direction	Sign $(\rho_1 - \rho_2)$	Sign $(\mu_1 - \mu_2)$	Stable displacement at flowrates
↑	+	+	none
	+	−	high
	−	+	low
	−	−	all
↓	+	+	high
	+	−	none
	−	+	all
	−	−	low

account.

Stability criteria for liquid-liquid miscible displacement from inert packed beds are discussed in this section. Some attention is given to flow phenomena in the unstable regime, and some methods suggested in literature to describe unstable displacement are given. Stability critera were verified experimentally for a stepwise concentration change of the solute which increases the viscosity of the liquid flowing through a densely packed bed. This study was then extended to the case of a gradually falling concentration in the displacing liquid in Section 4.2. This situation is relevant to solid-liquid extraction, where the concentration of the solute rises in the direction of the liquid flow. Finally, the effect of mass transfer on the flow stability was studied. Two different cases were considered. When the liquid in the interstitial voids of the packed bed is initially in equilibrium with the liquid in the internal pores of the packing material, mass transfer is expected to stabilize the displacement. Due to mass transfer in the protrusion, the viscosity ratio for the liquids outside and inside the protrusion is decreased. The growth rate of the disturbance is thus reduced by mass transfer. When the liquid in the interstitial voids is initially not in equilibrium with the solids, mass transfer occurs both inside and outside the disturbance. Then the overall effect depends on displacement conditions and the physical properties of the liquid. The extraction efficiency in a packed column has been measured over a wide range of displacement velocities to establish these effects.

4.1.1 Stability criteria

For liquid-liquid displacement, both miscible and immiscible, stability criteria are reported in literature. In general, interaction between the porous medium and the flowing liquid, e.g. adsorption, is neglected. When gravity effects are negligible, as in horizontal or matched density experiments, Muskat (1949) found that the flow is stable when the mobility ratio of the displacing and the displaced liquid exceeds 1. The mobility is defined as the ratio of permeability and viscosity. Hill (1952) included stabilization by

gravity during miscible displacement in the analysis. He assumed a sharp interface between the displaced and the displacing liquids, as shown in Fig. 37. At z the pressure in both the displaced and the displacing phase, p_2 and p_2 respectively, is assumed equal to p. The pressures in the phases at $z + \Delta z$ can be calculated from this value when the pressure gradients in the phases are known. The hypothetical disturbance indicated in the figure will then grow when $p_1' < p_2'$ and will be suppressed when $p_1' > p_2'$. According to the expression for p_1' and p_2', the condition for marginal stability can now be formulated as:

$$\left.\frac{dp}{dz}\right|_1 = \left.\frac{dp}{dz}\right|_2 \tag{4.1}$$

The pressure gradients in both phases can be calculated from the Darcy Law. When v_c is the maximum stable velocity we obtain:

$$-\frac{v_c \mu_1}{\kappa_1} + \rho_1 g = -\frac{v_c \mu_2}{\kappa_2} + \rho_2 g \tag{4.2}$$

The displacement is thus stabilized when $<v> < v_c$ where v_c is given by:

$$v_c = \frac{g(\rho_2 - \rho_1)}{\frac{\mu_2}{\kappa_2} - \frac{\mu_1}{\kappa_1}} \tag{4.3}$$

It can be verified easily that this result is in agreement with Table 9.

During the flow through packed beds, any concentration jump between two miscible liquids, one of which displaces the other, will be smoothed out by diffusion or dispersion effects. Thus the stability criterion derived by Hill was reformulated by Dumoré (1964) to account for a continuous concentration change in the liquids. Since for downward displacement any disturbance in the equi-concentration planes will grow when the local pressure gradient is lower than the pressure gradient in the liquid downstream, the displacement will be stable when the pressure gradient increases continuously in the flow direction. The condition for marginal stability thus reads:

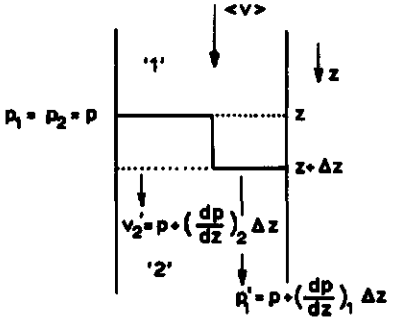

Fig. 37. Definition sketch of a hypothetical disturbance at the displacement front.

$$\frac{d}{dz}\left(\frac{dp}{dz}\right)=0 \tag{4.4}$$

Combining the Darcy Law with Eqn 4.4 gives for a constant permeability κ

$$\frac{1}{g\,\dfrac{d\mu}{dz}}\,\frac{d^2p}{dz^2}=-\frac{v_s}{\kappa g}+\frac{d\rho}{d\mu} \tag{4.5}$$

where v_s is the maximum stable displacement velocity in the situation under consideration. When the viscosity in the liquid increases in the direction of the flow, $d\mu/dz$ is greater than zero and the stability condition that is obtained for this case is that $< v > < v_s$, with v_s given by:

$$v_s=\kappa g\,(d\rho/d\mu) \tag{4.6}$$

The value of $(d\rho/d\mu)$ is only a function of the concentration of the solute. Since Eqn 4.6 should be satisfied everywhere in the packed column to prevent the formation of viscous 'fingers', the minimum value of $(d\rho/d\mu)$ is inserted in Eqn 4.6. Thus usually $(d\rho/d\mu)$ has to be determined for the concentration of the displaced liquid in the present case.

The stability criteria of Hill and Dumoré do not take into account the stabilizing effect of axial and radial dispersion in the liquid phase. Small amplitude distortions of the displacement front can be smoothed out by axial dispersion. On the other hand, radial dispersion tends to supress small wavelength perturbations irrespective of their amplitude. Perkins (1965) stated that the smallest channel that was not smoothed out by radial dispersion has a wavelength:

$$\lambda_{min}=2\sqrt{3.95\,\mathbb{D}_{E,T}\,t} \tag{4.7}$$

This result can be obtained assuming a Fourier number of 0.25 required for smoothing of the radial concentration gradients in the protrusion. From this discussion it can be concluded that the perturbations with a large amplitude and a long wavelength are the least affected by dispersion. The least stable distortion of the displacement front thus has a wavelength that is bounded by the size of the apparatus under consideration.

A marginal stability condition that takes dispersion effects into account can be obtained from the simultaneous solution of the equation of change for component A assuming dispersion with a dispersion coefficient $\mathbb{D}_E$, the equation of motion with the Darcy constitutive equation for the velocity vector $\vec{v}$ and the continuity equation in a three-dimensional velocity field. For a binary mixture of A and B:

$$\frac{\partial \rho_A}{\partial t}+\nabla\cdot\rho_A\vec{v}-\nabla\cdot\mathbb{D}_E\,\rho\,\nabla\,(\rho_A/\rho)=0 \tag{4.8}$$

$$\vec{v}+(\kappa/\mu h)\,(\nabla p-\rho\,\vec{g}+\rho\,D\vec{v}/Dt)=0 \tag{4.9}$$

$$\frac{\partial \rho}{\partial t}+\nabla\cdot\rho\,\vec{v}=0 \tag{4.10}$$

$\partial/\partial t$ denotes the partial derivative with respect to t, D/Dt the Lagrangian or substantial derivative. In these equations, both the liquid density ρ and viscosity μ are dependent on the concentration of component A. For the determination of marginal conditions for stable displacement, only the stability of the displacement front when it is subjected to small distortions has to be examined. This problem is usually solved by perturbation analysis. For small differences between the pure component densities, $\Delta\rho/\rho_A$, Perrine (1961) derived an expression for the initial growth rate γ_n of a perturbation of the form:

$$\rho_n = \bar{\rho}_n \, e^{i(\alpha x + \beta y + n\pi z)} \, e^{-\gamma_n t} \tag{4.11}$$

where $\bar{\rho}_n$ is the solution for stable flow; x, y and z are the spatial coordinates of a rectangular coordinate system extending infinitely in the x and y directions while bounded in the z direction between 0 and L. The bulk liquid flow is in the positive x direction. The growth rate parameter γ_n characterizes the initial growth rate of a perturbation with a specific wavelength. For stability analysis in miscible displacements, only the real part of γ_n has to be considered, because the flow instabilities observed in laboratory experiments are found to be of non-oscillatory nature (Schowalter, 1965). This result was derived analytically for small density differences between the displaced and the displacing liquid by Lapwood (1948). A condition for marginal stability can thus be obtained by setting the value of the growth rate parameter γ_n for the least stable distortion equal to zero, thus forcing all possible perturbations to be just suppressed. Only the solution for downward, vertical displacement is given here. Bearing in mind that the least stable perturbation has a maximum possible wavelength and amplitude, we obtain for the maximum stable displacement velocity v'_s:

$$v'_s = \frac{\dfrac{\kappa g}{\mu}\dfrac{\partial \rho}{\partial c}}{\dfrac{\partial \ln \mu}{\partial c} - \dfrac{\pi^2}{Bo_T}\left(\dfrac{D_p}{L}\right)^2 \left(\dfrac{\partial c}{\partial x'}\right)^{-1}} \tag{4.12}$$

where $Bo_T = v'_s D_p / \mathbb{D}_{E,T}$ is the transverse Bo number and $x' = \bar{x}/D_p$, $\bar{x}$ being the distance coordinate in the direction of the liquid flow in a coordinate system moving with the mean flow velocity. For negligible radial dispersion $Bo_T \to \infty$, this equation reduces to the stability condition that was later derived by Dumoré (1964). Schowalter (1965) analysed the case where no restriction is put on the maximum pure component density differences. He assumed that the effective dispersion coefficient $\mathbb{D}_E$ has the same value in both the transverse and longitudinal direction. According to Perkins (1965) the following empirical relation can be used to estimate radial Pe values in porous media that can be characterized by a tortuosity factor F and an interstitial void fraction h:

$$Bo_T^{-1} = \frac{\mathbb{D}_c}{Fh < v > D_p} + 0.0157\,\sigma \tag{4.13}$$

where $\mathbb{D}_c$ is the molecular diffusion coefficient of component A in the liquid phase and the parameter σ measures the inhomogenity of the packing. A similar expression holds for the Bo number in the longitudinal direction:

$$Bo_L^{-1} = \frac{\mathbb{D}_c}{Fh < v > D_p} + 0.5\,\sigma \tag{4.14}$$

From these equations it is observed that equal dispersion coefficients can only be assumed in the low flow velocity range, where dispersion is controlled by molecular diffusion. From perturbation analysis Schowalter found that the condition for marginal stability was determined by four dimensionless groups, quantifying the relative importance of the effects of gravity, viscosity, dispersion and permeability. For perturbations with a wavelength smaller than some critical wavelength λ_c, the displacement front is stabilized by dispersion and gravity effects. In his paper the author presented graphs of λ_c against the parameters that characterize the displacement condition. A similar analysis is given by Heller (1966) who did not assume the same value for the dispersion coefficients in both the longitudinal and the transverse direction. For a ramp-shaped concentration distribution in the mixing zone at the displacement front, the value of the growth rate parameter of the least stable perturbation is given for various displacement conditions.

In conclusion, simple stability conditions describing the stabilizing effect of gravity segregation at the onset viscous fingering are directly obtained from the Darcy Law. A more complete analysis that includes dispersion effects shows that the onset of viscous fingering depends on the wavelength of the perturbations. The development of the least stable distortion of the displacement front is retarded by transverse dispersion effects, and also by longitudinal dispersion when small amplitude perturbations are considered. The wavelength of the least stable distortion is determined by the size of the experimental equipment, and consequently the onset of flow instabilities depends on the size of the apparatus considered.

4.1.2 Flow behaviour in the unstable regime

In addition to the formulation of stability criteria, many attempts have been made to describe the flow phenomena in the unstable flow regime. The mathematical modelling of viscous fingering commonly proceeds along one of the following two routes:

– Numerical solution of the equations of motion, dispersion and continuity, Eqns 4.8–4.10. Since the 'dispersion equation', i.e. the continuity equation for a component A, is a mixed parabolic and hyperbolic partial differential equation, simple finite difference methods lead to numerical smearing of the concentration profiles when the dispersion term is small compared with the convective term (Chhatwal, 1973). Therefore, one has to resort to complex numerical schemes, see for example Peachman & Ratchford (1962).

– Phenomenological description of the flow behaviour based on the Buckley-Leverett model. This model was origionally derived for the prediction of breakthrough curves for immiscible displacement of liquids with equal densities. Two basic equations are involved in this model. Firstly the frontal advance equation:

$$\left.\frac{\partial x}{\partial t}\right|_s = \frac{< v >}{h} \frac{\partial f}{\partial s} \tag{4.15}$$

the result from a simple mass balance, that embodies the rate at which an equi-satura-

tion plane with solvent saturation s proceeds through the porous medium in terms of the mean linear flow rate $< v >/h$ and the relation between the fraction of solvent that is actually flowing and the local saturation of solvent s. Secondly, the fractional flow equation that relates the quantity f to the viscosity ratio of the immiscible liquids, M:

$$f = \frac{v_1 A}{<v>(A_1 + A_2)} = \left\{1 + \frac{1}{\alpha} \cdot \frac{1}{M} \cdot \frac{1}{\gamma}\right\}^{-1} \tag{4.16}$$

where $\alpha = A_1/A_2$, $M = \mu_2/\mu_1$ and $\gamma = \kappa_1/\kappa_2$ (Fig. 36). This equation can be derived from the Darcy Law assuming an equal pressure drop in both the pure solvent channel and the displaced liquid regions. Koval (1963) followed this approach for simulating matched density displacements. In order to fit his results with experimental data, he replaced M in Eqn 4.16 by the effective viscosity ratio M_e, which is related to the actual viscosity ratio M by:

$$M_e = (0.78 + 0.22\, M^{0.25})^4 \tag{4.17}$$

Dougherty (1963) included both gravity effects and mixing in the analysis. This results in a fractional flow equation of the form:

$$f = \left\{1 + \frac{1}{\alpha} \cdot \frac{1}{M} \cdot \frac{1}{\gamma}\right\}^{-1} \left\{1 - \frac{\alpha}{\alpha + 1} \frac{\kappa g (1-c) \Delta\rho / \bar{\mu}_o}{<v>}\right\} \tag{4.18}$$

where a linear relation between ρ and c is assumed, when c is the local solvent concentration in the liquid mixture; $\bar{\mu}_o$ is defined by:

$$\bar{\mu}_o = \left\{c\, \mu_s^{-0.25} + (1-c)\, \mu_o^{-0.25}\right\}^{-4} \tag{4.19}$$

The mass balance on slice dz in Fig. 35 now reads for the solvent channels:

$$\frac{<v>}{h} \frac{\partial f}{\partial z} + \frac{\partial s}{\partial t} = -B s^{p_1} (1-s)(1-c)^{p_2} \tag{4.20}$$

and for the solvent dissolved in the displaced liquid:

$$\frac{<v>}{h} \frac{\partial (1-f)c}{\partial z} + \frac{\partial (1-s)h}{\partial t} = B s^{p_1} (1-s)(1-c)^{p_2} \tag{4.21}$$

The dispersive mixing terms are lumped in the term on the right in the equations. Claridge (1972) solved these equations (4.18–4.21) numerically. The parameters γ, B, p_1 and p_2 were adjusted to obtain acceptable agreement between calculated and measured breakthrough curves. B was found to depend on displacement velocity, viscosity ratio, concentration of solvent in the oil phase and the degree of fingering.

Both the methods result in fairly close agreement between calculated and observed breakthrough curves, the latter however only after scaling of several model parameters.

In addition to the above studies on the onset and progression of viscous fingers, some

interesting features of fully developed fingers are reported in the literature. Mathematical relations were derived for the shape of both the front end (Saffman & Taylor, 1958) and the rear end (Outmans, 1963) of the fingers. Apart from this front and rear end, the channel occupies a constant fraction of the column cross-sectional area. This fraction ranges from about 1 for very low flow rates to an asymptotic value 0.5 at higher displacement velocities (Saffman & Taylor, 1958). Numerical simulations and electric analogue studies have shown that in this portion of the channel the flow is in the direction of the main liquid flow vector. Only at the front end and at the rear lateral flow of liquid was found from the finger towards the surrounding liquid and the reverse. (Richardson, 1961; Perkins, 1965).

4.1.3 Experimental verification from literature data

Many experimental investigations on liquid displacement in packed beds have been reported in the literature. Most of these are concerned with the efficiency of the displacement in the stable and in the unstable flow regime, when a liquid is displaced from an inert porous medium (Hill, 1952; Brigham, 1961; Slobod & Howlett, 1964; King & Denizman, 1961). The results of these measurements are in qualitative agreement with Table 9. In most cases, the critical velocity v_c where the flow instabilities just develop is determined by plotting the length of the mixing zone against the displacement velocity $\langle v \rangle$. A more or less sharp increase of this length is observed near $\langle v \rangle = v_c$. The actually measured value of this mixing length is dependent on the displacement conditions and the experimental setup that was used. Slobod (loc. cit.) found that the mixing length correlated well with the ratio of the actual displacement velocity and the critical displacement velocity, as shown in Fig. 38. This ratio $\langle v \rangle / v_c$ can be interpreted as the ratio of viscous and gravity force terms in the Darcy equation:

$$\frac{\langle v \rangle}{v_c} = \frac{\langle v \rangle \Delta \mu / \kappa}{g \Delta \rho} \tag{4.22}$$

The effect of a graded mobility zone, i.e. a continuously falling viscosity of the injected fluid, on the stability of the flow through a porous medium was first studied by Slobod & Lestz (1960). They reported macroscopic stability of the flow when the displacement was carried out with a linear falling viscosity of the injected fluid. The displacement condi-

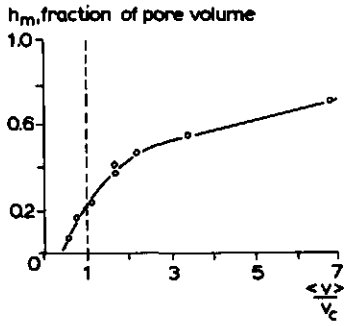

Fig. 38. Transition zone length h_m for displacement with favourable density and unfavourable viscosity ratio. From Slobod, 1964.

tions were such that Eqn 4.12 predicted unstable displacement. Kyle & Perrine (1965) applied a linear concentration gradient in the displacing liquid. They observed that any tendency for viscous fingers to develop was completely suppressed at steeper concentration gradients than those predicted by theory, Eqn 4.12. They concluded that formulating the stability criterion based on the least stable perturbation is quite conservative. Increasing the steepness of the concentration gradient increased the tendency for viscous fingers to develop. Mungan (1971), who used a Hele Shaw model in his experiments, found qualitatively that an exponential falling concentration of the injected liquid increased flow stability in his immiscible displacement experiments.

The effect of mass transfer from the packing to the liquid, as occurs in solid-liquid extractors, on the stability of the flow has been given little attention. King & Denizman (1972) mentioned the existence of unstable flow during solid-liquid adsorption chromatography. In their experimental study they measured the height of the mixing zone, h_m, as a function of the displacement velocity, for both porous and non-porous packing material. h_m was defined by the authors as the time interval between passage of the 10 and 90% concentration levels in the liquid effluent, multiplied by the mean displacement velocity. In all cases they observed a decreased height of the mixing zone when a porous packing was applied instead of a non-porous one. In their analysis they did not discriminate between the effect of finite mass transfer rates and hydrodynamic instabilities on the value of h_m. Nevertheless it can be concluded from their experiments that the mass transfer process considerably stabilizes the flow. The conclusion agrees with the discussion on this subject in Section 4.1.

The growth of viscous fingers once they are initiated at the liquid-liquid interface or equiconcentration plane has been measured for both miscible and immiscible displacement by many authors, e.g. Benham & Olsen (1963) and Gupta et al. (1974b). It is generally concluded that the growth rate of the fingered region is virtually constant during the major portion of the displacement. For short times after the onset of the channels the growth rate may be apparently slower or faster, and at long times stabilization by transversal dispersion may reduce finger growth rate, although theoretically the mechanism seems rather ineffective in practical systems (Benham & Olsen, 1963; Wooding, 1969). When gravity effects can be neglected in comparison with the viscous effects, the growth rate of a channel becomes independent of the displacement velocity (Scheidegger, 1960). For normal flow rates the fractional area that is occupied by the channels in the mixing zone is approximately 0.5; at very low flow rates this value can be considerably higher (Perkins, 1965; Saffman & Taylor, 1958).

The observations just mentioned contribute to the basic understanding of the behaviour of viscous fingers during liquid displacement in packed beds in the unstable regime. On the other hand it should be realized that the onset and growth of these fingers is strongly dependent on the scale of the apparatus used in the experiments (Blackwell, 1959), local inhomogenities of the packing (Hawthorne, 1960), preferent flow along the wall etc. Thus the quantitative result cannot easily be extrapolated to other displacement conditions and packing materials.

4.2 Experimental study of miscible liquid displacement from packed beds

Experiments reported in the literature are mostly concerned with the determination of critical displacement velocities and the growth of viscous fingers in the unstable flow regime, when a liquid is displaced from an inert packed bed by a miscible or immiscible solvent, see Section 4.1. However, little experimental evidence is available on the stabilizing effect of concentration gradients between displacing and displaced liquid, especially when those gradients arise from mass transfer between the solids that constitute the porous medium and the interstitial liquid. It is the aim of this study to contribute to the knowledge on flow phenomena under these conditions. To facilitate the interpretation of the measurements, the effect of a concentration gradient on both the onset and growth of viscous fingers is established in the first part of the study. The experimental setup that was used is sketched in Fig. 39. Both the experimental procedure and the apparatus are discussed in detail in Appendix E. The column packed with glass beads and the top and bottom mixer were initially filled with glycerol solution. Water was injected in the top mixer during the downward displacement experiments. The liquid concentration at the bed inlet thus fell exponentially with time. In this way, an arbitrary exponential concentration gradient can be applied by varying the size of the top mixed region. The breakthrough curve was measured by taking samples at the column outlet and by continuously monitoring the sample density. In order to assure representative sampling, the

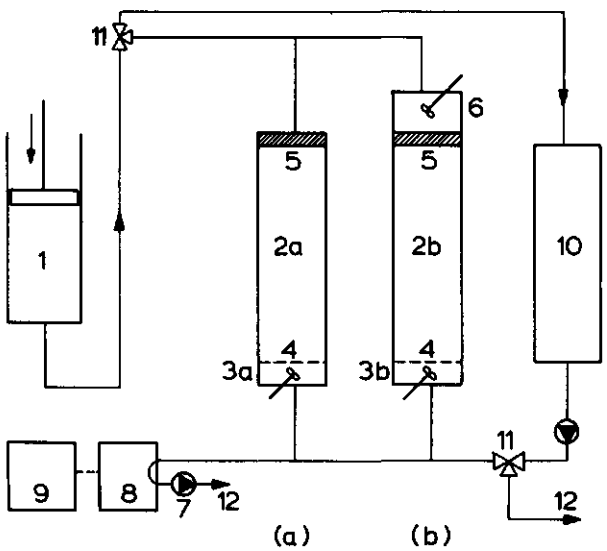

Fig. 39. Schematic diagram of the experimental setup. Item list:

1. storage vessel
2. packed column section
3. mixed sample region
4. mesh wire
5. porous glass disk
6. gradient mixer
7. sample pump
8. density meter
9. paper tape punch
10. storage vessel viscous solution
11. three-way cock
12. drain

outlet stream was mixed in the lower mixed region so that any radial concentration difference caused by channelling was smoothed efficiently. In the second part of the experimental study the more complicated case of displacement with simultaneous mass transfer between the packing and the interstitial liquid was investigated. The packing consisted of porous silica spheres, impregnated with sugar solutions prior to the experiments. The apparatus used and the experimental procedure that was followed are analogous to the one just described.

4.2.1 Effect of a concentration gradient in the liquid phase on flow stability

Experiments were designed to determine the effect of a concentration gradient in the displacing liquid on the stability of the displacement. The measured breakthrough curves give information on the residence time distribution in the packed section of the column which arises from dispersion effects and channelling. Once some mixing model is adopted to describe the measured data, several methods are available to adjust the mixing parameters involved in the model in order to obtain agreement with the experimental data. These methods include time-domain, s-plane and frequency domain curve fitting techniques (Johnston, 1971; Abbi & Gunn, 1976), as well as graphical procedures (Vergnes, 1975; Gupta, 1974a). Since in the present experimental study the residence time distribution can originate from viscous fingering, wall flow, axial dispersion etc., no mixing model was assumed beforehand. Instead, the residence time distribution in the packed section of the apparatus is characterized by the relative variance of residence times in this column section, $(\sigma/\tau)^2_{col}$, where the variance and the mean residence time are given by respectively:

$$\sigma^2 = \int_0^\infty (t-\tau)^2 \, E(t)\, dt \tag{4.23}$$

and:

$$\tau = \int_0^\infty t\, E(t)\, dt \tag{4.24}$$

Later on, parameters involved in mixing models can be adjusted to produce the same value of τ and $(\sigma/\tau)^2_{col}$, when model fitting should be required. $(\sigma/\tau)^2_{col}$ can easily be derived from the relative variance of the frequency distribution of residence times $E_t(t)$ of the total flow system, $(\sigma/\tau)^2_t$. The latter can be calculated from the moments of the distribution function, which are defined as:

$$M_n = \int_0^\infty t^n \, E(t)\, dt \tag{4.25}$$

Combining Eqns (4.23 – 4.25), we obtain the well-known relation:

$$(\sigma/\tau)^2_t = \frac{M_2 M_0}{M_1^2} - 1 \tag{4.26}$$

where M_0 equals 1 if a normalized frequency distribution is used in the calculation. The

procedure followed to calculate the moments from the measured residence time distribution function is discussed at length in Appendix F. The relative variance caused by the packed section $(\sigma/\tau)^2_{col}$ can be calculated from $(\sigma/\tau)^2_t$ by making use of the additivity of variance and mean residence times for cascaded equipment. Since for a complete mixed region $(\sigma/\tau)^2_m$ equals 1, the following relation holds:

$$(\sigma/\tau)^2_{col} = (\sigma/\tau)^2_t\,(1 + \xi_1 + \xi_2)^2 - \xi_1^2 - \xi_2^2 \tag{4.27}$$

where ξ_1 is the ratio of the mean residence times in the bottom mixer and the packed section, and ξ_2 represents the same value for the upper mixed region.

As a base case the breakthrough curve for a steep concentration jump using an inert packing material was measured. The results are shown in Fig. 40, where the value of $2/(\sigma/\tau)^2_{col}$ is plotted against the dimensionless displacement velocity $<v>/v_s$, representing the ratio of inert to viscous forces in the packed bed. For single phase flow through packed beds, where the residence time distribution is determined by axial dispersion that can be described with an eddy diffusion coefficient $\mathbb{D}_{E,L}$ the following relation holds (van der Laan, 1958):

$$\left(\frac{\sigma}{\tau}\right)^2_{ax.\ disp.} = \frac{2}{Pe_L^2}\{Pe_L - 1 + \exp(-Pe_L)\} \tag{4.28}$$

Single phase flow Pe_L-measurements revealed that $Pe_L = 0.25\ (L/D_p)$. This value was virtually independent of the Re-number in the range where the experiments were performed ($Re = \rho<v>D_p/\mu < 10$). This behaviour in the low Re-number regime is in agreement with literature data (Miller & King, 1966; Levenspiel, 1957). For the high

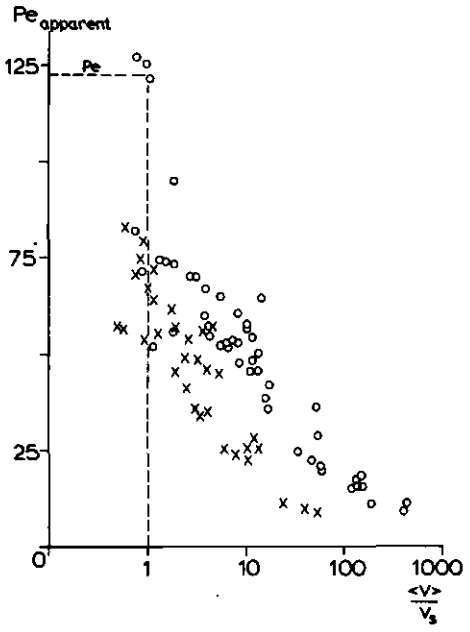

Fig. 40. Efficiency of miscible liquid-liquid displacement from packed beds: the effect of a concentration gradient in the displacing liquid. ξ_1 is ratio of the volume of the gradient mixer and the pore volume of the packed section of the column; Column: length 0.7 m, diameter 0.07 m; Key: x – $\xi_1 = 0$, o – $\xi_1 = 0.21$.

Pe_L-numbers encountered in the experiments the above relation reduces to:

$$\left(\frac{\sigma}{\tau}\right)^2_{\text{ax.disp.}} = \frac{2}{Pe_L} \tag{4.29}$$

or $Pe_L = 2/(\sigma/\tau)^2$. For miscible displacement stabilized by gravity segregation somewhat higher Pe_L numbers can be measured resulting from the favourable density difference. The Pe_T number, characterizing the transversal or radial mixing in the column, can be estimated from Eqn 4.13. For the high values of Pe_T calculated from this relation and because of the steep concentration gradient that is applied at the liquid inlet end of the bed, no stabilisation of the flow by transverse mixing is expected as can be verified from Eqn 4.12. For displacement velocities below v_s, the maximum stable displacement velocity, we thus expect Pe_L values of about 125. In the unstable flow regime, where $<v>/v_s > 1$, viscous fingering is likely to occur, so that the variance of the residence time distribution curve increases considerably. For very high values of $<v>/v_s$, the effect of gravity forces becomes negligible, and the growth growth rate of the disturbances is essentially independent of the displacement velocity (Scheidegger, 1960). This can be verified easily from a simple model shown in Fig. 41. Lumping all viscous fingers into a single hypothetical parallel channel and assuming the same pressure drop over the parallel channel and the 'main' flow, we can derive the following relation for the ratio of the velocity inside and outside the channel from the Darcy Law:

$$\Gamma = \frac{v_1}{v_2} = \left[(\alpha+1)\ \frac{M\gamma\alpha+1}{M\gamma(\alpha+1) - \dfrac{\gamma(M-1)}{R}} - \alpha\right]^{-1} \tag{4.30}$$

where $\alpha = A_1/A_2$, $\gamma = \kappa_1/\kappa_2$, $M = \mu_2/\mu_1$, and $R = \dfrac{<v>\Delta\mu}{\kappa_2 g \Delta\rho}$, the ratio of viscous and intertial forces. In essence, this equation is identical to the fractional flow equation derived by Dougherty (1963), expressed in Eqn 4.18. The value of the relative variance $(\sigma/\tau)^2$ of the residence time distribution function shown in Fig. 41, resembling the pulse

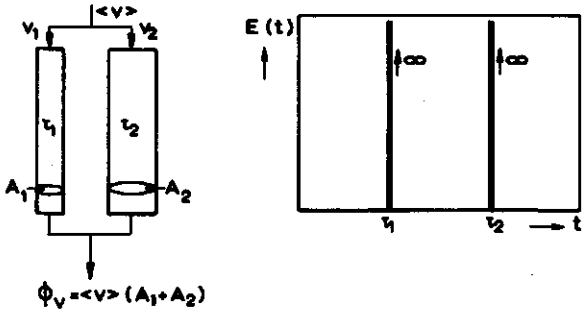

Fig. 41. Two-stream model for the description of liquid-liquid displacement from inert packed beds in the unstable flow regime; and the hypothetical pulse response of this two-stream model.

response of such a two parallel stream model, is given by:

$$\left(\frac{\sigma}{\tau}\right)^2_{\text{parr.}} = \frac{\frac{\alpha}{1+\alpha} + \frac{1}{1+\alpha}\Gamma^2}{\left[\frac{\alpha}{1+\alpha} + \frac{1}{1+\alpha}\cdot\Gamma\right]^2} - 1 \tag{4.31}$$

where we made use of the relation $\tau_2/\tau_1 = \nu_1/\nu_2 \equiv \Gamma$. Thus, for high displacement velocities $<v>$, the value of Γ is virtually independent of the R number. Eqn 4.31 shows that then $(\sigma/\tau)^2$ reaches an asymptotic value that is determined by the parameters γ, M and α. In Section 4.1.2 it was mentioned that α reaches a constant value at high displacement velocities; Miscible displacement experiments in packed beds that were designed to confirm this asymptotic value are reported in Appendix G. Thus for high R values the relative variance of the distribution curve reaches a constant value. From the simplified model we also learn that $(\sigma/\tau)^2_{\text{col}}$ is independent of the column length when the residence time distribution is controlled by channelling, while for flow of a liquid with uniform physical properties through packed beds, the value of $2/(\sigma/\tau)^2_{\text{col}}$ is known to increase linearly with the column length in the high Pe_L-number range, as can be verified from Eqn 4.29. Experimental results for two different column lengths are shown in Fig. 42. The results are in qualitative agreement with the simple flow model.

From Eqn 4.12 it can be derived that the onset of channelling is not retarded significantly when a concentration gradient of the form $c = c_0 \exp(-t/\tau_m)$ is applied at the column inlet, and τ_m is 21% of the mean residence time in the packed section of the column. From the simple flow model we expect, however, that the growth rate of the fingers will be attenuated due to a decrease of the effective viscosity ratio M. This

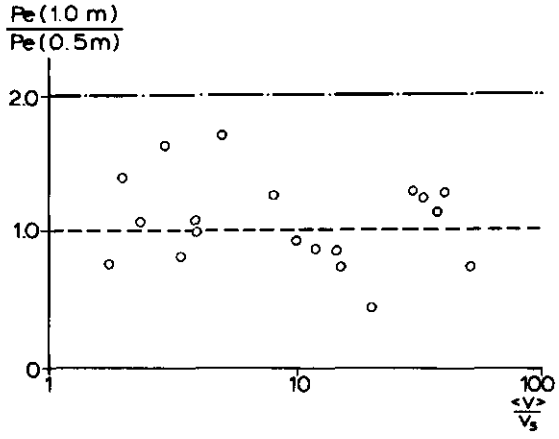

Fig. 42. Effect of column length on the apparent Péclet number in the unstable flow regime. The columns used had diameter 0.054 m, and length 0.5 and 1.0 m, respectively. (——.——) Dispersion is the controlling mechanism; (– – –) Channelling is the controlling mechanism.

parameter represents the ratio of the average viscosity in the channel and in the main flow. Due to this decreased finger growth rate, the variance of the breakthrough curve is reduced, as is shown in Fig. 40. Applying an even less steep concentration gradient in the displacing liquid causes considerable problems in the data analysis. From Eqn 4.27, it is observed that the contribution of the mixing zones in the top and bottom section of the apparatus to the total variance in residence time is quite significant. The small additional variance caused by the packed section of the apparatus is thus more difficult to determine accurately for higher τ_m values. This fundamental problem is discussed by Otto & Gestrich, (1974), who proposed the assemblage of a mixer-column-mixer system for residence time distribution measurements in single phase flow.

From the above experiments it is concluded that in the interpretation of the measurements, the ratio of the actual and the maximum stable displacement velocity can be used to discriminate between a stable and unstable flow regime. Although a smooth concentration gradient with an exponential decaying solute concentration attenuates viscous finger growth rate, channelling is not completely inhibited. The displacement efficiency in the unstable flow regime can be described qualitatively with a very simple model based on the Darcy Law.

4.2.2 Effect of mass transfer from the packing to the liquid on flow stability

The effect of mass transfer on flow stability was studied with the aid of a porous packing. The experimental setup was quite similar to the one used with an inert packing material, see Fig. 39 sub a. These porous particles were impregnated with a concentrated sugar solution before the experiment. Dependent on the initial condition that was requested the interstitial liquid was either washed out of the column with pure water, or the liquid remained in the column until equilibrium between the interparticle liquid and the pore liquid was attained. Subsequently the breakthrough curves were recorded when pure water was injected in the apparatus. In all cases, the flow direction was downwards. Properties of the packing material and details of the experimental procedure are given in Appendix E. In order to detect flow instabilities in this system, the measured breakthrough curves were compared with theoretical extraction curves obtained from a simple mathematical model. For plug flow of liquid through a fixed bed, such a model is given by Eqns 2.12 to 2.15, where a constant mass transfer coefficient is assumed. These equations were slightly modified to account for axial dispersion. The final result reads:

$$\frac{\partial c}{\partial \theta} = \frac{1}{Pe}\frac{\partial^2 c}{\partial z^2} - \frac{\partial c}{\partial z} + N(\omega - c) \tag{4.32}$$

$$\frac{\partial \omega}{\partial \theta} = -ND(\omega - c) \tag{4.33}$$

where $Pe = <v>L/ID_{E,L}$ and the other dimensionless variables are defined in Eqns 2.6 to 2.11. The initial and boundary conditions that apply in our case are:

$$\theta = 0 \qquad c = s_0 \qquad \text{and} \quad \omega = 1 \qquad z \geqslant 0 \tag{4.34}$$

$$\theta > 0 \qquad c = 0 \qquad z = 0 \tag{4.35}$$

$$\partial c/\partial z = 0 \qquad z = 1 \tag{4.36}$$

In Eqn 4.34, s_0 embodies the initial saturation of the interstitial liquid. For $s_0 = 1$, initial equilibrium exists between the pore liquid inside and outside the porous particle. When $s_0 = 0$, the external pore liquid is free from the solute. To simplify the mathematics involved in solving these equations the second boundary condition has been replaced by:

$$\theta > 0 \qquad c = s_0 = \text{finite} \qquad z = \infty \tag{4.37}$$

Extrapolating from similar dispersion problems it is expected that the effect of this modification on the final expression $c = c\ (\theta)$ is small for the high Peclet numbers encountered in the present study under stable flow conditions (Gerson & Nir, 1969). Adjustment of the parameters involved in the model to match the predicted breakthrough curve with the measured data is achieved by moment analysis. The zeroth and the first moments calculated from the analytical solution of Eqns 4.32 to 4.37 are given below:

$$M_{c,0} = (1 + s_0 D)/D \tag{4.38}$$

$$M_{c,1} = \frac{1}{D^2}\left[\frac{1}{N} + \left(\frac{1}{2} + \frac{1}{Pe}\right)(1 + D)(1 + s_0 D)\right] \tag{4.39}$$

The index c implies that the moments pertain to the breakthrough curve at the exit of the packed section of the apparatus. The moments $M_{m,i}$ of the actually measured concentration-time curve in the mixed sample region are related to the moments of the breakthrough curve at the exit of the packed section of the column $M_{c,i}$. The mass balance on the mixed region with volume V_m reads:

$$V_m \frac{dc_m}{dt} = \phi_v (c_c - c_m) \tag{4.40}$$

where the subscript m refers to the mixed region and c to the exit of the packed section of the column. Introducing dimensionless variables $\theta = t/(V_{col}h/\phi_v)$ and $\xi = V_m/V_{col}h$ leads to the following equation:

$$\xi \frac{dc_m}{d\theta} = c_c - c_m \tag{4.41}$$

After Laplace transformation and some rearrangement we obtain:

$$\tilde{c}_c = \tilde{c}_m (\xi s + 1) - \xi s_0 \tag{4.42}$$

From this equation the moments are readily obtained by the well-known method:

$$M_i = \lim_{s \to 0} (-1)^i \frac{\partial^i \tilde{c}(s)}{\partial s^i} \tag{4.43}$$

with the following result:

$$M_{c,0} = M_{m,0} - \xi s_0 \qquad i = 0 \tag{4.44}$$

$$M_{c,i} = M_{m,i} - i \xi M_{m,i-1} \qquad i > 0 \tag{4.45}$$

Combining Eqns 4.38 and 4.39 with Eqns 4.44 and 4.45 gives the normalized first moment of the breakthrough curve:

$$\frac{M_{1,m}}{M_{0,m}} = \frac{\frac{1}{D^2}\left[\frac{1}{N} + \left(\frac{1}{2} + \frac{1}{Pe}\right)(1+D)(1+s_0 D)\right]}{\frac{1+s_0 D}{D} + \xi s_0} + \xi \tag{4.46}$$

Thus, the value of the Peclet number can be calculated once the other parameters D and N are given. Since D is only determined by the geometry of the packing, it remains unchanged for all the runs. For stable flow, the Pe number can be estimated from previous measurements, see Section 4.2, to be $Pe = 100$. For the same reason as discussed in Section 4.2.1. this value is essentially independent of the Re number in the low Re number regime where the measurements are carried out, as long as dispersion is the only mechanism that causes deviations from plug flow. Estimation of the other parameters D and N from stable flow displacements is discussed in Appendix H. The results show that $D = 0.9$, and $N = 0.0125\ \tau$, when stable flow occurs.

Experiments were performed with initial saturation $s_0 = 0$ and $s_0 = 1$, over a wide range of displacement velocities and initial concentration levels. The measured breakthrough curves were reduced to their zeroth and first moment. The Pe number was determined from these assuming the theoretically predicted value for N. Also, the apparent number of transfer units N is calculated from Eqn 4.46 assuming $Pe = 100$. The results are summarized in Table 10. The Pe and N values contain essentially the same information; from Eqn 4.39 it can be derived that:

$$\frac{N}{N_{ref}} = 1 + N(1+D)(1+s_0 D)\left(\frac{1}{Pe_{ref}} - \frac{1}{Pe}\right) \tag{4.47}$$

Therefore, only the Pe number will be considered in the further analysis. When channelling occurs, some fraction of the solute is recovered at a later stage of extraction. Thus the first moment $M_{1,m}$ increases accordingly, resulting in a decrease of the apparent Pe number, see Eqn 4.39. Thus when the Pe number falls below 100, or alternatively N/N_{ref} below 1, it can be concluded that viscous fingering contributes to the residence time distribution, together with axial dispersion and finite mass transfer rates.

The results of the $s_0 = 1$ runs are shown in Fig. 43 and Table 10. The dimensionless flow velocity along the horizontal axis is calculated from Eqn 4.6. The minimum value of

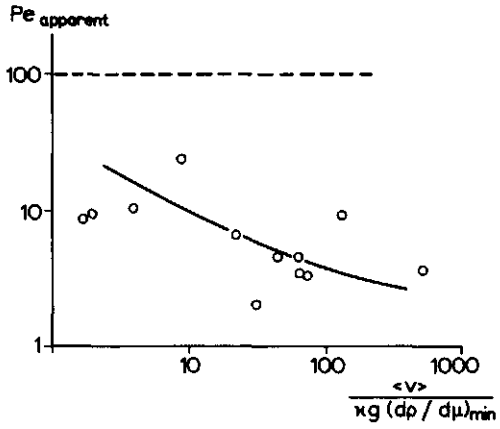

Fig. 43. Effect of hydrodynamic instabilities in systems with simultaneous mass transfer on the apparent Péclet number: pore liquid initially saturated ($s_0 = 1$). (– – –) Stable displacement limit.

$(d\rho/d\mu)$ is inserted in this equation, which is the value attained at the initial concentration in both the particles and the interstitial liquid. The figure clearly shows that the *Pe* number is far below 100. The existence of flow instabilities is indicated by breakthrough of displacing liquid before $t/\tau = 1$ and by deformation of the regular s-shape in the more unstable cases. Due to excessive tailing of the breakthrough curve, especially in the unstable flow regime, the curves were sometimes truncated before the solute was completely recovered. This tailing can originate from limited mass transfer rates, but also from inclusion of displaced liquid when the leading edges of viscous fingers coalesce (Perkins, 1965). Inspection of Eqn 4.39 shows that when the breakthrough curve is prematurely truncated, the value of *Pe* is overestimated. The data shown in Fig. 43 are conservative in these cases. From the figure it can thus be concluded that the stabilizing effect of mass transfer is not sufficient to prevent viscous finger growth in case $s_0 = 1$ under the prevailing experimental conditions.

Fig. 44 and Table 10 show the results of the $s_0 = 0$ runs. In the interpretation of the breakthrough curves an additional problem arises here compared with the previous case. In the prewash step there is some diffusional loss of the solute when the sucrose solution is removed from the interstitial voids of the packing. Since this loss is not known exactly, the initial interparticle concentration has to be determined from the zeroth moment of the breakthrough curve. Only when the solute is completely recovered from the bed, does the value thus obtained equal the actual initial concentration. The maximum concentration that occurs inside the packed column determines the value of the dimensionless displacement velocity along the horizontal axis of Fig. 44. This maximum concentration is calculated from the solution of the mass transfer model for a packed bed, Eqns 2.12 to 2.15. In this calculation the theoretical number of transfer units $N = 0.0125\ \tau$ is assumed. This method was believed to give a more reliable reference condition for the $(d\rho/d\mu)$-term in the expression for the stable velocity than the concentration at the maximum of the actually measured breakthrough curve. Even though this measured maximum equals the maximum concentration obtained in the packed section of the column under stable flow conditions, see Eqn 4.40, it may be considerably lower when radial concentration differences occur since these differences are efficiently smoothed in the sample region. The results of the calculations show less then 20% difference between the maximum concen-

Table 10. Results of displacement runs with simultaneous mass transfer.

$s_0 = 1$

Run	Initial liquid conc. (kg/m³)	Mean residence time τ (s)	$\frac{\langle v \rangle}{v_s}$ (1)	$\frac{N}{N_{ref}}$ (1)	Pe (1)
1	600	560	22	0.22	6.5
2	350	560	4	0.32	10.5
3	200	560	1.7	0.27	8.7
4	620	350	45	0.24	4.6
5	140	350	2	0.40	9.5
6	615	200	70	0.28	3.3
7	590	97	65	0.45	3.5
8	550	67	130	0.77	9.3
9	111	67	9	0.91	24.0
10	700	38	500	0.69	3.7
11	370	38	60	0.74	4.6
12	190	38	30	0.54	2.0

$s_0 = 0$

Run	Theoretical maximum liquid conc.	Mean residence time τ (s)	$\frac{\langle v \rangle}{v_s}$ (1)	$\frac{N}{N_{ref}}$ (1)	Pe (1)	Initial particle conc. ω_0 (kg/m³)
1	187	590	1.4	0.43	9.4	360
2	128	590	1.1	0.43	9.6	240
3	73	590	0.9	0.45	10.0	140
4	259	195	6.7	0.80	15.0	500
5	173	195	4.1	0.74	12.0	330
6	150	195	3.5	0.76	13.0	290
7	108	195	3.0	0.74	12.0	210
8	71	195	2.5	0.81	17.0	140
9	212	98	10.2	0.79	8.1	450
10	179	98	8.7	0.68	4.8	380
11	156	98	7.7	0.73	6.0	330
12	152	98	7.7	0.76	6.9	325
13	98	98	5.6	0.70	5.2	210
14	154	47	15.5	0.75	3.3	425
15	133	38	17.0	0.74	2.5	430
16	131	38	17.0	0.80	3.3	425

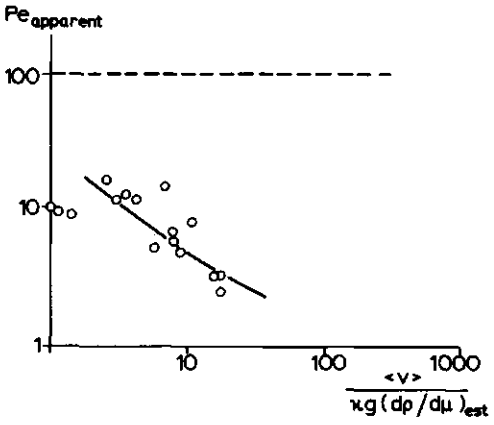

Fig. 44. Effect of hydrodynamic instabilities in systems with simultaneous mass transfer on the apparent Péclet number: pore liquid initially free from solute ($s_0 = 0$). (– – –) Stable displacement limit.

tration obtained from the measurements and the calculated value. The final results of the $s_0 = 0$ runs, shown in Fig. 44, show that considerable effects of channelling are observed in the $s_0 = 0$ case where miscible displacement is accompagnied by transfer of a viscosity increasing solute.

In conclusion, without putting emphasis on the numerical value of the results, the experiments clearly show that in systems where there is simultaneous miscible displacement and mass transfer of a solute that increases the viscosity of the liquid, viscous fingers may develop and reduce extraction efficiency.

5 Conclusions

From mathematical models the effect of local phase contact in countercurrent separation cascades is established for diffusion batteries and belt type solid-liquid extractors. The results are presented as concise correlations between the number of exterior apparent and true transfer units. These correlations show that the separation efficiency of a diffusion battery with 4 or more columns in series is within 10% of a purely countercurrent extractor under normal operating conditions. Similarly, a belt extractor as shown in Fig. 12 performs much like a countercurrent extractor when it contains 6 or more extraction stages. The beneficial effect of dripping sections is quantitatively discussed. When the solvent is recirculated in each section, complete mixing of the solvent in the stages can often be assumed. Liquid recirculation restricts the separation efficiency of an extractor, especially when the number of transfer units per section is high and mixing in the liquid phase becomes controlling.

Asymptotic values of the mass transfer coefficient in the dispersed phase have been calculated for purely cocurrent and countercurrent extraction. A simplified design procedure based on these values is proposed. Only a minor error is introduced when the asymptotic values are used directly in the solutions of the lumped parameter model for countercurrent extraction. The error in the estimated residence time required for a specified separation in such an extractor decreases with increasing dimensionless Fourier time, decreasing ratio of mass transfer resistance inside and outside the particle or Biot number and decreasing extraction factor. For cocurrent extraction the use of asymptotic transfer-coefficients in combination with the solutions of the lumped parameter models seems less promising; for the high Biot numbers that normally prevail in solid-liquid extractors, the critical Fourier value above which the asymptotic solution applies is only in the region of practical interest for a high extraction factor and slab geometry. For those cases where the approach just mentioned fails, an accurate short-cut calculation method is proposed which combines the penetration and asymptotic solutions.

Hydrodynamic instabilities, i.e. viscous fingering, can occur in solid liquid extraction systems, in spite of the stabilizing effect of viscosity gradients in the liquid phase. Such gradients, rather than viscosity jumps in the liquid flowing through a densely packed bed, significantly reduce the channelling intensity in the unstable flow regime. However, a significant effect on the point of onset of flow instabilities is not observed. For inert packing materials, the onset can be predicted from simple stability criteria reported in literature. More experimental results are required to warrant a conclusion about the onset of channelling during displacement with simultaneous mass transfer. However, in the unstable flow regime viscous fingering considerably reduces the overall mass transfer efficiency of the extractor. Finally it was concluded that the preferent flow along the wall of a packed column can be very much higher in the unstable flow regime than one would estimate from the usual correlations that apply for liquids with uniform physical properties.

Summary

Large scale solid-liquid extractors often consist of countercurrently cascaded mass transfer sections. The local mode of phase contact within each section usually differs from the overall countercurrent. A design procedure for solid-liquid extractors, which incorporates the mode of phase contact in the extraction stages, is presented for a diffusion battery or Shanks extractor, and for a rotary or belt type extractor. The effect of dripping sections, which are often applied to prevent interstage liquid entrainment, is included in the analysis. The mathematical models developed in this study are based on the equations describing mass transfer in a single-stage fixed bed. The results are reduced to ready-to-use correlations that can be applied over a wide range of process conditions. The estimation of mass transfer coefficients is an essential part of the current design procedures for solid-liquid extractors. Asymptotic values of the transfer coefficients are calculated for cocurrent and countercurrent extraction of particles with simple geometry. It is shown that these asymptotic values are a convenient tool in design calculations, especially for countercurrent extraction. For countercurrent extraction, an explicit semi-theoretical equation for the asymptotic mass transfer coefficient is derived which applies for an extraction factor greater than 0.5. Very accurate short-cut calculation methods are suggested based on the combination of mass transfer rates derived from the penetration theory and the asymptotic solutions.

In percolation type extractors, which are often used for large scale extraction processes, the solid particles form a densely packed bed. In this study the effect of non-uniform liquid flow through this layer of solids on extractor performance is studied. Special attention is given to channelling phenomena caused by differences in viscosity and density in the solvent. Measurements are performed to establish the effect of both the concentration gradients in the liquid phase and the mass transfer between the packing material and the solvent on the stability of the flow. The results qualitatively show that channelling caused by viscosity gradients in the solvent flow direction can occur in many solid-liquid extraction systems. The effect of this phenomenon on the extractor performance was studied experimentally for a single-stage fixed-bed extractor.

Samenvatting

Extractie van vaste materialen met behulp van een oplosmiddel is een, met name voor de voedingsmiddelenindustrie, belangrijke unit operation. Dit onderzoek richt zich op twee aspecten van het extractieproces. Eerst wordt ingegaan op het dimensioneren van extractieapparaten, die gebruikt worden voor processen op grote schaal. In het tweede deel wordt de stroming van het oplosmiddel door een laag van vaste deeltjes bestudeerd.

Extractieprocessen op grote schaal worden vaak uitgevoerd in apparatuur die bestaat uit in tegenstroom geschakelde secties, waarin de vaste en vloeistoffase met elkaar in contact worden gebracht. Het fasecontact in elke sectie zal in het algemeen afwijken van zuiver tegenstroom. Twee voor de voedingsmiddelen industrie belangrijke voorbeelden hiervan zijn de diffusiebatterij of Shanks-extractor, en de band-type-extracteur. Aan de hand van mathematische modellen is het extractierendement van deze apparaten vergeleken met het rendement van een pure tegenstroomextracteur. De bij deze berekeningen gebruikte modellen zijn gebaseerd op de vergelijkingen die het instationair stoftransport in een gepakte kolom beschrijven. Zowel voor de diffusie batterij als voor verschillende uitvoeringsvormen van de band-type-extracteur zijn de resultaten verwerkt tot correlaties, die over een groot gebied van extractiecondities bruikbaar zijn.

Voor het berekenen van extractieprocessen kan de lokale stoftransportsnelheid vaak voldoende nauwkeurig worden beschreven met een constante stofoverdrachtscoëfficiënt. Voor het bepalen van de voor een gespecificeerd extractierendement benodigde apparaatgrootte is een nauwkeurige schatting van de waarde van deze overdrachtscoëfficiënt essentieel. Voor zowel meestroom- als tegenstroomextractie van vlakke, cylindervormige of bolvormige deeltjes is de asymptotische waarde berekend die de stofoverdrachtscoëfficiënt na lange contacttijden aanneemt. Het gebruik van deze asymptotische waarde in ontwerpberekeningen wordt besproken. Vooral voor tegenstroomextractie is de afwijking van de uit de exacte oplossingen berekende apparaatgrootte klein. Voor dit praktisch interessante geval is een semi-theoretische vergelijking opgesteld, waarmee de asymptotische waarde van de stofoverdrachtscoëfficiënt direct kan worden berekend.

In vast-vloeistof-extracteurs van het percolatietype vormt de vaste fase tijdens het transport door het apparaat een stationair gepakt bed. Het effect van niet-uniforme stroming van het oplosmiddel door de laag vaste deeltjes op het extractierendement is experimenteel bepaald in een gepakte kolom. Behalve door inhomogeniteit van de pakking kan kanaalvorming optreden ten gevolge van viscositeits- en dichtheidsverschillen in de extractievloeistof. Met name aan dit laatste aspect is in dit onderzoek aandacht besteed. Zowel de invloed van een concentratiegradient in de vloeistoffase als van stoftransport van de vaste deeltjes naar de vloeistof op de stroming door de laag vaste deeltjes is bestudeerd. De resultaten laten zien dat kanaalvorming ten gevolge van concentratieverschillen in de vloeistoffase de scheidende werking van een extracteur nadelig kan beïnvloeden.

References

Abbi, Y.P. & D.J. Gunn, 1976. Trans. Instn. Chem. Engrs. 54: 225-231.
Acrivos, A., 1956. Ind. Engng. Chem. 48: 703.
Anzelius, A., 1926. Angew. Math. u. Mech. 6: 291.
Backstrom D.M., 1935. Int. Vet. Akad. Handlinger. 136:.
Bakal, A., G. Timbers & K. Hayakawa, 1970. Can. Inst. Fd Technol. I. 3: 76.
Barbouteau, I., 1956. Revue Inst. Fr. Pétrol. 11: 358-388.
Barker, J.J., 1965. Ind. Engng. Chem. 57: 43-51.
Beckenbach, E.F., 1961. Modern Mathematics for the Engineer, McGraw Hill N.Y. p. 350.
Beek, W.J. & K.M.K. Muttzall, 1972. Paper presented at the Int. Symposium Heat and Mass Transfer Problems in Food Eng., Paper D5, Wageningen, the Netherlands.
Beek, W.J. & K.M.K. Muttzall, 1975. Transport Phenomena. Wiley & Sons, London.
Benham, A.L. & R.W. Olsen, 1963. Soc. Pet. Engrs. J. June: 138-144.
Berg, C. v.d., 1972. Dechema Monogr. 70: 27.
Bernardini, E., 1973. Oil and Fat Technology. Technologie s.r.l. Rome. p. 228.
Bernardini, E., 1976. J. Am. Oil Chem. Soc. 53: 275-278.
Bichsel, B., S. Gál & R. Signer, 1976. J. Fd Technol. 11: 637-646.
Blackwell, W.E., J.R. Rayne & W.M. Terry, 1959. Trans. Am. Inst. Min. metall. Engrs. 216: 1-8.
Bomben, J.L., E.L. Durkee, E. Lowe & G.E. Secor, 1974. J. Fd Sci. 39: 260-263.
Brigham, W.E., P.W. Reed & J.N. Dew, 1961. Soc. Pet. Engrs. J. March: 1-7.
Brüniche Olsen, H., 1962. Solid liquid extraction. Nyt Nordish Verlag Copenhagen.
Brüniche Olsen, H., 1969. Sugar Technol. Rev. 1: 3-42.
Carslaw, H.S. & J.C. Jaeger, 1959. Conduction of Heat in Solids. Oxford University Press.
Chen, J.W., F.L. Cunningham & J.A. Buege, 1972. Ind. Engng. Chem. Process Des. Dev. 11: 430-444.
Chhatwal, S.S., R.L. Cox, D.W. Green & B. Ghandi, 1973. Wat. Resour. Res. 9: 1369-1377.
Chuoke, R.L., P. v. Meurs & C. v.d. Poel, 1959. Trans. Am. Inst. Min. metall. Engrs. 216: 188-194.
Claridge, E.L., 1972. Soc. Petr. Engrs. J. April: 143-155.
Colburn, A.P., 1939. Trans. Am. Inst. Chem. Engrs. 35: 211.
Cooney, D.O., 1974. A.I.Ch.E.Jl. 20: 1010-1011.
Cornish, A.R.H., 1965. Trans. Instn. Chem. Engrs. 43: T332-T333.
Crank, J., 1956. The Mathematics of Diffusion. Oxford University Press.
Dombrowski, H.S. & L.E. Brownell, 1954. Ind. Engng. Chem. 46: 1207-1219.
Dougherty, E.L., 1963. Soc. Pet. Engrs. J. June: 155-163.
Dumoré, J.H., 1964. Soc. Pet. Engrs. J. Dec: 357-362.
Dwivedi, P.N. & S.N. Upadhyay, 1977. Ind. Engng. Chem. Process Des. Dev. 16: 157-165.
Eder, B.D., 1971. Ph. D. Thesis, St. Univ. East Lansing, Michigan, USA.
Edeskuty, F.J. & N.R. Amundson, 1952. Ind. Engng. Chem. 44: 1698-1703.
Fan, H.P. & J.C. Morris, 1948. Ind. Engng. Chem. 40: 195-199.
Farritor, F.J. & L.C. Tao, 1972. Int. J. Heat Mass Transfer 15: 1179-1183.
Fornwalt, H.J. & R.A. Hutchins, 1966. Chem. Engng. 9: 155.
Frössling, N., 1938. Beitr. Geophys. 52: 170-216.
Furnas, C.C., 1930. Trans. Am. Inst. Chem. Engrs. 24: 142-193.
Gangwal, S.K., R.R. Hudgins & P.L. Silveston, 1977. Proceedings Europ. Congr. Particle Systems, Neurenberg, March 1977, pr1-pr29.
Gardner, G.C., 1966. Ind. Engng. Chem. Process Des. Dev. 5: 275-280.
Gardner, K. & J. Taborek, 1977. A.I.Ch.E.Jl. 23: 777-786.

Gerson, N.D. & A. Nir, 1969. Wat. Resour. Res. 5: 830-838.
Gibilaro, L.G. & A.A.H. Drinkenburg, 1972. Chem. Engng. Sci. 27: 445-447.
Gillespie, B.M., E.D. Crandall & J.J. Carberry, 1968. A.I.Ch.E.Jl. 14: 483.
Gunn, D.J., 1970, Chem. Engng. Sci. 25: 53-66.
Gupta, S.P. & R.A. Greenkorn, 1974a. Wat. Resour. Res. 10: 839-846.
Gupta, S.P. & R.A. Greenkorn, 1974b. Wat. Resour. Res. 10: 371-374.
Hartland, S. & J.C. Mecklenburg, 1966. Chem. Engng. Sci. 21: 1209-1221.
Hawthorne, R.G., 1960. Trans. Am. Inst. Min. metall. Engrs. 219: 81-87.
Hayakawa, K., 1975. Lebensm. Wiss. Technol. 8: 231-233.
Heller, J.P., 1966. J. Appl. Phys. 37: 1566-1579.
Higbie, R., 1935. Trans. Am. Inst. Chem. Engrs. 31: 365.
Hill, S., 1952. Chem. Engng. Sci. 1: 247-253.
Hutchins, R.P., 1976. J. Am. Oil Chem. Soc. 53: 279-282.
Jeschar, R., 1966. Arch. Eisenhütt Wes. 37: 193-200.
Johnston, J.L., L.T. Fan & Y.S. Wu, 1971. Ind. Engng. Chem. Process Des. Dev. 10: 425-431.
Kasten, P.R. & N.R. Amundson, 1952. Ind. Engng. Chem. 44: 1704-1711.
Kerkhof, P.J.A.M. & H.A.C. Thijssen, 1974. Chem. Engng. Sci. 29: 1427-1434.
King, P.J. & E. Denizman, 1972. Chem. Engng. May: 177-181.
Klaus, R., R.C. Aiken & D.W.T. Rippin, 1977. A.I.Ch.E.Jl. 23: 579-586.
Klinkenberg, A., 1954. Ind. Engng. Chem. 46: 2285.
Klinkenberg, A. & A. Harmens, 1960. Chem. Engn. Sci. 11: 260-266.
Kondratiev, G.M., 1964. Regular Thermal Regime, Gostekhizdat, Moscow.
Koval, E.J., 1963. Soc. Pet. Engrs. J. June: 145-154.
Krasuk, J.H., J.L. Lombardi & C.D. Ostrovsky, 1967. Ind. Engng. Chem. Process Des. Dev. 6: 187-195.
Kumar, S., S.N. Upadhyay & K.K. Mathur, 1977. Ind. Engng. Chem. Process Des. Dev. 16: 1-8.
Kyle, C.R. & R.L. Perrine, 1965. Soc. Pet. Engrs. J. Sept: 189-195.
Laan, E.T. v.d., 1958. Chem. Engng. Sci. 7: 187-191.
Lapwood, E.R., 1948. Proc. Camb. phil. Soc. math. phys. Sci. 44: 508.
Levenspiel, O. & W.K. Smith, 1957. Chem. Engng. Sci. 6: 227-233.
Luikov, A.V., 1968. Analytical Heat Diffusion Theory. Academic Press, N.Y.
Mandelbaum, J.A. & U. Böhm, 1973. Chem. Engng. Sci. 28: 569-576.
Martin, H., 1978. Chem. Engng. Sci. 33: 913-919.
McGaw, D.R., 1976. Powder Technol. 13: 231.
Mecklenburg, J.C. & S. Hartland, 1968. Chem. Engng. Sci. 23: 1421-1430.
Mikhailov, M.D., 1966. Forsch. Ing. Wes. 32: 101-110, 147-150.
Mikhailov, M.D., 1973. Int. J. Heat Mass Transfer 16: 2155-2164.
Mikhailov, M.D., 1977. Int. J. Heat Mass Transfer 20: 1409-1415.
Miller, J.S.F. & C.J. King, 1966. A.I.Ch.E.Jl. 12: 767-773.
Milligan, E.D., 1976. J. Am. Oil Chem. Soc. 53: 286-290.
Miyauchi, T., 1971. J. Chem. Engng. Jpn. 4: 238-245.
Miyauchi, T., H. Kataoka & T. Kikuchi, 1976a. Chem. Engng. Sci. 31: 9-13.
Miyauchi, T., T. Kikuchi & K. Hsu, 1976b. Chem. Engng. Sci. 31: 493-498.
Miyauchi, T., K. Matsumoto & T. Yoshida, 1975. J. Chem. Engng. Jpn. 8: 228-232.
Miyauchi, T. & T. Vermeulen, 1963. Ind. Engng. Chem. Fund. 2: 113-126.
Molyneaux, F., 1975. Fd Technol. Aust. 231-234.
Mungan, N., 1971. Can. J. Chem. Engng. 49: 32.
Munro, W.D. & N.R. Amundson, 1950. Ind. Engng. Chem. 42: 1481-1488.
Muskat, M., 1949. Physical Principles of Oil Production. McGraw Hill, N.Y.
Nelson, P.A. & T.R. Galloway, 1975. Chem. Engng. Sci. 30: 1-6.
Neretnieks, I., 1974. Svensk Papptidn. 11: 407-411.
Neretnieks, I., 1975. Chem. Ing. Techn. 47: 773.
Nusselt, W., 1930. Tech. Math. Therm. 1: 47.
Olçer, N.Y., 1964. Int. J. Heat Mass Transfer. 7: 307-314.
Oplatka, G., 1954. Z. Zuck Ind. 79: 471.

Otto, E. & W. Gestrich, 1974. Chem. Engng. Sci. 29: 1294-1296.
Outmans, H.D., 1963. J. Geophys. Res. 68: 5735-5737.
Paynter, H.M., 1957. Proc. Symposium on Control, Heidelberg sept. 1956. p. 243.
Peachman, D.W. & H.H. Ratchford, 1962. Soc. Pet. Engrs. J. Dec: 338.
Perkins, K., O.C. Johnston & R.N. Hoffman, 1965. Soc. Pet. Engrs. J. Dec: 301-317.
Perrine, R.L., 1961. Soc. Pet. Eng. J. March: 9-16.
Pfeffer, R. & J. Happel, 1964. A.I.Ch.E.Jl. 10: 605-611.
Pflug, I.J. & J.L. Blaisdell, 1963. ASHRAE J. 5: 33-49.
Pflug, I.J., P.J. Fellers & D. Gurevitz, 1967. Fd Technol. 21: 90-94.
Pillai, K.K., 1977. Chem. Engng. Sci. 32: 59-61.
Plachco, F.P. & M.E. Lago, 1972. Can. J. Chem. Engng. 50: 611-615.
Plachco, F.P. & M.E. Lago, 1975. Ind. Engng. Chem. Process Des. Dev. 15: 361-365.
Plachco, F.P. & J.H. Krasuk, 1970. Ind. Engng. Chem. Process Des. Dev. 9: 419-433.
Plachco, F.P. & J.H. Krasuk, 1972. Chem. Engng. Sci. 27: 221-226.
Pratt, H.R.C., 1975. Ind. Engng. Chem. Process Des. Dev. 14: 74-80.
Pratt, H.R.C., 1976. Ind. Engng. Chem. Process Des. Dev. 15: 544.
Rein, P.W., 1976. Sug. J. Dec: 15-22.
Richardson, R.G., 1961. Handbook of Fluid Dynamics. McGraw Hill N.Y., sect. 16.
Rickles, R.N., 1965. Chem. Engng. 15: 157.
Rietema, K., 1976. Fysische Transport en Overdrachtsverschijnselen. Het Spectrum Utrecht, Prisma Technica 60. p. 253.
Roetzel W. & F.J.L. Nicole, 1975. J. Heat. Transfer. Febr: 5.
Rosenbrock, H.H. & C. Storey, 1966. Computational Techniques for Chemical Engineers. Pergamon Press. p. 127.
Rutov, D.G., 1958. Annexe Bull. Int. Inst. Refr. (Moscow). 2: 415-421.
Saffman, P.G. & G. Taylor, 1958. Proc. R. Soc. A245: 312-329.
Scheidegger, A.E., 1960. Phys. Fluids 3: 94-104.
Schoeber, W.J.A.H., 1976. Ph. D. Thesis, Eindhoven University of Technology.
Schowalter, W.R., 1965. A.I.Ch.E.Jl. 11: 99-105.
Schwartzberg, H.A. & M. Desai, 1977. Paper no. 2054 Mass. Agr. Exp. Station, University of Massachusetts.
Sideman, S., 1966. Adv. Chem. Engng. 6: 207-286.
Sideman, S. & H. Shabtai, 1964. Can. J. Chem. Engng. June: 107-117.
Silin, P.M., 1964. Technology of Beet Sugar Refining. Israel Progr. for Sci. Transl., Jerusalem.
Sivetz, M.S., 1963. Coffee Processing Technology, AVI Westport Connecticut.
Sleicher, C.A., 1959. A.I.Ch.E.Jl. 5: 145-149.
Sleicher, C.A., 1960. A.I.Ch.E.Jl. 6: 529-530.
Slobod, R.L. & W.A. Howlett, 1964. Soc. Pet. Engrs. J. March: 1-9.
Slobod, R.L. & S.J. Lestz, 1960. Producers Mon. Penn. Bil Prod. Ass. Aug: 12-19.
Stanek, V. & J. Szekeley, 1972. Can. J. Chem. Engng. 50: 9-14.
Stemerding, S. & F.J. Zuiderweg, 1963. Trans. Instn. Chem. Engrs., Chem. Eng. (London) CE156.
Suzuki, M., 1975. J. Chem. Engng. Jpn. 8: 163-165.
Svedberg, U.G., 1976. Chem. Engng. Sci. 31: 345.
Tettamanti, K., J. Manczinger, J. Hunek & R. Stomfai, 1975. Acta Chim. Hung. 85: 27-47.
Thibodeaux, L.J., 1969. Chem. Engng. 2: 165.
Thibodeaux, L.J., D.R. Daner, A. Kimura, J.D. Millican & R.J. Parikh, 1977. Ind. Eng. Chem. Process Des. Dev. 16: 325.
Thijssen, H.A.C., 1969. Lecture notes Mass Transfer Processes, Eindhoven University of Technology.
Tolić, A., V. Rod & V. Jevtovic, 1973. Glasn. Hem. Dvušt., Beogr. 38: 571-602.
Tondeur, D., 1970. Chim Ind. 103: 2799-2808.
Treyball, R.E., 1968. Mass Transfer Operations. 2nd. ed., McGraw Hill N.Y.
Upadhyay, S.N. & G. Tripathi, 1975. J. Sci. Ind. Res. 34: 10.
Vergnes, F., 1976. Chem. Engng. Sci. 31: 88-90.
Vorstman, M.A.G. & H.A.C. Thijssen, 1971. Proc. Int. Solv. Extr. Conf. ISEC, April 1971. The Hague, the Netherlands, Paper 166, p. 1071.

Vorstman, M.A.G. & H.A.C. Thijssen, 1972. Proceedings Int. Symposium Heat Mass Transf. Problems in Fd Eng., Wageningen, the Netherlands. Paper D4.
Wakao, N., 1976. Chem. Engng. Sci. 31: 1115-1122.
Wakao, N. & T. Funazkri, 1978. Chem. Engng. Sci. 33: 1375-1384.
Wartman, R. & H. Mertes, 1966. Arch. Eisenhütt Wes. 37: 201-207.
Watson, J.S. & H.D. Cochran, 1971. Ind. Engng. Chem. Process Des. Dev. 10: 83.
Wooding, R.A., 1969. J. Fluid Mech. 39: 477-495.
Wucherpfenning, K., P. Possman & T. Özmen, 1976. Flüss. Obst 43: 119-121.
Yang, H.H. & J.C. Brier, 1958. A.I.Ch.E.Jl. 4: 453-459.

Appendices

Appendix A. Numerical solution of the equations describing mass transfer in a fixed bed

In Section 2.2.1, the equations describing mass transfer in a fixed bed were derived:

$$\frac{\partial c}{\partial \theta} + \frac{\partial c}{\partial \zeta} = N_{t,c}(\omega - c) \tag{2.12}$$

$$\frac{\partial \omega}{\partial \theta} = -N_{t,c} D (\omega - c) \tag{2.13}$$

Solving these equations by finite difference techniques gives accurate results only when the number of true transfer units, $N_{t,c}$ is high and the step size used in the integration is very small. The reason for this unfortunate situation is that any discontinuity in the concentration profiles in the liquid phase is suppressed by numerical dispersion (Rosenbrock & Storey, 1966). Therefore, Acrivos (1956) suggested the method of characteristics for solving the above equations. The principle of this method is that first the position of the solid and liquid elements are calculated as a function of time. The solution of the equations 2.12 and 2.13 is then calculated along these curves. Since $\omega = \omega(\zeta, \theta)$ and $c = c(\zeta, \theta)$ one can write:

$$d\omega = (\partial\omega/\partial\zeta) \cdot d\zeta + (\partial\omega/\partial\theta) \cdot d\theta \tag{A.1}$$

$$dc = (\partial c/\partial\zeta) \cdot d\zeta + (\partial c/\partial\theta) \cdot d\theta \tag{A.2}$$

The above equations can be considered as four simultaneous equations in the unknowns $\partial c/\partial\zeta$, $\partial c/\partial\theta$, $\partial\omega/\partial\zeta$ and $\partial\omega/\partial\theta$. These equations can be summarized in matrix notation as $\mathbf{[A] \cdot b = c}$, or

$$\begin{bmatrix} 1 & 1 & 0 & 0 \\ 0 & 0 & 0 & 1 \\ d\zeta & d\theta & 0 & 0 \\ 0 & 0 & d\zeta & d\theta \end{bmatrix} \cdot \begin{bmatrix} \partial c/\partial\zeta \\ \partial c/\partial\theta \\ \partial\omega/\partial\zeta \\ \partial\omega/\partial\theta \end{bmatrix} = \begin{bmatrix} N_{t,c}(\omega - c) \\ -N_{t,c} D (\omega - c) \\ dc \\ d\omega \end{bmatrix} \tag{A.3}$$

The characteristic directions can be obtained by setting the determinant of [A] equal to zero (Beckenbach, 1961). Thus the two characteristic curves, indicated by I and II, are obtained:

$$\left.\frac{d\zeta}{d\theta}\right|_{I} = 1 \tag{A.4}$$

$$\left.\frac{d\zeta}{d\theta}\right|_{II} = 0 \tag{A.5}$$

The characteristic grid for the hyperbolic system (2.12) and (2.13) is shown in Fig. A.1.

The differential equations that hold along the characteristics can be obtained by combining the origional PDE with the equations for the characteristic curves. For the derivative of c with respect to time along characteristic I the result is:

$$\left.\frac{dc}{d\zeta}\right|_{I} = N_{t,c}\,(\omega - c) \tag{A.6}$$

Similarly, the derivative of ω with respect to time along characteristic II is obtained by combining Eqns 2.13 and A.6:

$$\left.\frac{d\omega}{d\theta}\right|_{II} = -N_{t,c}\,D(\omega - c) \tag{A.7}$$

Eqn (A.6) is solved numerically along the characteristic I, by applying the following finite difference approximation:

$$c_{j+1,i+1} = c_{j,i} + \frac{\Delta\zeta}{2}\left(\left.\frac{dc}{d\zeta}\right|_{j+1,i+1} + \left.\frac{dc}{d\zeta}\right|_{j,i}\right) \tag{A.8}$$

Substitution of (A.6) and rearrangement gives:

$$c_{j+1,i+1} = \frac{c_{j,i}\left(\dfrac{2}{\Delta\zeta N_{t,c}} - 1\right) + \omega_{j,i} + \omega_{j+1,i+1}}{\left(\dfrac{1}{\Delta\zeta N_{t,c}} + 1\right)} \tag{A.9}$$

Similarly the resulting finite difference approximation of $d\omega/d\theta$ along characteristic II is obtained:

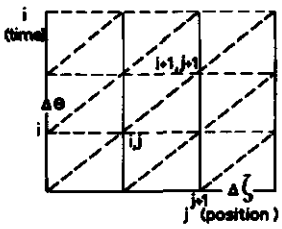

Fig. A1. Characteristic grid. (– – –) I-characteristic; (——) II-characteristic.

$$\omega_{j+1,i+1} = \frac{\omega_{j+1,i}\left(\dfrac{2}{\Delta\theta N_{t,c} D} - 1\right) + c_{j+1,i} + c_{j+1,i+1}}{\left(\dfrac{2}{\Delta\theta N_{t,c} D} + 1\right)} \tag{A.10}$$

The above equations are solved simultaneously. The initial conditions (2.14) provide the values of $c_{j,0}$ and $\omega_{j,0}$ at the beginning of a cycle. The liquid concentration $c_{0,i}$ is given by Eqn 2.15. The concentration in the solid phase at $\xi = 0$, $\omega_{i,0}$, is calculated from Eqn A.7:

$$\left.\frac{d\omega_{0,i}}{d\theta}\right|_{II} = -D N_{t,c} (\omega_{0,i} - c_{0,i}) \tag{A.11}$$

During the time interval $\Delta\theta$ the concentration $c_{0,i}$ is assumed to remain constant. After integration of the above equation the following boundary condition at the liquid inlet side of the column results:

$$\omega_{0,i} = c_{0,i} + (\omega_{0,i-1} - c_{0,i}).\ \exp(-N_{t,c} D \Delta\theta) \tag{A.12}$$

The differential equations (2.12) and (2.13) with the initial and boundary conditions can thus be replaced by the finite difference equations (A.9) and (A.10).

Appendix B. Criteria for the validity of the simplified model of a belt extractor

The concentration in each section is nearly constant when the concentration of liquid, sprayed on a section, c_{in}, and the concentration of liquid leaving the solids beds, c_{out}, do not differ too much. From analytical solutions of Eqns 2.12 and 2.13, one can calculate the liquid concentration at the bed exit at the moment of breakthrough, c_b, when the solids entering the section have uniform initial concentration over the bed height.

$$c_b - c_{in} = 1 - e^{-N_{t,r}/n} \tag{B.1}$$

where $N_{t,r}/n$, the number of true transfer units on overall liquid phase basis in one section, is defined as:

$$\frac{N_{t,r}}{n} = \frac{k_{oc} a V/n}{\phi_{c,r}} = \frac{N_{t,c}}{n}\ \frac{1}{R} \tag{B.2}$$

It will be clear that here $c_b - c_{in}$ is the maximum concentration difference within a section.

From Eqn B.1 it can be seen that for high recirculation rates $R = \phi_{c,r}/\phi_c$ and low mass transfer rates $N_{t,c}$, the concentration of liquid in the bed is nearly constant. In interpreting this result it should be realized that in general R is not an independent variable, but is normally adjusted to assure complete filling of the interstitial voids in the packing. A maximum concentration difference of, say, 10% is attained when $N_{t,c}/n\ R = 0.1$, as can be seen from Eqn B.1. Assuming no liquid entrainment, $N_{t,c}$ can be calculated from Eqns

Table B.1. Recirculation ratio resulting in 10% maximum concentration difference at 90% efficiency.

	Number of sections n	
Λ	5	8
1.5	9	5
2	5	3
4	2	1

1.3 and 2.59. For $\eta = 0.90$, the resulting recirculation ratio required to meet the above condition is shown in Table B1. The situations are often met in practice.

The simplified model will not be applicable in extraction of deep beds and when the number of sections is low. For these situations, the equations describing mass transfer in a fixed bed must be solved to account for concentration gradients in the liquid phase, and in the solid phase perpendicular to the flow direction of the solids.

Appendix C. Approximate relation for estimating $Sh_{d,a}$ values

In Section 3.3.2, it is shown that the $Sh_{od,a}$ value for countercurrent extraction with an extraction factor $\Lambda > 1$ is given by:

$$Sh^{od,a}_{\Lambda,Bi,\nu} = \frac{\Lambda}{\Lambda - 1} \frac{2}{\nu} \lambda_1^2 \tag{C.1}$$

where λ_1 is the first non-zero root of the related characteristic equation and the indices Λ, Bi and ν refer to arbitrary value of Λ, the Biot number Bi and the geometrical shape factor ν. For a linear equilibrium relation it was further shown in Section 3.1 that:

$$Sh^{-1}_{d,a,\Lambda,Bi,\nu} = Sh^{-1}_{od,a,\Lambda,Bi,\nu} - (2\,Bi)^{-1} \tag{C.2}$$

Combining the foregoing equations yields the following relation for $Sh_{d,a}$

$$Sh^{d,a}_{\Lambda,Bi,\nu} = \frac{1}{2}\left(\frac{\Lambda - 1}{\Lambda} \frac{1}{\lambda_1^2} - \frac{1}{Bi}\right) \tag{C.3}$$

The aim of this appendix is to provide a simple method for estimating the first eigenvalue λ_1, thus allowing a straightforward calculation of $Sh_{d,a}$. For convenience this approach is followed for slab geometry. The results for this case are there after extended to the basic geometries cylinder and sphere.

For infinite Λ, i.e. a constant bulk concentration, several authors presented simple

Table C.1. Approximate relation for the first root of $\tan \lambda_1 = Bi/\lambda_1$

$\lambda_{\infty,Bi,1}$	Source
$\frac{2.5\,Bi}{Bi + 2.4}$	Rutov, 1958
$\frac{2.67\,Bi}{Bi + 2.67}$	Backstrom, 1935
$\frac{(\pi^2/4)\,Bi^{1.02}}{Bi^{1.02} + 2.24}$	Kondratiev, 1964

equations for estimating the first eigenvalue $\lambda_{\infty,Bi,1}$. For slab geometry, some equations are summarized in Table C.1. In the present analysis the Kondratiev equation was adopted since it produces the exact solution for infinite *Bi* numbers. The equation was used in a somewhat simplified form, without forcing the accuracy significantly:

$$\lambda_{\infty,Bi,1} = \frac{\pi^2}{4}\,\frac{Bi}{Bi + 2.25} \tag{C.4}$$

To extend this equation to finite values of the extraction factor, it was written as:

$$\lambda_{\Lambda,Bi,1} = \frac{\pi^2}{4}\,\frac{Bi}{Bi + 2.25}\,f(\Lambda, Bi) \tag{C.5}$$

Since the $Sh_{d,a}$ value for a slab subjected to countercurrent extraction with extraction-factor $\Lambda = 1$ is 6, irrespective of the *Bi* number, a combination of Eqns C.3 and C.5 sets a constraint to the function $f(\Lambda, Bi)$:

$$f(\Lambda, Bi) = \frac{\Lambda - 1}{\Lambda}\,\frac{1}{\frac{1}{3} + \frac{1}{Bi}}\,\frac{Bi + 2.25}{Bi\,\pi^2/4}\;; \quad \Lambda = 1 \tag{C.6}$$

or

$$\frac{\Lambda}{\Lambda - 1}\,f(\Lambda, Bi) = p^* = \frac{Bi + 2.25}{Bi + 3}\,\frac{12}{\pi^2}\;; \quad \Lambda = 1 \tag{C.7}$$

From the values of $f(\Lambda, Bi)$ calculated from Eqn C5 the Fig. C1 is constructed. It is noted that for any Λ the following relation holds with reasonable accuracy:

$$\frac{\Lambda}{\Lambda - 1}\,f(\Lambda, Bi) = 1 + \frac{1}{\Lambda}\,(p^* - 1) \tag{C.8}$$

The final result is obtained from Eqns C3, C5 and C8 with $\nu = 1$

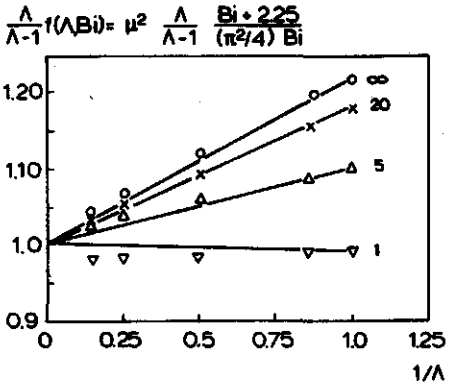

Fig. C1. Graphical determination of f(Λ, *Bi*); Parameter *Bi*.

$$Sh_{\substack{d,a \\ \Lambda, Bi, 1}} = \frac{Bi\left[6(Bi+2.25)+(\Lambda-1)\frac{\pi^2}{2}(Bi+3)\right]}{\Lambda Bi(Bi+2.25)+(\Lambda-1)\left[3(Bi+2.25)-(Bi+3)\pi^2/4\right]} \tag{C.9}$$

The deviation of Eqn C9 from the exact solution is shown in Fig. C2. The extension to other geometries is based on approximate equations given by Schoeber (1976) which he used for correlating $Sh_{d,a}$ values for concentration dependent diffusivities and constant surface concentration:

$$Sh_{\substack{d,a \\ \Lambda, Bi, 2}} = 2.07\ Sh_{\substack{d,a \\ \Lambda, Bi, 1}} - 4.45 \tag{C.10}$$

$$Sh_{\substack{d,a \\ \Lambda, Bi, 3}} = 3.18\ Sh_{\substack{d,a \\ \Lambda, Bi, 1}} - 2.30 \tag{C.11}$$

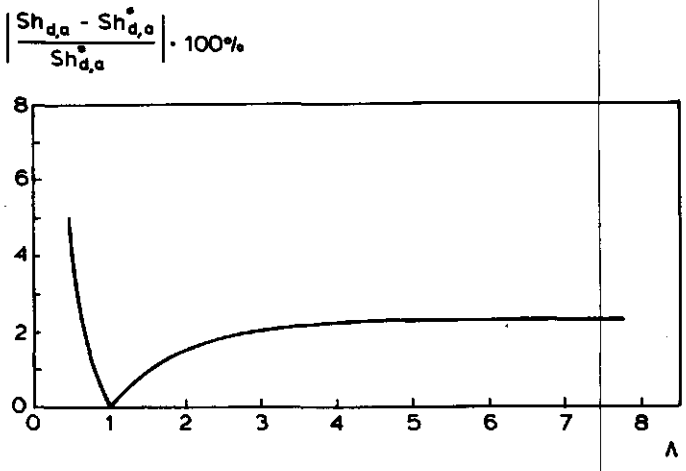

Fig. C2. Error bound of the approximate Eqn C.9.

These relations were reduced to a single equation, which increased the accuracy slightly for the case of variable extraction factor and constant diffusivity:

$$Sh_{\substack{d,a \\ \Lambda, Bi, \nu}} = \nu \; Sh_{\substack{d,a \\ \Lambda, Bi, 1}} - (\nu - 1)4 \tag{C.12}$$

As can be verified, the approximate equations presented here are exact for $\Lambda = 1$. Also for extraction factors slightly below 1 they can be used to estimate $Sh_{d,a}$ values with reasonable accuracy.

Appendix D. Mass transfer efficiency in the penetration period

In the following an analytical solution will be derived for the mass transfer problem for a slab subjected to cocurrent or countercurrent extraction with finite mass transfer resistance in the continuous phase in the penetration period.

The mass transfer process can be described with Eqn 3.29 with $\nu = 1$:

$$\frac{\partial W}{\partial t_d} = \frac{\partial^2 W}{\partial \xi^2} \tag{D.1}$$

The dimensionless distance coordinate is now defined according to Fig. D1. The boundary and initial conditions are given by:

$$t_d = 0 \qquad W = 0 \tag{D.2}$$

$$\xi = 0 \qquad \partial W/\partial \xi = Bi\,\{W - C(t_d)\} \tag{D.3}$$

$$\xi \to \infty \qquad \partial W/\partial \xi = 0 \tag{D.4}$$

Again, the value of $C(t_d)$ is obtained from a mass balance, with the following result:

$$\Lambda_t \frac{\partial C}{\partial t_d} + \nu \left.\frac{\partial W}{\partial \xi}\right|_{\xi=0} = 0 \tag{D.5}$$

with the initial condition $t_d = 0$, $C = 1$. The solution is derived using Laplace transforma-

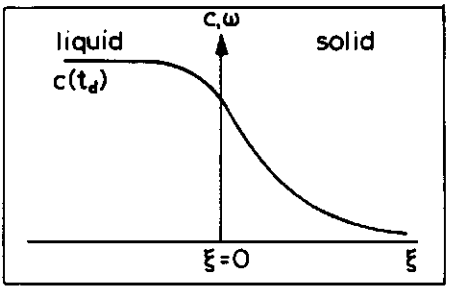

Fig. D1. Concentration profile near the solid liquid interface: semi infinite solid.

tion. Thus, the expression for $\partial W/\partial\xi|_0$ and $\bar{W}$ are readily obtained, where $\bar{W}$ has been defined as

$$\bar{W} = W_0 - \int_0^t \mathbb{D}_d \left.\frac{\partial W}{\partial r}\right|_{r=0} \frac{A_p}{V_p}\, dt = -\int_0^{t_d} \left.\frac{\partial W}{\partial \xi}\right|_{\xi=0} dt_d \tag{D.6}$$

The final relation for the Sh_{od} number then reads:

$$\frac{1}{2} Sh_{od} = \frac{\partial W/\partial \xi\,|_0}{\bar{W} - C} =$$

$$\frac{a_1 f(-a_1\sqrt{t_d}) - a_2 f(-a_2\sqrt{t_d})}{\frac{1}{a_1} f(-a_1\sqrt{t_d}) - \frac{1}{a_2} f(-a_2\sqrt{t_d}) + \frac{1}{a_2} - \frac{1}{a_1} - \sqrt{1 + \frac{4}{Bi\Lambda_t}}} \tag{D.7}$$

In the above equation the following variables are used:

$$f(x) = e^{x^2}\ \mathrm{erfc}\,(x) \tag{D.8}$$

$$a_1 = \frac{1}{2} Bi \left\{ -1 + \sqrt{1 + \frac{4}{Bi\,\Lambda_t}} \right\} \tag{D.9}$$

$$a_2 = \frac{1}{2} Bi \left\{ -1 - \sqrt{1 + \frac{4}{Bi\,\Lambda_t}} \right\} \tag{D.10}$$

For $Bi \to \infty$, the relation can be reduced to:

$$\tfrac{1}{2} Sh_{od} = \frac{\frac{1}{\sqrt{\pi t_d}} + \frac{1}{\Lambda_t} f(-\sqrt{t_d}/\Lambda_t)}{1 + (\Lambda_t - 1)\{1 - f(-\sqrt{t_d}/\Lambda_t)\}} \tag{D.11}$$

The average concentration in the solid phase can be determined from:

$$\bar{W} = \frac{Bi}{a_1 - a_2}\left[\frac{1}{a_1}\{-1 + f(-a_1\sqrt{t_d})\} - \frac{1}{a_2}\{-1 + f(-a_2\sqrt{t_d})\}\right] \tag{D.12}$$

Appendix E. Apparatus and experimental procedures: measurement of breakthrough curves

Apparatus: The experimental setup used in this study is shown in Fig. 39. Two columns which were kept at a constant temperature were used, one with a diameter of 0.07 m and a length of 0.7 m and a second with diameter 0.054 m and length 0.5 or 1 m.

Table E1. Properties of the packing material used in the experimental study.

Property of the packing material		Inert packing	Mass transfer experiments
diameter	(m)	1.4×10^{-3}	1.4×10^{-3}
permeability	(m^2)	0.49×10^{-9}	0.28×10^{-9}
interstitial void fraction	(1)	0.35	0.35
effective internal porosity calculated from measured value of the distributionratio	(1)	–	0.6
material		glass ballotini	porous silica
geometry		sphere	sphere

The properties of the packing material used are summarized in Table E.1. Since the concentration of the liquid flow leaving the packed section of the column may vary over the cross section of the bed, a complete mixed sampling region was constructed at the column outlet. The displacement velocity is kept constant by means of a positive displacement plunger pump. The plunger was driven by an electrical motor with variable speed, thus allowing easy control of flow velocity. A sample was withdrawn from the sample region and pumped continuously through a PAAR digital density meter. The density is measured over a time interval of about 4 seconds. With this time interval as a minimum, the measured density is stored on paper tape.

For experiments directed towards the effect of a concentration gradient on the flow stability the configuration shown in Fig. 39b was used. The mixer on top of the column provides an exponentially decreasing concentration at the inlet of the packed section of the column, when a step function in concentration is applied on the inlet stream:

$$\frac{c - c_\infty}{c_0 - c_\infty} = \exp\left(-\frac{t\phi_v}{V_m}\right) \tag{E.1}$$

where c_0 and c_∞ are the initial and final concentration in the mixer respectively. V_m is the volume of the mixed section. The resulting concentration gradient travelling downwards through the column is thus:

$$\frac{c - c_\infty}{c_0 - c_\infty} = \exp\left(-\frac{V_k}{V_m} z'\right) \tag{E.2}$$

$V_k = hAL$ is the free volume of the column and $z' = z/L$ is the distance coordinate in the flow direction. The shape of the concentration profile thus obtained resembles the one that is expected in countercurrent extractors with plug flow in both phases, when the extraction factor is greater than 1, see Eqn 1.3. It should be noted that the profile is independent of the displacement velocity when plug flow of the liquid occurs. Both from literature data (Miller & King, 1966; Levenspiel, 1972) and our own experiments, it was concluded that the axial Pe number is virtually independent of Re in the region of

interest. The former conclusion can thus be extended to stable displacement conditions in general. This allows us to evaluate easily the effect of displacement velocity on the hydrodynamic stability of the flow for a fixed concentration gradient.

The experiments designed to determine the effect of mass transfer on flow stability were performed in a set up similar to the one shown in Fig. 39a. The properties of the packing material are summarized in Table E.1.

Experimental procedure: Experiments run with an inert packing material i.e. glass beads proceeded in the following way. From a liquid reservoir a glycerol solution was recirculated through the bed until a uniform concentration was observed throughout the column. In order to assure complete deaeration of the packed section of the column, the flow was directed upwards. After closing the circulation loop, water was injected with a constant velocity in a downward direction, and the breakthrough curve was measured. When a porous packing was applied, the experiments proceeded in three steps. First, a sugar solution was recirculated through the bed until equilibrium between the liquid in the pores of the particles and the flowing liquid was obtained. There after the column was left to drain for several minutes. In the second step, the liquid adhering to the particles was washed off with water. To maximize the rinsing effect while reducing diffusional losses of sugar from the interior of the particle, the wash liquid was fed to the column at a relatively high speed. Measurements of the concentration of sugar in the wash water indicated that the desired effect was obtained when 5 pore volumes of wash water were collected. The flow direction was then reversed and the breakthrough curve was measured at the selected flow velocity. This third step is analogous to the final step in the experiments where an inert packing material was used.

Scouting experiments with inert packing material using dyed solutions indicated that considerable wall flow occurred in the unstable flow regime: the shape of the breakthrough curve showed a sudden decrease when breakthrough at the wall occurred. This is caused by the higher permeability in this region, a fact that triggers the formation of protuberances near the wall. The magnitude of the wall flow was dependent on the size of the equipment and the displacement conditions. To avoid the above effect, glass beads were mounted at the wall surface. It was ensured that a glue layer of Tensol cement occupied the voids fraction up to about half a particle diameter from the wall. Reruns

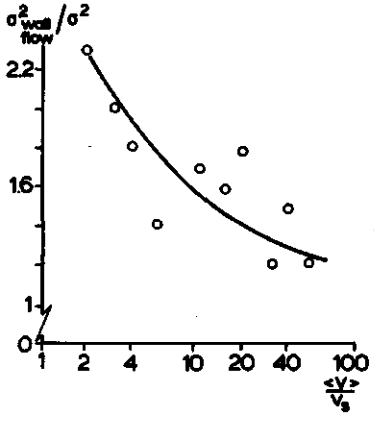

Fig. E1. Effect of preferent flow along the wall on the variance of the residence time distribution curve.

showed a considerable attenuation of the wall flow, see Fig. E.1. At the same time, the scatter in experimental data was considerably reduced. Reinterpretation of the residence time distribution curves that were affected by wall flow, which showed a significant concentration jump when breakthrough in the wall region occured, produced results that were very close to the measurements in the wall treated column.

Appendix F. Determination of the moments of the breakthrough curves

Several methods have been suggested in literature to determine the moments of the distribution function. Direct application of Eqn 4.23 has some significant drawbacks. Firstly, since in the experiments a cumulative distribution function $F(t)$ is measured, differentiation of the experimental data is required to obtain the frequency distribution $E(t)$. Numerical differentiation is a cumbersome procedure that requires careful smoothing of the measured data. Secondly, when the second moment M_2 is calculated, measurements in the tail of the distribution curve may contribute significantly because of the weighting function t^2. Therefore experimental errors in the trailing edge of this curve are largely amplified. Procedures that are proposed in literature try to overcome the forementioned difficulties. The method adopted here was suggested by Gunn (1970) and by Paynter (1957). Here the moments are obtained from the Laplace transform of the frequency distribution of residence times $E(t)$, that can be written as:

$$\mathcal{L}\{E(t)\} = \tilde{E}(s) = \int_0^\infty e^{-st} E(t)\,dt \tag{F.1}$$

After series expansion of the exponent and neglecting higher order terms, which is correct for small values of s, we obtain

$$\tilde{E}(s) = \int_0^\infty E(t)\,dt - s\int_0^\infty t\,E(t)\,dt + \tfrac{1}{2}s^2\int_0^\infty t^2\,E(t)\,dt \tag{F.2}$$

The moments of the distribution function can be recognized on the right side of this equation. After some rearrangement the following result is obtained for small values of s:

$$\frac{1}{s}\,\frac{\tilde{E}(s) - M_0}{M_0} = -\frac{M_1}{M_0} + s\,\frac{M_2}{2\,M_0} \tag{F.3}$$

M_1 and M_2 can thus be easily determined by linear regression. Even though the range of s is restricted to small values, an optimum choice exists. For very low values of s the truncation error of the computing device may set limits to calculation accuracy. Moreover, for higher s values the weighting function $\exp(-st)$ slightly suppresses the effect of errors in the tail of the breakthrough curve. According to Gibilaro & Drinkenburg (1972) the values of s should be selected in the range $0.02 < s\tau < 0.1$, where τ is the mean residence time in the flow system. Since the weighting function $\exp(-st)$ is always close to or smaller than unity, the accuracy in the determination of the moments is considerably increased compared to direct application of Eqn 4.23. In most of the experiments the cumulative distribution of residence times $F(t)$ is measured. By definition, the relation

between $E(t)$ and $F(t)$ is:

$$E(t) = d\,F(t)/d\,t \tag{F.4}$$

Since $F(0) = 0$ by definition, taking the Laplace transform of this equation gives:

$$\tilde{E}(s) = s\,\tilde{F}(s) \tag{F.5}$$

where $\tilde{F}(s)$ is defined analogous to Eqn F.1. After substitution of Eqn F.5 in Eqn F.3 the final result reads after slight rearrangement:

$$\mathcal{L}\{M_0 - F(t)\}/M_0 = M_1 - s\,M_2/2 \tag{F.6}$$

Note that M_1 can be determined directly from this equation when $s = 0$ is inserted. The resulting equation is then identical to the one proposed by Van der Laan (1958):

$$M_n = \int_0^\infty t^n\,E(t)\,dt = -\int_0^\infty t^n\,d(M_0 - F) = n\int_0^\infty (M_0 - F)\,t^{n-1}\,dt \tag{F.7}$$

For the calculation of M_2, the weighting function t that occurs in the procedure proposed by van der Laan is replaced by $\exp(-st)$, with some gain in accuracy.

Appendix G. Locating the position of the displacement front in downward miscible liquid-liquid displacement from packed beds

In order to get information on the behaviour of viscous fingers during unstable flow in liquid-liquid miscible displacement, an experimental setup was designed in which the location of the displacement front could be monitored. As pointed out in Appendix E, considerable wall flow may occur during unstable displacement. For this reason we aimed at a setup where measurements could be made in the interior of the column packing, while wall flow was suppressed as much as possible. This technique is likely to provide more reliable information on viscous finger growth than interpretation of frontal position measurements near the wall, see e.g. Chuoke et al., (1959).

The rectangular column used in these experiments is shown schematically in Fig. G1. In order to suppress preferent flow along the wall as much as possible, a pretreatment of the wall surface as discussed in Appendix E was followed. The column packing consisted of glass ballotini with a diameter of 0.0014 m. Glycerol solutions are displaced downwards with pure water. The location of the displacement front is determined by measuring the conductivity of the interstitial liquid between a common electrode and gold plated electrodes with the same dimension as the packing material. 100 Of these electrodes were mounted in a 10 x 10 matrix in a vertical plane in the centre of the column. To speed up the sample rate and to simplify recording of the data measured, only the order of magnitude of the conductivity is determined. This signal is converted to either a 0 or 1 logic level. Thus, at every moment the liquid concentrations inside the column are represented by a 10 x 10 matrix of 0 or 1 coded elements. The electronics were calibrated to produce a 0 signal for pure water and a 1 signal for the glycerol solution. Every

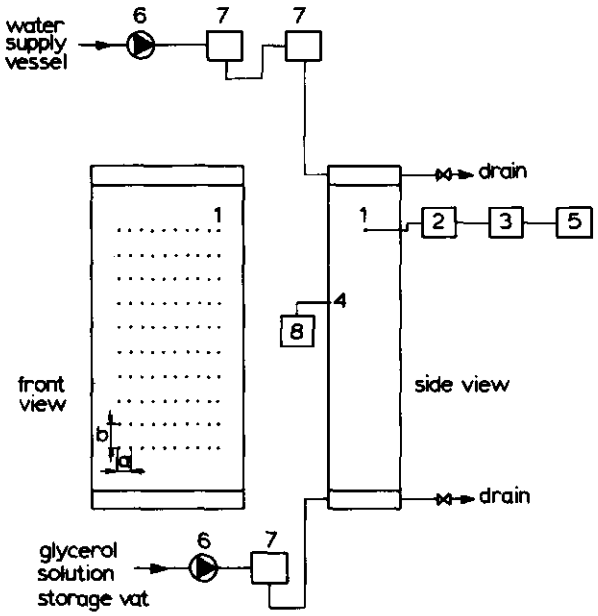

Fig. G1. Schematic picture of the experimental setup.

Dimensions	(m)	Item list
length	0.2	1. gold plated electrode
width	0.1	2. digitizer, 100 channels
height	0.5	3. multiplexer, 10 channels
a	0.01	4. common electrode
b	0.03	5. digital printer
Packing: glass beads		6. positive displacement pump
diameter	0.0014	7. pulse damper
porosity	0.35 (–)	8. sinewave generator

row of 10 electrodes thus constitutes a binary number. The decimal representation of this binary number is stored for further analysis. This figure can later be uniquely decoded to the binary representation. From these data, the time when the displacement front passed a specific electrode can be determined. By interpolation, the position of the front can be calculated at all times. To transform these results into smooth curves for further analysis, spline interpolation was used. Typical results are shown in Fig. G2 for stable displacement conditions, and in Fig. G3 and Fig. G4 for ambient and strongly unstable conditions, respectively.

From the measured front positions, the growth rate of the viscous fingers and the relative channel width were determined. At low displacement velocity, $\langle v \rangle / v_c < 3$, the fingers once initiated did not grow in size during the displacement. For higher flow velocities, the growth rate was essentially constant. The growth rate of the fingers is further increased with flow rate, until an asymptotic value is reached where the stabilizing effect of gravity can be neglected. The results confirm data reported in literature (e.g. Benham & Olsen, 1963; and others); Most of these data have been obtained from measurements in Hele Shaw models, a hydrodynamic analogon of a packed bed. Channel

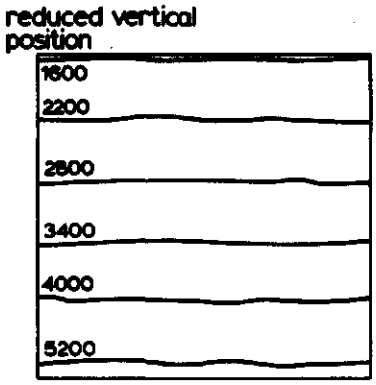

Fig. G2. Front positions under stable displacement conditions. $M = 60$; $\langle v \rangle / v_c = 0.6$; $\langle v \rangle = 0.33 \times 10^{-4}$ m/s; Parameter time.

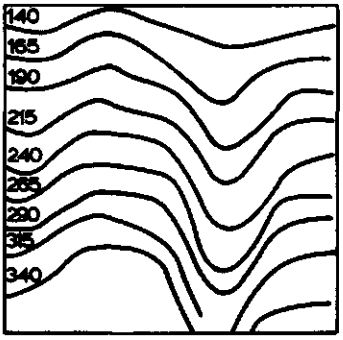

Fig. G3. Front positions under slightly unstable displacement conditions. $M = 20$; $\langle v \rangle / v_c = 5$; $\langle v \rangle = 6.2 \times 10^{-4}$ m/s; Parameter time.

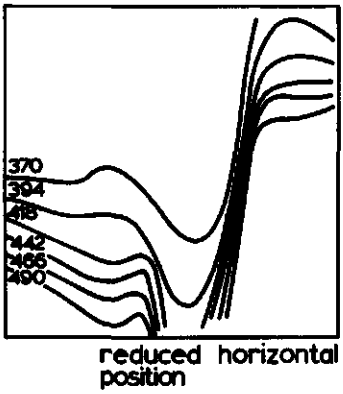

Fig. G4. Front positions under unstable displacement conditions. $M = 60$; $\langle v \rangle / v_c = 10$; $\langle v \rangle = 51.0 \times 10^{-4}$ m/s; Parameter time.

width was only well defined for high viscosity ratios and displacement velocities. The fraction of the column cross section occupied by the channels varied from 0.4 to 0.7 with increasing displacement velocity. This value compares reasonably with the asymptotic value of 0.5 for high displacement velocities reported by Safmann & Taylor (1958). For more ambient displacement conditions the area occupied by the fingers varies in the flow direction.

Appendix H. Experimental determination of model parameters D and (k_0a)

In principle the distribution ratio D can be determined from properties of the packing material, i.e. the internal and external void fraction ϵ_i and h. Yet we preferred to measure the value of D in situ since the internal pore volume might not be occupied completely with the presaturation liquid. Therefore experiments were designed with relatively low initial sugar concentration and rather low displacement velocities. Experimental conditions were chosen such that stable displacement could be expected. At the beginning of the experiment equilibrium conditions between the packing and the interstitial liquid was assured, $s_0 = 1$. Under this condition the initial solute concentration in both phases is known exactly and, moreover, mass transfer stabilizes the liquid flow. From the zeroth moment of the breakthrough curve the value of D is calculated with the aid of Eqn 4.36. The result, averaged over three runs, showed that the distribution ratio equals:

$$D = 0.90 \pm 0.05 \tag{H.1}$$

From the first moment of the breakthrough curve the number of transfer units is calculated with Eqn 4.37, assuming that Pe equals 100. From this value the apparent (k_0a) is determined. The effective interfacial area a is dependent on the packing geometry only and thus has the same value for all experiments. The overall mass transfer coefficient k_0 is dependent on k_c and k_d. The former coefficient is determined by the physical properties of the liquid and by the flow velocity. Fortunately it can be shown from Eqn 3.20 that the Biot number $Bi = mk_cD_p/\mathcal{D}_d$ is higher than 50, even for the runs with high sugar concentration and low flow velocity. This implies that the mass transfer rate is limited by interparticle diffusion. Although the value of k_0 is thus in principle a function of time and dependent on the concentration history in the liquid surrounding the particle, a constant value of k_0 is assumed here. This figure serves as a reference value for other experiments. Averaging over three runs we obtained:

$$(k_0a)_{ref} = (N/\tau)_{ref} = 0.0125 \pm 0.0015\ (s^{-1}) \tag{H.2}$$